A facile screening strategy to construct auto-fluorescent protein-based biosensors

Shunsuke Tajima

Kyoto University

Acknowledgements

The studies in this thesis have been carried out under the direction of Professor Takashi Morii at the Graduate School of Energy Science, Kyoto University, during April 2015 to March 2022. The study focuses on the development of a facile strategy to detect structural change of proteins and to enhance the signal response of biosensors based on auto fluorescent protein.

I would like to express the deepest appreciation to Professor Takashi Morii for his guidance, valuable suggestions, fruitful discussions and encouragement throughout the work.

I am deeply grateful to Associate professor Eiji Nakata for his kind advices, helpful discussions and encouragement. I would like to thank Lecturer Rajendran Arivazhagan for his helpful advices, guidance for English writing, discussions and encouragement.

I am sincerely grateful to Dr. Shun Nakano for his technical support, helpful guidance, suggestion, discussions and encouragement.

I am sincerely grateful to Dr. Masayuki Saimura for his technical support, kind guidance, fruitful discussions and valuable suggestions to perform the protein expression.

I would like to express my thank Professor Yasuo Mori for his collaboration works and the technical supports. I would like to express my thank to Lecture Reiko Sakaguchi for her technical supports, kind guidance, fruitful discussions and valuable suggestion to perform mammalian cell experiment in chapter 5.

I would like to show my greatest appreciation to Professor Emeritus Isao Saito for his helpful guidance, suggestions, fruitful discussions and encouragement.

I would like to express my sincere gratitude and appreciation to my thesis committee members, Professor Masato Katahira and Professor Takashi Sagawa for their

fruitful discussions and valuable suggestions in the writing and revising this thesis.

I thank the past and the present members of Professor Morii laboratory for their suggestions, cooperation and discussions.

I thank Ms. Yuki Tashiro, Ms. Kaori Hashimoto, and Ms. Yukie Kajikawa for their kind supports for office jobs and encouragements.

Finally, I would like to my family for their constant encouragements and supports.

Shunsuke Tajima
Laboratory of Biofunctional Chemistry
Department of Fundamental Energy Science
Graduate School of Energy Science
Kyoto University
March, 2022

Table of contents

Chapter 3: A two-step screening to optimize the signal response of autofluorescence protein-based biosensor

Chapter 4: Evaluation of selectivity and kinetics of the putative fluorescence NO sensors

Chapter 1
General introduction

1. 1. Demands of utilization of the metabolic systems as the renewable energy sources

The worldwide demand and consumption of energy continues to rise, which are resulted from the increasing of the human population expected to increase up to 9 billions by 2050.[1-3] Currently, to fulfil these high energy demands of ongoing industrialization, economic growth and rising populations, most of the energy sources were relied on the fossil fuels such as carbon, natural gas and petroleum. However, these fossil fuels are non-renewable energy sources considered to be depletion in about 100 years. Additionally, vast amount of greenhouse gases produced in usage of fossil fuel, occupying around 87% of the global CO_2 anthropogenic activities, will cause global warming.[4,5] The global warming caused by greenhouse gases may cause the melting of glaciers and ice sheets, raising the sea level, which affects the ecosystem indirectly.[2] To solve these worldwide problems, the development of energy sources and transformation systems which are renewable and sustainable are required.

Metabolic systems, energy generation and transformation processes which were carried out in biosynthesis by living organism, are highly efficient and clean systems to produce the adequate molecules for their lives. Utilizing and engineering of metabolic systems of the living organisms for material production could shed light on the development of the sustainable society. Recently, a lot of effort for practical application of bioethanol, biogas, or biodiesel, which were synthesized from the living organisms, are made to utilize their efficient and clean systems as the new renewable energy source.[1,2,6] Furthermore, biosynthesis of effective chemicals, such as microbial cellulose and ethylene, could also save the energy consumption at producing them to daily used materials.[7,8]

The metabolic pathways of living organisms have developed very sophisticated parallel multi-step reaction processes performed by various enzymes. To proceed these multi-step reactions exactly, enzyme in each step was strictly regulated in the appropriate time and location. To regulate such coordinated generation by appropriate enzymes, cells produce appropriate signaling molecules as second messengers inside cells following signal transduction systems. Therefore, understanding the signal transduction system is the key to control the metabolic reactions.

1. 2. Signal transduction systems in the living organisms

Signal transduction were regulated by various small molecules and proteins. Physiological and chemical stimulation from the environmental condition such as heat, cold, or acidity, or intercellular molecules, such as hormone or neurotransmitter, activate the receptor on the surface of the transmembrane of the cells, such as G protein-coupled receptors, receptor tyrosine kinase, or ligand-gated ion channel. To transduce these outer information inside the cells, activated receptors further activate other proteins with the chemical reaction, such as phosphorylation of the tyrosine residues of adenylate cyclase or phospholipase C-β, to synthesize cAMP or decompose phosphatidylinositol 4,5-bisphosphate (PtdIns(4,5)P_2) into D-*myo*-inositol-1,4,5-trisphosphate (Ins(1,4,5)P_3) and DAG, called as second messenger. These second messengers further propagate the signal to other biomolecules or proteins in the downstream, to induce various vital reactions finally. Some important second messengers and proteins related to signal transduction are introduced here.

Inositol polyphosphates

Inositol polyphosphates (IPs) form the largest family of second messengers, where over thirty kinds of IPs have been discovered. Ins(1,4,5)P_3 is the first IP to be identified as the second messenger and most extensively characterized.[9,10] Ins(1,4,5)P_3 is synthesized with the hydrolysis of PtdIns(4,5)P_2, which is catalyzed by members of the family of phospholipases C (PLC). Ins(1,4,5)P_3 can bind to Ins(1,4,5)P_3 receptors, which are Ca^{2+} channels located on intracellular organelles such as the endoplasmic reticulum (ER) and Golgi apparatus. Binding mediates Ca^{2+} release from intracellular stores,

resulting in Ca^{2+} accumulation in the cytosol and in organelles such as mitochondria and lysosomes (Figure 1. 1).

$Ins(1,3,4,5)P_4$ was synthesized by the phosphorylation of $Ins(1,4,5)P_3$ with the ositol-trisphosphate3-kinases ($InsP_3$Kinase; gene name: ITPK).[11-13] $Ins(1,3,4,5)P_4$ also function as the second messenger in many physiological processes, such as synaptic plasticity, hematopoietic cell survival, development and function, mRNA export, transcriptional regulation and chromatin remodelling.[14-16]

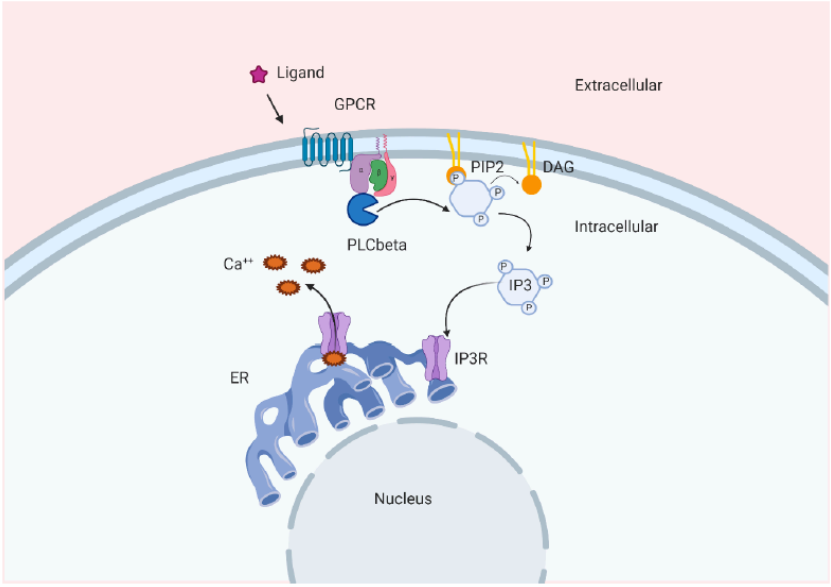

Figure 1.1. Schematic representation of signal transduction pathway related to the synthesis and function of $Ins(1,4,5)P_3$. GPCR, G protein-coupled receptor, activate the PLCbeta, phospholipase C-β, upon the ligand binding on the GPCR PLC beta decompose PIP_2, phosphatidylinositol 4,5-bisphosphate, to IP_3, $Ins(1,4,5)P_3$, and DAG, diacylglycerol. IP_3 bind to IP3R, IP_3 receptor, located on the ER, endoplasmic reticulum, to induce Ca^{2+} release

Nitric oxide

NO is also known as the cell signaling molecule that controls diverse biological functions, such as cardio vascular[17,18], nervous[19,20] and immune systems.[21] The tumor cell signaling[22], plant physiology, such as stomatal closure, growth, and development[23], and cellular morphology[24] are also found to be controlled by cellular NO dynamics. In animal cells, biosynthesis of NO is primarily catalyzed by the enzyme NOS. Three NOS isoforms have been identified, termed on the basis of the tissue source from which they were

originally extracted: neuronal NOS (nNOS), inducible NOS in macrophages (iNOS), and endothelial NOS (eNOS).[25,26] Activities of nNOS and eNOS are strictly dependent on the elevation of intracellular free Ca^{2+} and resultant binding of the Ca^{2+}–CaM complex. Because of its high reactivity, NO regulates the functions of many proteins via post-translational modifications, such as S-nitrosylation of the side-chain of cysteine[19,23,27], such as TRPC5, or by regulating the metal ion binding of metalloproteins (Figure 1.2).[28-30]

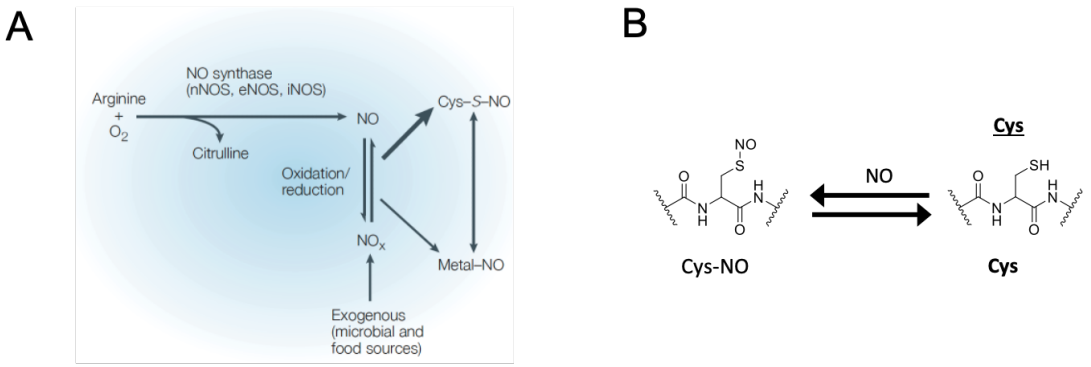

Figure 1.2. (A**)** Nitric oxide (NO) is generated, in most cell types, from Arg and O_2 by NO synthases (NOSs), neuronal NOS (nNOS), endothelial NOS (eNOS), or inducible/Ca^{2+}-independent NOS (iNOS). (B) NO regulates the functions of many proteins via the S-nitrosylation of the thiol of cysteine residues of the proteins.

TRPC5 channel

The transient receptor potential canonical (TRPC) channels are ubiquitously expressed in smooth muscle, endothelium, and brain and play important roles in a variety of physiological processes, including smooth muscle contraction, vascular function, neurotransmitter release, and neurological behavior.[31-33] The TRPC subfamily members are Ca^{2+}-permeable cation channels that depolarize cells and increase intracellular calcium levels and are potentiated by G protein-coupled receptors (GPCRs) or tyrosine kinase receptor-mediated activation of phospholipase C (PLC), which cleaves phosphatidylinositol 4,5-trisphosphate (PIP_2) into diacylglycerol (DAG) that directly activate TRPC subfamily[34] and inositol 1,4,5-trisphosphate (IP_3).[35] Among the seven mammalian TRPC members, a nonselective calcium-permeant cation channel TRPC5 is of considerable interest as a potential therapeutic target for progressive kidney disease, depression, anxiety, and other disorders.[33] TRPC5 assembles into tetramers to form a

channel, of which S5-S6 helices and the pore region between the S5 and S6 helices contribute to form the pore.[33,36] TRPC5 promotes Ca^{2+} uptake upon S-nitrosylation and/or disulfide bond formation of specific cysteine residues, providing the NO-sensing function of TRPC5 channels.[37] In the proposed NO-sensing mechanism of TRPC5, two cysteines, Cys553 and Cys558, located at the N-terminal side of pore-forming region are selectively modified by NO. The free thiol group of Cys558 nucleophilically attacks S-nitrosylated Cys553 to form a disulfide bond that stabilizes the open state.

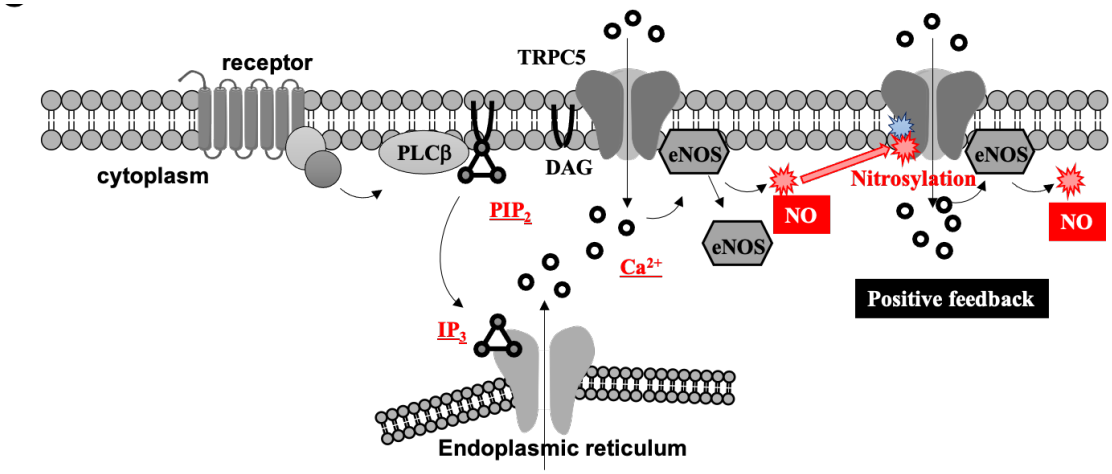

Figure 1.3. The schematic illustration of positive feedback regulation system of Ca^{2+} uptake concerned in nitric oxide (NO) and TRPC5. In endothelial cells, NO, which was produced by eNOS, acivate TRPC5 with S-nitrosylation and promote the Ca^{2+} influx.

1. 3. Strategy to understand signal transduction systems

To understand signal transduction, exploring the activation mechanism of proteins such as enzymes or channels and behavior of second messengers such as ions or small biomolecules are important.

To understand the structural change of proteins upon the activation, structural information of proteins was revealed by using NMR spectroscopy, X-ray crystallography, or Cryo-EM. However, information of structural changes of many proteins was still unknown because these methods have limitation resulted from the difficulty of the sample preparation. Therefore, development of convenient method to detect structural changes were desired.

Biosensors which allow real-time imaging of signal molecules in living cells were necessary to explore the behavior of second messngers.[38-41] Generally, biosensors consist of recognition module for binding targets and signal transduction module for converting binding event to measurable signal (Figure 1.4A). In more detail, fluorescence, chemiluminescence[41], electrochemical[39], electrical, thermal, and magnetic responses were utilized as the measurable signal (Figure 1.4B). Among these signals, fluorescence detection is the most useful method to detect signal molecules in living cells because of its advantage of property of high sensitivity and spatiotemporal resolution, low cost for use, and good tissue penetration.[43-47] On the other hand, biological macromolecules such as nucleic acids or proteins[42], synthetic receptor[48-56], and aptamer[56] were considered as the recognition module (Figure 1.4B). Especially, proteins possess high specificity and affinity to recognize biomolecules to strictly mediate and regulate chemical reactions in living cells. Therefore, proteins were superior for using as the recognition module to detect desirable target with high affinity and selectivity. Considering these contexts, fluorescent biosensors which consist of proteins as the recognition module were the most widely adaptable tool for detecting biomolecules in living cells.

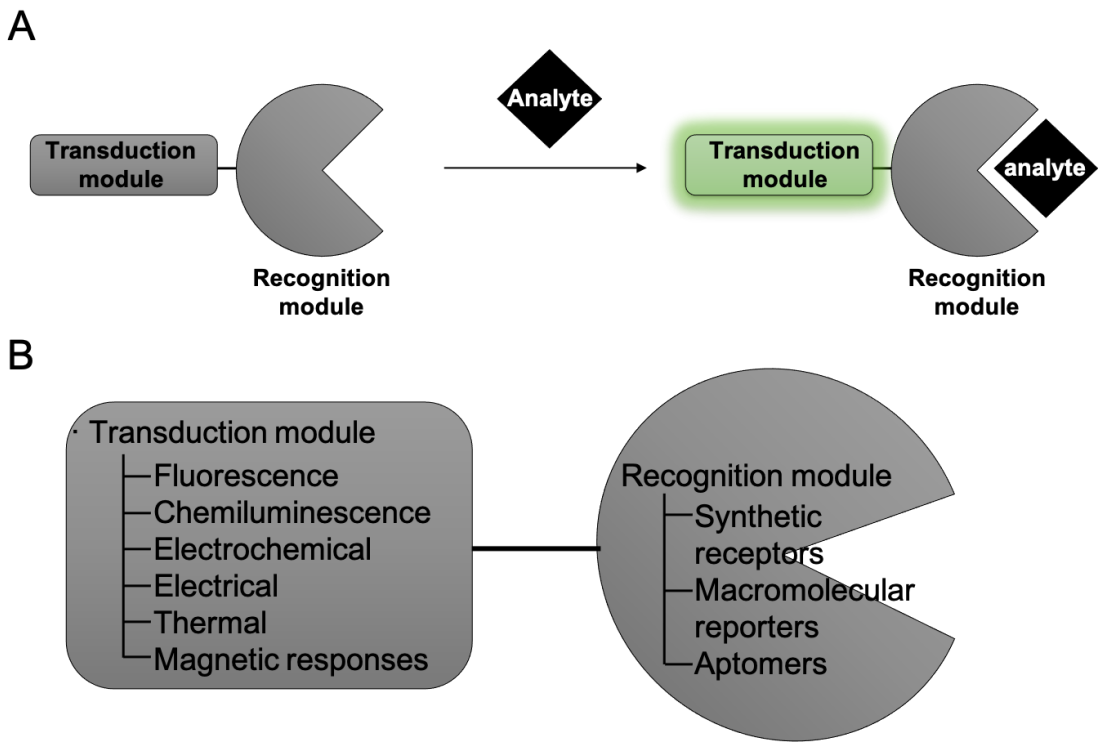

Figure 1.4. Schematic representation of biosensors. (A) In biosensors, target-binding events of recognition modules are converted to measurable signal of signal transduction

module. (B) Some elements were applicable for both transduction module and recognition module.

1. 4. Fluorescent biosensors using the protein recognition module

Depending on the type of fluorescence molecule in signal transduction module, the protein-based fluorescent biosensors could be classified into two categories;[42] 1) The first category is the chemically-modified biosensors, of which artificial fluorescent molecules were used as the signal transduction module. 2) The second category is the auto-fluorescent protein (AFP) based biosensors, of which auto-fluorescent proteins (AFPs), such as green fluorescent protein (GFP) and its variants were used as the signal transduction module. In this section, properties of these two categories of protein-based biosensors are explained.

1. 4. 1. Chemically-modified protein-based biosensors

In the chemically-modified protein-based biosensors, synthetic fluorescent molecules were modified into the receptor proteins of recognition module. The advantages of this kind of fluorescent biosensor are below;[38,42,57] 1) Synthetic fluorophore induce less perturbation to the functions of receptor proteins because of its relatively smaller size. 2) A superior characteristic of dye, not only the fluorescence changes in intensity and wavelength but also the microenvironmental sensitivity such as pH, polarity or molecular recognition, could be introduced to the receptor protein. 3) The introduction site of dye to the protein framework is more flexible compared to the auto-fluorescent protein (AFP)-based biosensors. While, in the AFP-based biosensors, the introduction sites of AFP are generally limited to the N- and C termini of receptor proteins, small dye can be introduced into the middle of loop regions or proximity to the binding pocket of receptor proteins. Chemically-modified biosensors generally detect the target based on the alteration of microenvironment of the modified fluorophore upon the target-binding event. Chemically-modified biosensors have been developed for maltose[58], glucose[59], ribose[60], and glutamine[60] by attaching environmentally sensitive fluorophores covalently to mutated thiols of receptor proteins.

Morii and coworkers have constructed novel Ins(1,4,5)P_3 and Ins(1,3,4,5)P_4 biosensors by utilizing the pleckstrin homology (PH) domain of PLCδ_1[61] and phosphoinositides 1 (GRP1)[62] as the recognition modules, respectively (Figure 1.5). These biosensors were constructed by introducing synthetic fluorophores into the proximity of the ligand-binding site of each PH domain by means of structure-based design. Binding of Ins(1,4,5)P_3 or Ins(1,3,4,5)P_4 induce the structural change of each PH domain, that effects a sufficient fluorescence response resulted from the changes in orientation of the fluorophore. This design strategy of chemically-modified biosensors is a powerful strategy to construct biosensors for inositol derivatives with high selectivity and appropriate affinity.[62,70]

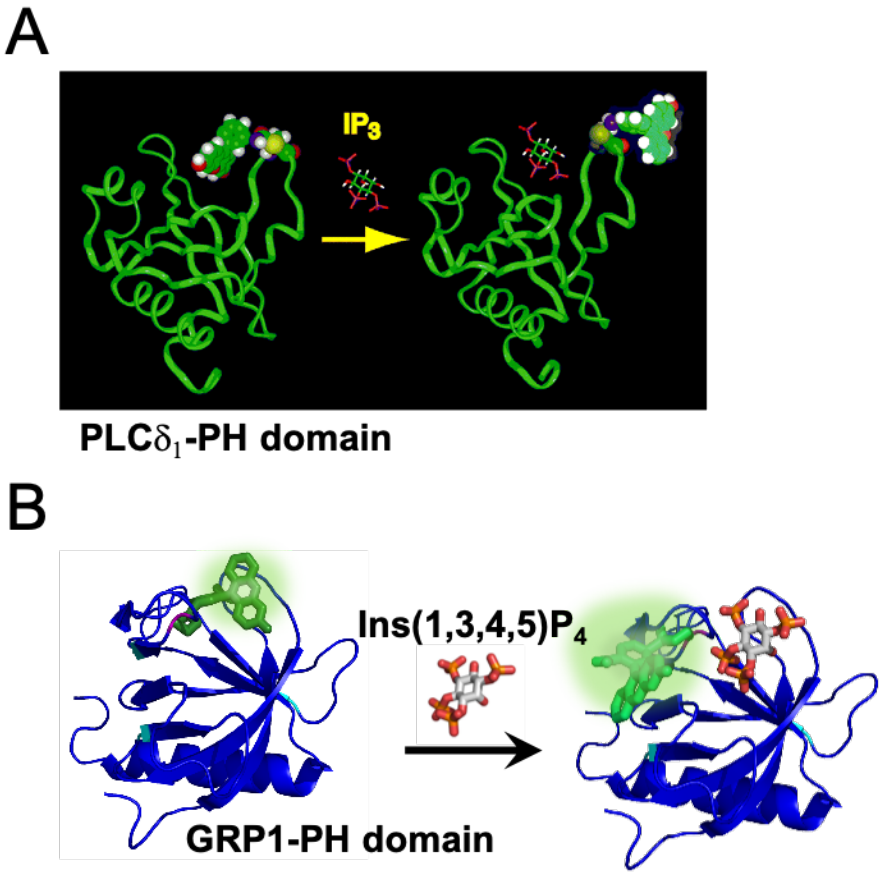

Figure 1.5. Schematic illustrations of fluorescent biosensors for (A) Ins(1,4,5)P_3 and (B) Ins(1,3,4,5)P_4.[62] The fluorophore was introduced at Glu 82 (magenta), near the binding pocket.

However, unlike AFP-based biosensors, synthetic fluorophores cannot be

introduced flexibly with the conventional genetic engineering. Consequently, other efficient methods to introduce synthetic fluorophores into receptor proteins are required. Additionally, unlike AFPs based biosensor, chemically-modified biosensors generally require the invasive introduction to living cells, such as electroporation[63-65], lipofection[66,67], microinjection[68], and tagging cell-permeable peptide sequences[69,70].

1. 4. 2. Auto-fluorescent protein (AFP) based biosensors

Green fluorescent protein (GFP), which is the first auto-fluorescent proteins (AFPs), was isolated from jellyfish[71]. AFPs form their chromophore spontaneously by the air-oxidation after expression in organisms, that is, AFPs do not require additives to show fluorescence. AFPs are automatically expressed in the cells by noninvasively introducing the vector encoding AFPs. Therefore, AFPs were utilized for noninvasive fluorescent markers to monitor gene expression, protein localization, and intracellular protein targeting by conjugating the AFPs to target proteins.

Furthermore, to image and detect biomolecules such as the second messengers in living cells, many kinds of AFP-based biosensors have recently been developed. The advantages of AFP-based biosensor are below;[38] 1) AFP-based biosensors can be automatically expressed in living cells by transfecting the plasmid DNA encoding them. This noninvasive method contributes to the low damage to the cell upon imaging. 2) Because AFP-based biosensors can be constantly produced based on plasmid DNA in the cells, dilution of biosensors resulted from a vital activity, such as cell growth and division, can be suppressed. This character enables long time imaging. 3) It is easy to localize biosensors to the specific regions within cell by introducing a certain peptide sequence for organelle-specific targeting signal. Therefore, AFP-based biosensors favorable for tracing the biomolecules functioning in various vital phenomena in the living cells.

AFP-based biosensors are designed so that the structural changes of the receptor proteins associated with the ligand-binding event transduces to a significant fluorescence response of AFPs. AFP-based biosensors could be classified in three categories; 1) Dual AFP-fused fluorescent resonance energy transfer (FRET)-based biosensors (Figure 1.6A), 2) Single AFP-based biosensors (Figure 1.6B).

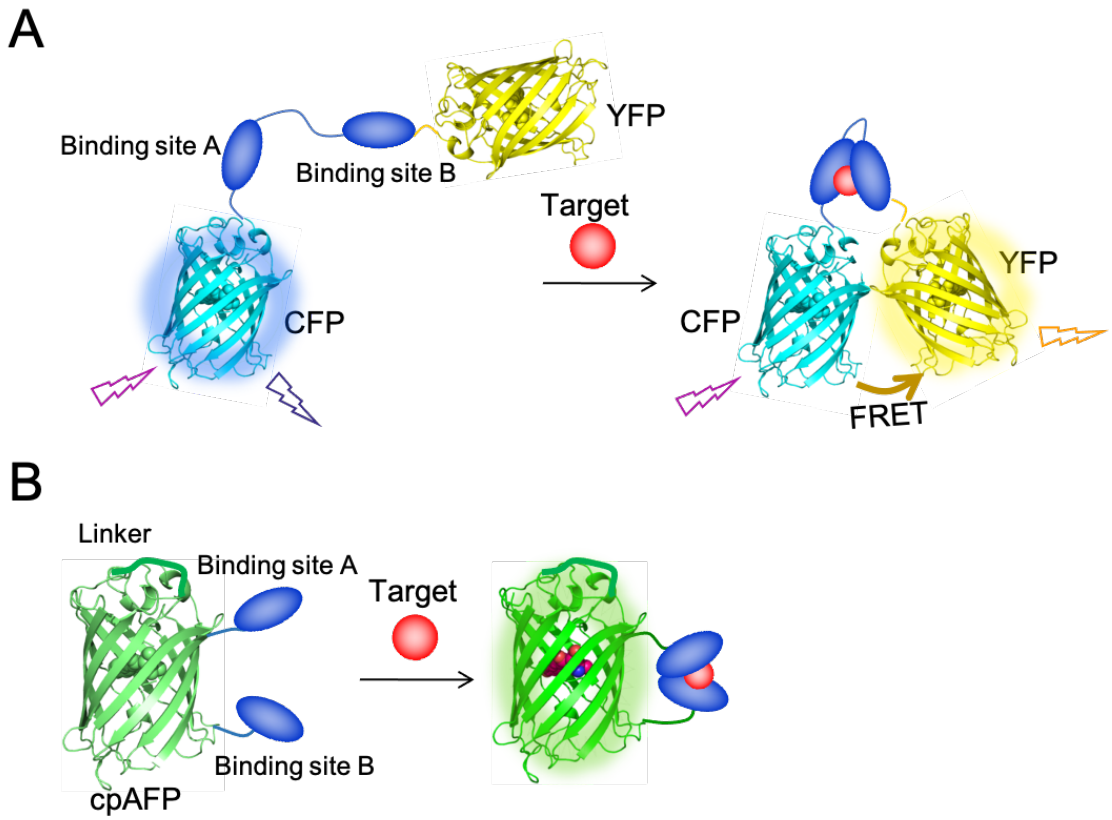

Figure 1.6. (A) Dual AFP-fused fluorescent resonance energy transfer (FRET)-based biosensors. Two AFPs, CFP and YFP, were connected with the target binding protein and peptide linkers. A structural change of the target binding protein upon binding the target induced the change of the FRET efficiency between CFP and YFP. (B) Single AFP-based biosensors.

FRET-based biosensors

FRET is a energy transfer between two fluorophores. The emission spectrum of donor fluorophores and the excitation spectra of acceptor fluorophores need to be overlapped. FRET occurs when two fluorophores are in sufficient proximity (<10 nm).[72] FRET-based biosensors are constructed by conjugating a pair of AFPs with the receptor proteins. A dynamic structural change of receptor protein upon binding targets result in locating a pair of AFPs in proximal distance each other, enhancing the FRET efficiency of them. Various FRET-based biosensor have been developed to image intracellular events such as enzyme activities, such as protease[74-77], kinase[78,79], and phosphatase[80], and dynamics of intracellular second messengers, such as Ca^{2+}[81,82], cAMP[83], cGMP[84], and

IP_3[85] (Figure 1.7).

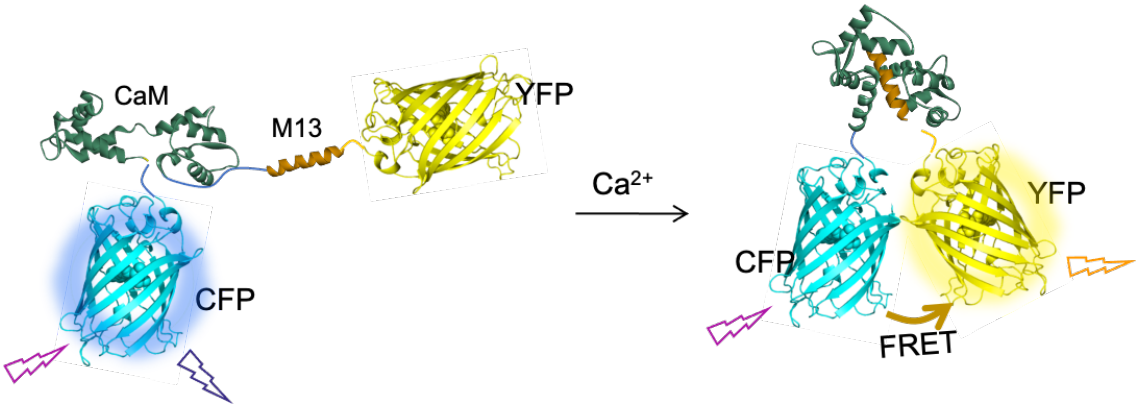

Figure 1.7. Schematic illustration of the FRET-based Ca^{2+} biosensor, cameleons.[81] They consist of tandem fusions of a BFP or CFP, calmodulin[87], the calmodulin-binding peptide M13[88], and an enhanced GFP or YFP. Binding of Ca^{2+} makes calmodulin wrap around the M13 domain, increasing the fluorescence resonance energy transfer (FRET) between the flanking GFPs.

To realize the sufficient energy transfer efficiency, the following two factors should be considered. 1) Suitable FRET pairs where emission spectrum of the donor and the acceptor excitation spectrum of acceptor were overlapped should be chosen. Generally, in the AFP-based FRET biosensors, CFP and YFP mutants have been widely used as a donor and an acceptor, respectively.[73] 2) The donor and the acceptor need to be located at a rational distance which can drastically change the FRET efficiency before and after binding target.[86] Therefore, to realize the sufficient change of FRET efficiency, the location of AFPs relative to the sensing domain need to be optimized by changing the linker between each protein unit. Especially, the large structural changes of the receptor proteins are the most important to realize drastic change of FRET efficiency. This requirement to the receptor protein severely limits the candidates of proteins available to construct FRET-based biosensors.

Single AFP-based biosensors

Single AFP-based biosensors have been developed for targeting Ca^{2+} [89-92], cGMP[93], H_2O_2[94,95], Zn^{2+} [96]. Single AFP-based biosensors were constructed by conjugating receptor proteins into single AFP. The structural change induced at the receptor protein upon the reaction with target is subsequently transduced as the change in fluorescence emission of AFP. Generally, to construct AFP-based biosensors, dynamic structural change of receptor proteins upon binding target is required.

Circulary permuated (cp) AFPs were constructed by connecting original C and N termini of AFPs with a short peptide linker and regenerating the new C and N termini at another position. In cpAFP-based biosensors, split receptor protein can be introduced near the AFP chromophore by generating new C and N termini near the AFP chromophore. Split receptor proteins are expected to show larger structural changes compared to wild type receptor proteins, enhancing signal response of AFP. Nakai and coworkers have developed Ca^{2+} biosensors, G-CaMP, which showed a high affinity and signal-to-noise ratio (Figure 1.8).[89] Since G-CaMP showed the dynamic signal responses in response to Ca^{2+}, this sensor have been widely used to visualize the intracellular dynamics of Ca^{2+} in living cells. However, these biosensors still required large structural change of target binding protein to detect as such high signal.[98]

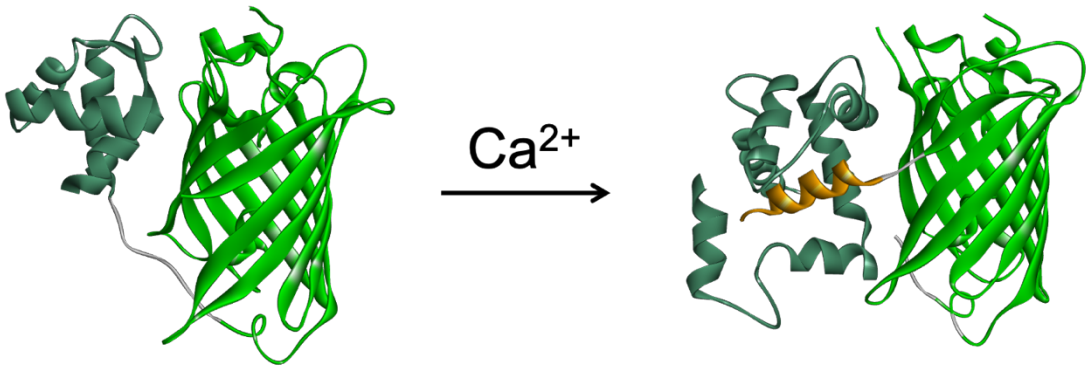

Figure 1.8. Crystal structures of G-CaMP in the Ca^{2+}-free form (PDB: 3EKJ) and Ca^{2+}-saturated form (PDB:3EK4).[98] CaM (dark green) and M13 (orange) were connected to new C- and N-terminal of cpGFP with peptide linker, respectively. Binding of Ca^{2+} makes calmodulin wrap around the M13 domain, transduced to the fluorescence change of the cpGFP. Large structural change upon the binding between CaM and M13 was required.

Morii and coworkers developed a novel Ins(1,3,4,5)P_4 biosensor by introducing a

designed split pleckstrin homology (PH) domain of Bruton's tyrosine kinase (Btk) into a single cpGFP (Figure 1.9 A).[94] Ins(1,3,4,5)P_4 biosensor shows two absorption maxima corresponding to the protonated and deprotonated states of the GFP chromophore (Figure 1.9B). Therefore, Ins(1,3,4,5)P_4 biosensor can detect Ins(1,3,4,5)P_4 with the change of fluorescence emission ratio when excited at each absorption maxima, and retained the affinity and selectivity of the original Btk-PH domain. Importantly, although Btk-PH domain shows subtle structural change upon binding Ins(1,3,4,5)P_4, introducing the Btk-PH domain near the cpGFP chromophore of cpGFP contribute to detect as a measurable fluorescence change. (Figure 1.9).

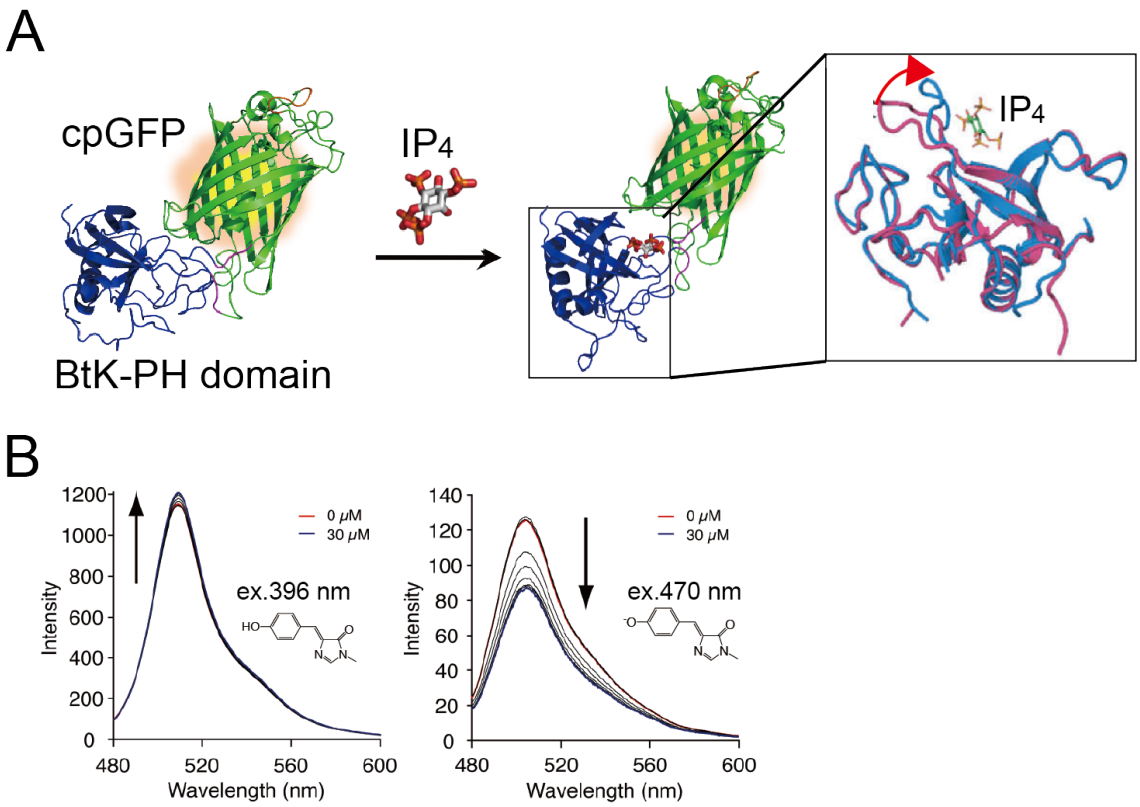

Figure 1.9. (A) Schematic illustration of single cpAFP-based Ins(1,3,4,5)P_4 biosensor.[94] Btk-PH domain was introduced near the cpGFP chromophore. Btk-PH domain shows subtle structural difference between unliganded (magenda, PDB: 1BTK) and Ins(1,3,4,5)P_4-bound (blue, PDB: 1B55) state. (B) Upon binding Ins(1,3,4,5)P_4, Ins(1,3,4,5)P_4 biosensor showed the increment of the fluorescence intensity excited at 396 nm corresponding to protonated state and decrease of the fluorescence intensity excited at 470 nm corresponding to deprotonated state.

1. 5. Construction strategy of AFP-based biosensors

For construction of AFP-based biosensor, the structurally well-characterized native proteins, which were analyzed by NMR spectroscopy, X-ray crystallography, or Cryo-EM, are suitable for the recognition domain.[57,88,89,92,99-102] However, the information of the structural changes of recognition modules binding targets of interest is not always available because these methods consume a lot of times and labors for acquiring the structural information. Additionally, even when structures of proteins are well-characterized, proteins do not always show the sufficient structural changes for being utilized to AFP-based biosensors. Some efforts to make the construction of AFP-based biosensors effectively in the case of less structural information of receptor proteins have been made. Circularly permutation, as described in the previous section, is one method for amplifying the structural change of receptor proteins. In cpAFP-based biosensors, receptor proteins can be divided into to two parts to introduce receptor proteins to N- and C-terminal of cpAFPs, respectively, as the recognition module. Introduction of the divided receptor proteins could cause the enhancement of the structural changes of recognition modules upon binding target, which induce the enhancement of the signal response of AFP-based biosensors. Additionally, in the single AFP-based biosensors, the receptor proteins could be placed in the vicinity of the residues that would critically affect the photochemical property of the chromophore in AFP, like Ins(1,3,4,5)P_4 biosensor as described in the previous section, to detect the slight structural change of receptor proteins.[94] However, in spite of these efforts, optimization processes for constructions of AFP-based biosensors still require the construction of large scale of library and multi-step screening.[100] To utilize the AFP-based biosensors more widely, development of a general construction strategy using smaller library and less step screening in the case of less structural information of receptor proteins are required.

1. 6. Aim of this research

In this thesis, two new strategies related to the application of AFP-based biosensors for investigating the signal transduction were developed.

Firstly, the putative structural change of TRPC5 upon reaction to NO was detected with utilizing the detection mechanism of AFP-based biosensors. In the proposed NO-

sensing mechanism, TRPC5 is proposed to stabilize the open state by forming the disulfide bond between Cys558 and S-nitrosylated Cys553, located at the N-terminal side of pore-forming region. While the three-dimensional structure of TRPC5 has been reported by the cryo-EM analysis[36], dynamic structural changes at the NO-sensing domain in response to NO through the S-nitrosylation and the disulfide bond formation remain to be investigated. In this thesis, a partial NO-sensing segment of TRPC5 containing two cysteine residues, Cys553 and Cys558, was embedded into a near chromophore of AFP, termed as EGFP-TRPC5, to evaluate its structural changes in response to NO. Fluorescence response and the contents of the free thiol group of EGFP-TRPC5 upon reaction to NO were evaluated to investigate.

Secondly, a facile screening strategy for construction of the single AFP-based biosensors was tried to be developed. NO biosensor could be constructed with the optimization of a slight signal response of EGFP-TRPC5 with the disulfide bond formation upon reaction with NO. One of the strategies to efficiently transduce the structural change upon disulfide bond formation to the EGFP chromophore is deletion of amino acid residues of NO-sensing segment. However, even the simplest one by one deletion of amino acid residues from the N- and/or the C-terminal provided 47 mutants as the candidates of deletion mutants. Therefore, before the *in vitro* evaluation of 47 mutants, a degree of structural change of each mutant was estimated as a RMSD value based on *in silico* simulation. Three NO sensor candidates obtained from a two-step screening, *in silico* screening as first screening and *in vitro* screening as second screening, were further investigated to confirm whether these candidates could work as the NO sensor with *in vitro* and *in vivo* measurements.

These methods developed in this thesis with application of AFP-based biosensors could promote to explore the functions of the biomolecules and proteins in the signal transduction to utilize the bioenergy in the cells.

1. 7. References

1. Raheem A, Prinsen P, Vuppaladadiyam AK, Zhao M, Luque R. A review on sustainable microalgae based biofuel and bioenergy production: Recent development. J. Clean. Prod. 2018;181:42-59.
2. Chia SR, Ong HC, Chew KW, Show PL, Phang SM, Ling TC, Nagarajan D, Lee DJ, Chang JS. Sustainable approaches for algae utilisation in bioenergy production. Renew. Energy 2018;129:838-852.
3. Godfray HCJ, Beddington JR, Crute IR, Haddad L, Lawrence D, Muir JF, Pretty J, Robinson S, Thomas SM, Toulmi C. Food security: the challenge of feeding 9 billion people. Science 2010; 327:812-818.
4. Goli A, Shamiri A, Talaiekhozani A, Eshtiaghi N, Aghamohammadi N, Aroua, MK. An overview of biological processes and their potential for CO_2 capture. J. Environ. Manage. 2016;183:41-58.
5. Sipilä K, Johansson A, Saviharju K. Can fuel-based energy production meet the challenge of fighting global warming - a chance for biomass and cogeneration? Bioresour. Technol. 1993;43:7-12.
6. Yuan JS, Tiller KH, Al-Ahmad H, Stewart NR, Stewart CN. Plants to power: bioenergy to fuel the future. Trend Plant Sci. 2008;13:421-429.
7. Eckert C, Xu W, Xiong W, Lynch S, Ungerer J, Tao L, Gill R, Maness PC, Yu J. Ethylene-forming enzyme and bioethylene production. Biotechnol. Biofuels. 2014;7:33.
8. Nobles DR, Brown RM. Transgenic expression of Gluconacetobacter xylinus strain ATCC 53582 cellulose synthase genes in the cyanobacterium Synechococcus leopoliensis strain UTCC 100. Cellulose 2008;15:691-701.
9. Berridge MJ. Rapid accumulation of inositol trisphosphate reveals that agonists hydrolyse polyphosphoinositides instead of phosphatidylinositol. Biochem. J. 1983; 212:849-858.
10. Berridge MJ. Inositol trisphosphate and diacylglycerol as second messengers. Biochem. J. 1984; 220:345-360.
11. Choi KY, Kim HK, Lee SY, Moon KH, Sim SS, Kim JW, Chung HK, Rhee SG. Molecular cloning and expression of a complementary DNA for inositol 1,4,5-trisphosphate 3-kinase. Science 1990;248:64-66.

12. Dewaste V, Roymans D, Moreau C, Erneux C. Cloning and expression of a full-length cDNA encoding human inositol 1,4,5-trisphosphate 3-kinase B. Biochem. Biophys. Res. Commun. 2002;291:400-405.
13. Nalaskowski MM, Bertsch U, Fanick W, Stockebrand MC Schmale H. Mayr GW. Rat inositol 1,4,5-trisphosphate 3-kinase C is enzymatically specialized for basal cellular inositol trisphosphate phosphorylation and shuttles actively between nucleus and cytoplasm. J. Biol. Chem. 2003;278:19765-19776.
14. Windhorst S, Song K, Gazdar AF. Inositol-1,4,5-trisphosphate 3-kinase-A (ITPKA) is frequently over-expressed and functions as an oncogene in several tumor types. Biochem. Pharmacol. 2017;137:1-9.
15. Irvine RF, McNulty TJ, Schell MJ. Inositol 1,3,4,5-tetrakisphosphate as a second messenger–a special role in neurones? Chem. Phys. Lipids 1999;98:49-57.
16. Schurmans S, Pouillon V, Maréchal Y. Regulation of B cell survival, development and function by inositol 1,4,5-trisphosphate 3-kinase B (Itpkb). Adv. Enzyme Regul. 2011;51:66-73.
17. Loscalzo J, Welch G. Nitric Oxide and Its Role in the Cardiovascular System. Prog. Cardiovasc. Dis. 1995;38 87-104.
18. Lei J, Vodovotz Y, Tzeng E, Billiar TR. Nitric oxide, a protective molecule in the cardiovascular system, Nitric Oxide. 2013;35:175-185.
19. Bradley SA, Steinert JR. Nitric Oxide-Mediated Posttranslational Modifications: Impacts at the Synapse. Oxid. Med. Cell. Longevity. 2016;2016:5681036.
20. Steinert JR, Robinson SW, Tong H, Haustein MD, Kopp-Scheinpflug C, Forsythe LD. Nitic Oxide Is an Activity-Dependent Regulator of Target Neuron Intrinsic Excitability. Neuron. 2011;71:291-305.
21. Hirst DG, Robson T. Nitric oxide physiology and pathology. Methods Mol. Biol. 2011;704:1-13.
22. Xu W, Liu LZ, Loizidou M, Ahmed M, Charles IG. The role of nitric oxide in cancer. Cell Res. 2002;12:311-320.
23. Wendehenne D, Durner J, Klessig DF. Nitric Oxide: a new player in plat signaling and defense responses. Curr. Opin. Plant Biol. 2004;7:449-455.
24. Horenberg AL, Houghton AM, Pandey S, Seshadri V, Guilford WH. S-nitrosylation of cytoskeletal proteins. Cytoskeleton. 2019;76:243-252.

25. Wendehenne D, Pugin A, Klessig D, Durner J. Nitric oxide: comparative synthesis and signaling in animal and plant cells. Trends Plant Sci. 2001;6:177-183.
26. Alderton WK, Cooper CE, Knowles RG. Nitric oxide synthases: structure, function and inhibition. Biochem. J. 2001;357:593-615.
27. Hess DT, Matsumoto A, Kim SO, Marshall HE, Stamler JS. Protein S-nitrosylation: purview and parameters. Nat. Rev. Mol. Cell Biol. 2005;6:150-166.
28. Johnson DC, Dean DR, Smith AD, Johnson MK. STRUCTURE, FUNCTION, AND FORMATION OF BIOLOGICAL IRON-SULFUR CLUSTERS. Annu. Rev. Biochem. 2005;74:247-281.
29. Radi R. Reaction of Nitric Oxide with Metalloproteins. Chem. Res. Toxicol. 1996;9:828-835.
30. Serrano PN, Wang H, Crack JC, Prior C, Hutchings MI, Thomson AJ, Kamali S, Yoda Y, Zhao J, Hu MY, Alp EE, Oganesyan VS, Le Brun NE. Nitrosylation of Nitiric-Oxide-Sensing Regulatory Proteins Containing [4Fe-4S] Clusters Gives Rise to Multiple Iron-Nitrosyl Complexes. Angew. Chem. Int. Ed. 2016;55:14575-14579.
31. Gonzalez-Cobos JC, Trebak M. TRPC channels in smooth muscle cells. Front Biosci., Landmark Ed. 2010;15:1023-1039.
32. Zhang E, Liao P. Brain Transient Receptor Channels and Stroke. J. Neurosci. Res. 2015;93:1165-1183.
33. Gees M, Colsoul B, Nilius B. The Role of Transient Receptor Potential Cation Channels in Ca^{2+} Signaling. Cold Spring Harbor Perspect. Biol. 2010;2:a003962.
34. Vazquez G, Wedel B. J, Aziz O, Trebak M, Putney JW. The mammalian TRPC cation channels. Biochim. Biophys. Acta. 2004;1742:21-36.
35. Montell C. Drosophia TRP channels. Pflueg. Arch. Eur. J. Physiol. 2005;451:19-28.
36. Duan J, Li J, Chen GL, Ge Y, Liu J, Xie K, Peng X, Zhou W, Zhong J, Zhang Y, Xu J, Xue C, Liang B, Zhu L, Liu W, Zhang C, Tian XL, Wang J, Clapham DE, Zeng B, Li Z, Zhang J. Cryo-EM structure of TRPC5 at 2.8-Å resolution reveals unique and conserved structural elements essential for channel function. Sci. Adv. 2019;5:eaaw7935.
37. Yoshida T, Inoue R, Morii T, Takahashi N, Yamamoto S, Hara Y, Tominaga M, Shimizu S, Sato Y, Mori Y. Nitric oxide activates TRP channels by cysteine S-nitrosylation. Nat. Chem. Biol. 2006;2:596-607.

38. Nakata E, Liew FF, Nakano S, Morii T. Recent progress in the constructin methodology of fluorescent biosensors based on biomolecules. Biosensors-Emerging materials and Applications. Serra, P. A. Ed. pp. 123-140 (2011).
39. Thevenot DR, Toth K, Durst RA, Wilson GS. Electrochemical biosensors: recommended definitions and classification. J. Biosci. Bioeng. 2001;16:121-131.
40. Jelinek R, Kolusheva S. Carbohydrate biosensors. Chem. Rev. 2004;104:5987-6015.
41. Borisov SM, Wolfbeis OS. Optical Biosensors. Chem. Rev. 2008;108:423-461.
42. Wang H, Nakata E, Hamachi I. Recent Progress in Strategies for the Creation of Protein-Based Fluorescent Biosensors. Chembiochem 2009;10:2560-2577.
43. Giepmans BN, Adams SR, Ellisman MH, Tsien RY. The Fluorescent Toolbox for Assessing Protein Location and Function. Science 2006;312:217-224.
44. Johnsson N, Johnsson K. Chemical Tools for Biomolecular Imaging. ACS Chem. Biol. 2007;2:31-38.
45. Rao J, Dragulescu-Andrasi A, Yao H. Fluorescence Imaging *in vivo*: Recent Advances. Curr. Opin. Biotechnol. 2007;18:17-25.
46. Johnsson K. Visualizing Biochemical Activities in Living Cells. Nat. Chem. Biol. 2009;5:63-65.
47. Wang H, Nakata E, Hamachi I. Recent Progress in Strategies for the Creation of Protein-Based Fluorescent Biosensors. ChemBioChem 2009;10:2560-2577
48. de Silva AP, Gunaratne HQ, Gunnlaugsson T, Huxley AJ, McCoy CP, Rademacher JT, Rice TE. Signaling Recognition Events with Fluorescent Sensors and Switches. Chem. Rev. 1997;97:1515-1566.
49. Johnson I. Fluorescent Probes for Living Cells. Histochem. J. 1998;30:123-140.
50. Terai T, Nagano T. Fluorescent Probes for Bioimaging Applications. Curr. Opin. Chem. Biol. 2008;12:515-521.
51. Domaille DW, Que EL, Chang CJ. Synthetic Fluorescent Sensors for Studying the Cell Biology of Metals. Nat. Chem. Biol. 2008;4:168-175.
52. Cao H, Heagy MD. Fluorescent Chemosensors for Carbohydrates: a Decade's Worth of Bright Spies for Saccharides in Review. J. Fluoresc. 2004;14:569-584.
53. Gomes A, Fernandes E, Lima JL. Use of Fluorescence Probes for Detection of Reactive Nitrogen Species: a Review. J. Fluoresc. 2006;16:119-139.
54. Soh N. Recent Advances in Fluorescent Probes for the Detection of Reactive Oxygen Species. Anal. Bioanal. Chem. 2006;386:532-543.

55. Nolan EM, Lippard SJ. Small-Molecule Fluorescent Sensors for Investigating Zinc Metalloneurochemistry. Acc. Chem. Res. 2009;42:193-203.
56. Liu J, Cao Z, Lu Y. Functional Nucleic Acid Sensors. Chem. Rev. 2009;109:1948-1998.
57. Tainaka K, Sakaguchi R, Hayashi H, Nakano S, Liew FF, Morii T. Design Strategies of Fluorescent Biosensors Based on Biological macromolecular Receptors. Sensors 2010;10:1355-1376.
58. Marvin JS, Corcoran EE, Hattangadi NA, Zhang JV, Gere SA, Hellinga HW. The Rational Design of Allosteric Interactions in a Monomeric Protein and Its Applications to the Construction of Biosensors. Proc. Natl. Acad. Sci. USA 1997; 94:4366-4371.
59. Marvin JS, Hellinga HW. Engineering Biosensors by Introducing Fluorescent Allosteric Signal Transducers: Construction of a Novel Glucose Sensor. J. Am. Chem. Soc. 1998;120:7-11.
60. de Lorimier RM, Smith JJ, Dwyer MA, Looger LL, Sali KM, Paavola C., Rizk SS, Sadigov S, Conrad DW, Loew L, Hellinga HW. Construction of a Fluorescent Biosensor Family. Protein Sci. 2002;11:2655-2675
61. Morii T, Sugimoto K, Makino K, Otsuka M, Imoto K, Mori Y. A New Fluorescent Biosensor for Inositol Trisphosphate. J. Am. Chem. Soc. 2002;124:1138-1139.
62. Sakaguchi R, Tainaka K, Shimada N, Nakano S, Inoue M, Kiyonaka S, Mori Y, Morii T. An *in vivo* Fluorescent Sensor Reveals Intracellular Ins(1,3,4,5)P_4 Dynamics in Single Cells. Angew. Chem. Int. Ed. 2009;49:2150-2153.
63. Marrero MB, Schieffer B, Paxton WG, Schieffer E, Bernstein KE. Electroporation of $pp60^{c\text{-}src}$ Antibodies Inhibits the Angiotensin II Activation of Phospholipase C-γ1 in Rat Aortic Smooth Muscle Cells. J. Biol. Chem. 1995;270:15734-15738.
64. Fenton M, Bone N, Sinclair AJ. The Efficient and Rapid Import of a Peptide into Primary B and T Lymphocytes and a Lymphoblastoid Cell Line. J. Immunol. Methods 1998;212:41-48.
65. Sakaguchi R, Tainaka K, Shimada N, Nakano S, Inoue M, Kiyonaka S, Mori Y, Morii T. An in Vivo Fluorescent Sensor Reveals Intracellular Ins(1,3,4,5)P_4 Dynamics in Single Cells. Angew. Chem., Int. Ed. 2010;49:2150-2153.

66. Zelphati O, Wang Y, Kitada S, Reed JC, Felgner PL, Corbeil J. Intracellular Delivery of Proteins with a New Lipid-Mediated Delivery System. J. Biol. Chem. 2001;276:35103-35110.
67. Zheng X, Lundberg M, Karlsson A, Johansson M. Lipid-Mediated Protein Delivery of Suicide Nucleoside Kinases. Cancer Res. 2003;63:6909-6913.
68. Abarzua P, LoSardo JE, Gubler ML, Neri A. Microinjection of MonoclonalAntibody PAb421 into Human SW480 Colorectal Carcinoma Cells Restores the Transcription Activation Function to Mutant p53. Cancer Res. 1995;55:3490-3494.
69. Wadia JS, Dowdy SF. Transmembrane Delivery of Protein and Peptide Drugs by TAT-Mediated Transduction in the Treatment of Cancer. Adv. Drug. Deliv. Rev. 2005;57:579-596.
70. Sugimoto K, Nishida M, Otsuka M, Makino K, Ohkubo K, Mori Y, Morii T. Novel Real-Time Sensors to Quantitatively Assess in Vivo Inositol 1,4,5-Trisphosphate Production in Intact. Cells. Chem. Biol. 2004;11:475-485.
71. Shimomura O, Johnson FH, Saiga Y. Extraction, Purification and Properties of Aequorin, a Bioluminescent Protein from the Luminous Hydromedusan, Aequorea. J. Cell Comp. Physiol. 1962;59:223-239.
72. Sapsford KE, Berti L, Medintz IL. Materials for Fluorescence Resonance Energy Transfer Analysis: Beyond Traditional Donor-Acceptor Combinations. Angew. Chem. Int. Ed. 2006;45:4562-4589.
73. Piston DW, Kremers GJ. Fluorescent Protein FRET: The Good, the Bad and the Ugly. Trends Biochem. Sci. 2007;32:407-414.
74. Mahajan NP, Harrison-Shostak DC, Michaux J, Herman B. Novel mutant green fluorescent protein protease substrates reveal the activation of specific caspases during apoptosis. Chem. Biol. 1999;6:401-409.
75. Luo KQ, Yu VC, Pu Y, Chang DC. Application of the fluorescence resonance energy transfer method for studying the dynamics of caspase-3 activation during UV-induced apoptosis in living HeLa cells. Biochem. Biophys. Res. Commun. 2001; 283:1054-1060.
76. Rehm M, Dussmann H, Janicke RU, Tavare JM, Kogel D, Prehn JH. Single-cell fluorescence resonance energy transfer analysis demonstrates that caspase activation during apoptosis is a rapid process. Role of caspase-3. J Biol. Chem. 2002; 277:24506-24514.

77. Ai HW, Hazelwood KL, Davidson MW, Campbell RE. Fluorescent protein FRET pairs for ratiometric imaging of dual biosensors. Nat. Methods 2008;5:401-403.
78. Sato M, Ozawa T, Inukai K, Asano T. Umezawa Y. Fluorescent Indicators for Imaging Protein Phosphorylation in Single Living Cells. Nature Biotechnol. 2002;20:287-294.
79. Nagai Y, Miyazaki M, Aoki R, Zama T, Inoue S, Hirose K, Iino M, Hagiwara M. A fluorescent indicator for visualizing cAMP-induced phosphorylation in vivo. Nat. Biotechnol. 2000;18:313-316.
80. Newman RH, Zhang J. Visualization of phosphatase activity in living cells with a FRET-based calcineurin activity sensor. Mol. BioSyst. 2008;4:496-501.
81. Miyawaki A, Llopis J, Heim R, McCaffery JM, Adams JA, Ikura M, Tsien RY. Fluorescent Indicators for Ca^{2+} Based on Green Fluorescent Proteins and Calmodulin. Nature 1997;388:882-887.
82. Romoser VA, Hinkle PM, Persechini A. Detection in Living Cells of Ca^{2+}-Dependent Changes in the Fluorescence Emission of an Indicator Composed of Two Green Fluorescent Protein Variants Linked by a Calmodulin-Binding Sequence. A New Class of Fluorescent Indicators. J. Biol. Chem. 1997;272:13270-13274.
83. Nikolaev V, Bunemann OM, Hein L, Hannawacker A, Lohse MJ. Novel Single Chain cAMP Sensors for Receptor-induced Signal Propagation. J. Biol. Chem. 2004;279:37215-37218.
84. Sato M, Hida N, Ozawa T, Umezawa Y. Fluorescent Indicators for Cyclic GMP Based on Cyclic GMP-Dependent Protein Kinase Iα and Green Fluorescent Proteins. Anal. Chem. 2000;72:5918-5924.
85. Sato M, Ueada Y, Shibuya M, Umezawa Y. Locating Inositol 1,4,5-trisphosphate in the Nucleus and Neuronal Dendrites with Genetically Encoded Fluorescent Indicators. Anal. Chem. 2005;77:4751-4758.
86. Ohashi T, Galiacy SD, Briscoe G, Erickson HP. Experimental Study of GFP Based FRET, with Application to Intrinsically Unstructured Proteins. Protein Sci. 2007;16:1429-1438.
87. Crivici A, Ikura M. Molecular and structural basis of target recognition by calmodulin. Annu. Rev. Biophys. Biomol. Struct. 1995;24:85-116.

88. Ikura M, Clore GM, Gronenborn AM, Zhu G, Klee CB, Bax A. Solution structure of a calmodulin-target peptide complex by multidimensional NMR. Science. 1992;256:632-638.
89. Nakai J, Ohkura M, Imoto K. A High Signal-to-Noise Ca^{2+} Probe Composed of a Single Green Fluorescent Protein. Nat. Biotechnol. 2001;19:137-141.
90. Souslova EA, Belousov VV, Lock JG, Stromblad S, Kasparov S, Bolshakov AP, Pinelis VG, Labas YA, Lukyanov S, Mayr LM, Chudakov DM. Single Fluorescent Protein-Based Ca^{2+} Sensors with Increased Dynamic Range. BMC Biotechnol. 2007;7:37.
91. Baird GS, Zacharias DA, Tsien RY. Circular Permutation and Receptor Insertion within Green Fluorescent Proteins. Proc. Natl. Acad. Sci. USA 1999;96:11241-11246.
92. Nagai T, Sawano A, Park ES, Miyawaki A. Circularly Permuted Green Fluorescent Proteins Engineered to Sense Ca^{2+}. Proc Natl. Acad. Sci. USA 2001;98:3197-3202.
93. Nausch LW, Ledoux J, Bonev AD, Nelson MT, Dostmann WR. Differential Patterning of cGMP in Vascular Smooth Muscle Cells Revealed by Single GFP-Linked Biosensors. Proc. Natl. Acad. Sci. USA 2008;105:365-370.
94. Belousov VV, Fradkov AF, Lukyanov KA, Staroverov DB, Shakhbazov KS, Terskikh AV, Lukyanov S. Genetically Encoded Fluorescent Indicator for Intracellular Hydrogen Peroxide. Nat. Methods 2006;3:281-286.
95. Dooley CT, Dore TM, Hanson GT, Jackson WC, Remington SJ, Tsien RY. Imaging Dynamic Redox Changes in Mammalian Cells with Green Fluorescent Protein Indicators. J. Biol. Chem. 2004;279:22284-22293.
96. Mizuno T, Murao K, Tanabe Y, Oda M, Tanaka T. Metal-Ion-Dependent GFP Emission in vivo by Combining a Circularly Permutated Green Fluorescent Protein with an Engineered Metal-Ion-Binding Coiled-Coil. J. Am. Chem. Soc. 2007;129:11378-11383.
97. Sakaguchi R, Endoh T, Yamamoto S, Tainaka K, Sugimoto K, Fujieda N, Kiyonaka S, Mori Y, Morii T. A Single Circularly Permuted GFP Sensor for Inositol-1,3,4,5-Tetrakisphosphate Based on a Split PH Domain. Bioorg. Med. Chem. 2009;17:7381-7386.
98. Akerboom J, Rivera JDV, Guilbe MMR, Malavé ECA, Hernandez HH, Tian L, Hires SA, Marvin JS, Looger LL, Schreiter E.R. Crystal Structures of the GCaMP

Calcium Sensor Reveal the Mechanism of Fluorescence Signal Change and Aid Rational Design. J. Biol. Chem. 2009;284:6455-6464.

99. Berg J, Hung YP, Yellen G. A genetically encoded fluorescent reporter of ATP:ADP ratio. Nat. Methods. 2009;6:161-166.
100. Kitaguchi T, Oya M, Wada Y, Tsuboi T, Miyawaki A. Extracellular calcium influx activates adenylate cyclase 1 and potentiates insulin secretion in MIN6 cells. Biochem. J. 2013;450:365-373.
101. Qin Y, Sammond DW, Braselmann E, Carpenter MC, Palmer AM. Development of an Optical Zn^{2+} Probe Based on a Single Fluorescent protein. ACS Chem. Biol. 2016;11:2744-275.
102. Matsuda S, Harada K, Ito M, Takizawa M, Wongso D, Tsuboi T, Kitaguchi T. Generation of cGMP indicator with an Expanded Dynamic Range by Optimization of Amino Acid Linkers between a Fluorescent Protein and PDE5α. ACS Sens. 2017;2:46-51.

Chapter 2
Fluorescence detection of the nitric oxide-induced structural change at the putative nitric oxide sensing segment of TRPC5

2. 1. Introduction

Structural changes of proteins are crucial factor for the activation of proteins concerned in the signal transduction. To explore the signal transduction, it is important to understand the structural change of proteins. Studies on the structure and function of TRPC5 channel provided a novel gating mechanism of the Ca^{2+} entry activated by cysteine S-nitrosylation.[1,2] A nonselective calcium-permeant cation channel TRPC5 is of considerable interest as a potential therapeutic target for progressive kidney disease, depression, anxiety, and other disorders.[3] TRPC5 promotes Ca^{2+} uptake upon S-nitrosylation and/or disulfide bond formation of specific cysteine residues, providing the NO-sensing function of TRPC5 channels.[1] Regulation of TRPC5 activity is highly specific to NO against other oxidants such as H_2O_2.[4] In the proposed NO-sensing mechanism of TRPC5, two cysteines, Cys553 and Cys558, located at the N-terminal side of pore-forming region are selectively modified by NO. The free thiol group of Cys558 nucleophilically attacks S-nitrosylated Cys553 to form a disulfide bond that stabilizes the open state. The modification of Cys553 and Cys558 would cause structural changes at the pore-forming region of TRPC5. While the three-dimensional structure has been reported by the cryo-EM analysis (Figure 2.1A)[5], dynamic structural changes at the NO-sensing domain in response to NO through the S-nitrosylation and the disulfide bond formation remain to be investigated.

An appropriate conjugation of a recognition or reaction module for a given molecule to a transducing module, such as an auto-fluorescent protein (AFP), couples the recognition/reaction event to fluorescence signal changes, as has been widely applied for the general design strategy of AFP-based fluorescent biosensors.[6-8] In the single AFP-based sensor, a reaction module is introduced near the chromophore of AFP. The conformational change induced at the reaction module upon the reaction with target molecule is subsequently transduced as the change in fluorescence emission of AFP.[9,10] Importantly, even subtle conformational changes of the reaction module were effectively transduced to measurable fluorescence changes by introducing the reactive module near the chromophore of AFP.[11] Therefore, single AFP-based biosensors were considered to be suitable for obtaining the information about structural change of proteins.

In this chapter, a structural change at the NO-sensing module of TRPC5 in response to the modification of cysteine residues by NO was investigated. To evaluate the NO-induced structural change of the NO-sensing module, a partial segment of the putative NO-sensing module of TRPC5 channel containing Cys553 and Cys558 residues was fused as a loop structure by means of structure-based design to EGFP. The resulting TRPC5 segment-fused EGFP, termed as EGFP-TRPC5, exerted measurable fluorescence emission changes in response to the NO concentration changes. The EGFP-TRPC5 showed the expected NO-induced disulfide bond formation. The disulfide bond formation, not the S-nitrosylation alone, was responsible for the ratiometric fluorescence intensity changes during the formation of NO. These results support the proposed model of TRPC5 activation by NO that the structural change is induced by disulfide bond formation. That the conformational change would be reversible in the presence and absence of NO.

2. 2. Results and discussions

2. 2. 1. Incorporation of the NO-sensing segment of TRPC5 to EGFP

TRPC5 is six-transmembrane protein which contains S1-S6 helices and pore helices between S5 and S6 helix in the transmembrane domain (Figure 2.1A). TRPC5 assembles into tetramers of which S5 and S6 helices of another monomer lie in the space

among S1-S4 helices and S5-pore-S6 helices to form a channel, of which S5-S6 helices and the pore region contribute to form the pore (Figure 2.1).[3,5]

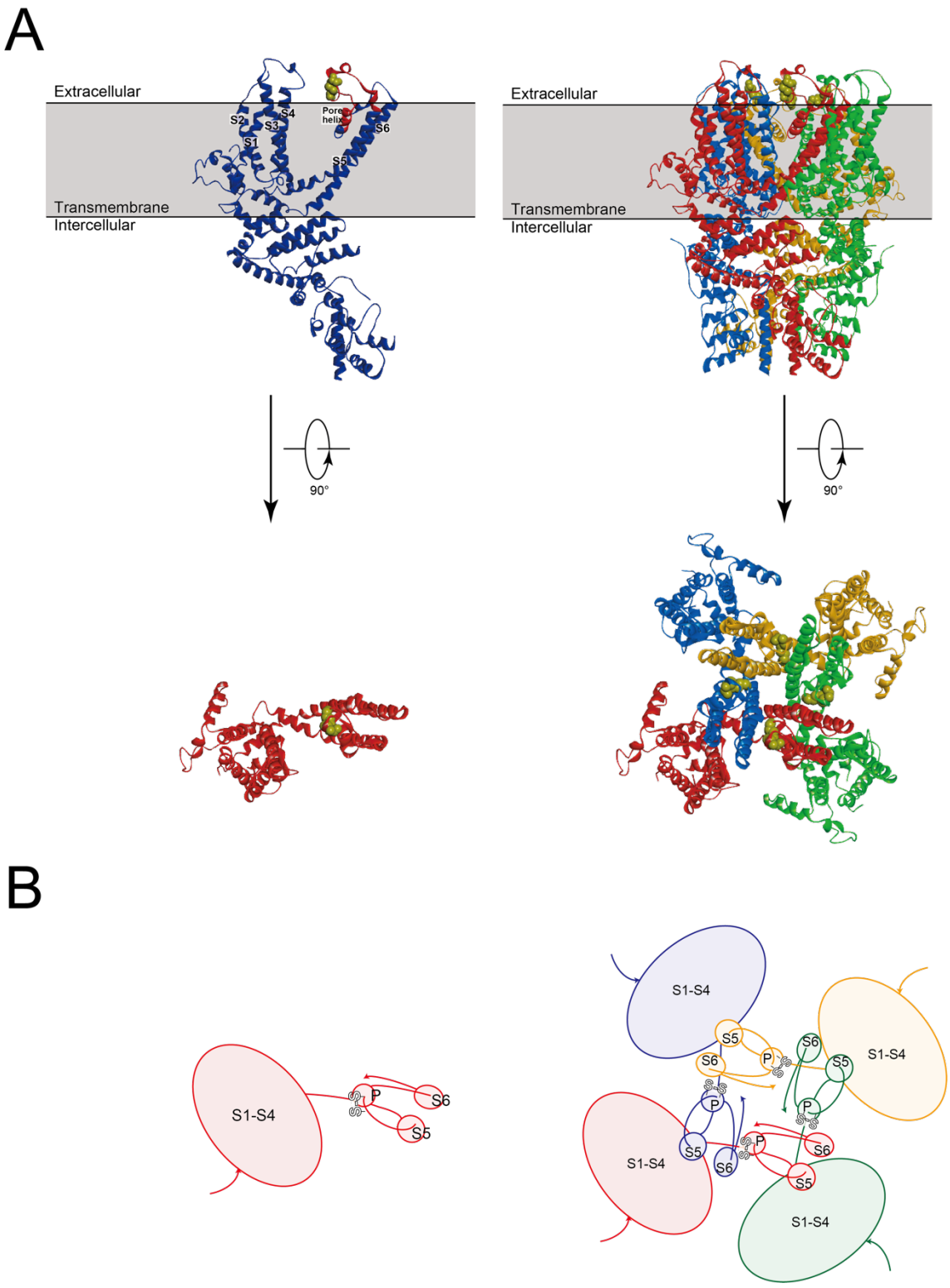

Figure 2.1. (A) A Cryo-EM structure of TRPC5 with the disulfide bond between Cys553 and Cys558 (PDB: 6AEI). Left: A monomer structure of TRPC5. TRPC5 is six-

transmembrane protein which contains S1-S6 helices and pore helices between S5 and S6 helix in the transmembrane domain. Right: homotetramer structure of TRPC5. Each monomer was shown in the red, blue, orange, and green, respectively. Side views, top view, and schematic picture on the top view were shown in the top, middle and blow. (B) Illustration of Cryo-EM structure of TRPC5 was shown. Each color indicate each monomer corresponding to each color in (A). S1-S4 helices were replaced into one circle for simplification. S5, S4, and pore helix were replaced into each circle. Lines indicated the coordinated arrangement of each helix.

In TRPC5, two cysteine residues, Cys553 and Cys558, locating between the S5 and S6 helices in the pore region, have been proposed as the NO reactive sites (Figure 2.1 and 2.2A).[1] Cys553 is S-nitrosylated by NO to open the pore region of TRPC5, followed by the attack of Cys558 to S-nitrosylated Cys553 to form a disulfide bond that stabilizes the open state of TRPC5 (Figure 2.2).[1] The region ranging from Leu568 to Leu575 consists of a part of pore helix and that from Leu538 to Tyr541 locates near the C-terminal end of S5 helix (Figure 2.2).[5] This segment Leu538 to Leu575 was adapted as an NO-reactive module to conjugate with EGFP (Figure 2.3B). Parent EGFP forms the β-barrel structure to incorporate the chromophore. The chromophore exists in the protonated or deprotonated form with each showing the absorption peak around 400 and 470 nm, respectively.[10-12] The equilibrium between these forms in the ground state is governed by hydrogen bond network that allows proton transfer between the chromophore and the side chains of neighboring amino acid residues. The configuration of Thr203 and His148 residues of EGFP against the chromophore likely shows the profound effect on the protonated or deprotonated state of chromophore.[10,13] To effectively transduce the conformational change in response to NO as the fluorescence change, the partial segment corresponding to the NO-reactive module of TRPC5, Leu538-Leu575, was introduced between Asn144 and Phe145 of EGFP, where a large structural perturbation to the chromophore was expected to effectively transduce the conformational change in response to NO to the fluorescence emission change (Figure 2.3).

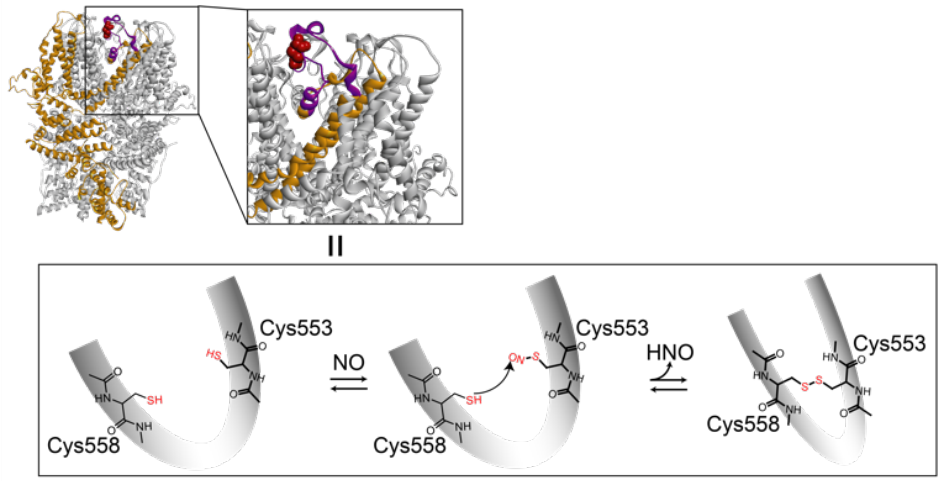

Figure 2.2. A cryo-EM structure of the TRPC5 homotetramer with the disulfide bond between Cys553 and Cys558 (upper, PDB ID: 6AEI) and NO-sensing mechanism of TRPC5.[5] One monomer of the TRPC5 homotetramer is represented in orange and the structural segment of TRPC5 Leu538-Leu575 embedded into EGFP is represented in purple. As the key residues, Cys553 and Cys558 are shown in CPK representation (red) with a zoomed up view. In the zoomed up view, the region locating between two helices S5 and S6 (in orange) contribute to form the pore structure. The amino acid residues ranging from Leu568 to Leu575 consist of a part of pore helix and Leu538 to Tyr541 locate near the C-terminal of S5 helix. The plausible reaction scheme of TRPC5 with NO is also represented (lower).[1,14,15]

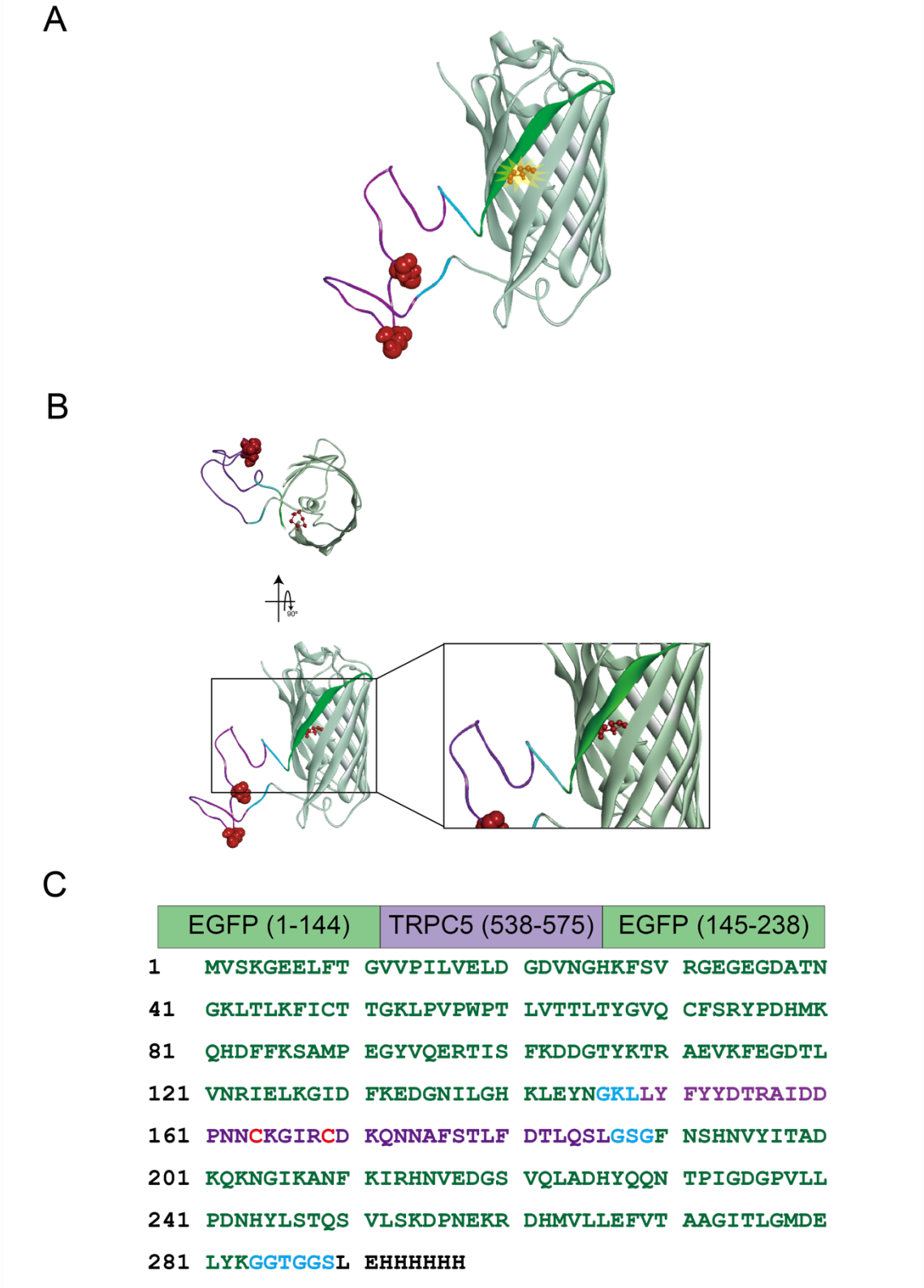

Figure 2.3. (A) A structural model of EGFP-TRPC5. The segment of TRPC5, from Leu538 to Leu575 (purple), was embedded into EGFP (green, PDB ID: 2B3P)[16] between Asn144 and Phe145 through linkers (blue). The chromophore of EGFP is represented by

ball and stick model (red). The segment of TRPC5 was introduced in the β-strand (dark green) locating in vicinity to the chromophore. The molecular model was constructed by using Discovery Studio (version 3.1, Accelrys Inc.). (B) The zoomed up view shows the TRPC5 segment introduced in the β-strand (dark green) located near the chromophore through the linker. (C) The partial segment of TRPC5 (Leu538-Leu575) was inserted between EGFP (upper) as indicated in the amino acid sequence (lower). Colors correspond to the highlighted segment in B (EGFP: green; linker: blue; a segment of TRPC5: purple; the cysteine residues in the TRPC5 segment: red).

2. 2. 2. Substitution of the cysteines in the parent EGFP

It should be noted that parent EGFP also contains two cysteine residues, Cys49 and Cys71, which would react with NO and to disturb the quantitation of the disulfide bond formation and the S-nitrosylation (Figure 2.3C). These two cysteine residues were mutated to non-cysteine amino acids as commonly applied in the previous reports[17-19], Cys49 was replaced with Ser49 (C49S) and Cys71 with Ser71 (C71S)[17], Met71 (C71M)[18], or Val71 (C71V)[19], respectively. The genes encoding three types of EGFP mutants (C49S/C71S, C49S/C71M, and C49S/C71V) appended with the structural segment of TRPC5 (L538-L575) and the parent EGFP with the structural segment of TRPC5 (L538-L575) were expressed in *Escherichia coli* (*E. coli*) (Figure 2.4A and B). The solubility and the fluorescence emission properties of the three mutants were compared with the parent EGFP with TRPC5 (L538-L575) in the *E. coli* cell lysate (Figure 2.4B). The soluble and insoluble fractions of cell lysate were separated by centrifugation and were analyzed by SDS-PAGE (Figure 2.4B and C). The fluorescence intensity of the bands corresponding to EGFP derivatives on the gel were analyzed by the fluorescence imager (Figure 2.4C). Among them, the C49S/C71V mutant showed a comparable solubility to the parent EGFP with TRPC5 (L538-L575) and a higher solubility compared to other two mutants, C49S/C71S and C49S/C71M. The C49S/C71V mutant also retained fluorescence emission property similar to the parent EGFP with TRPC5 (L538-L575). Other mutants, C49S/C71S and C49S/C71M, showed much smaller fluorescence intensity and lower solubility than the parent EGFP with TRPC5 (L538-L575). Therefore, the C49S/C71V mutant embedded with the structural segment TRPC5 (L538-L575), termed as EGFP-TRPC5, was used for further evaluation (Figure 2.5).

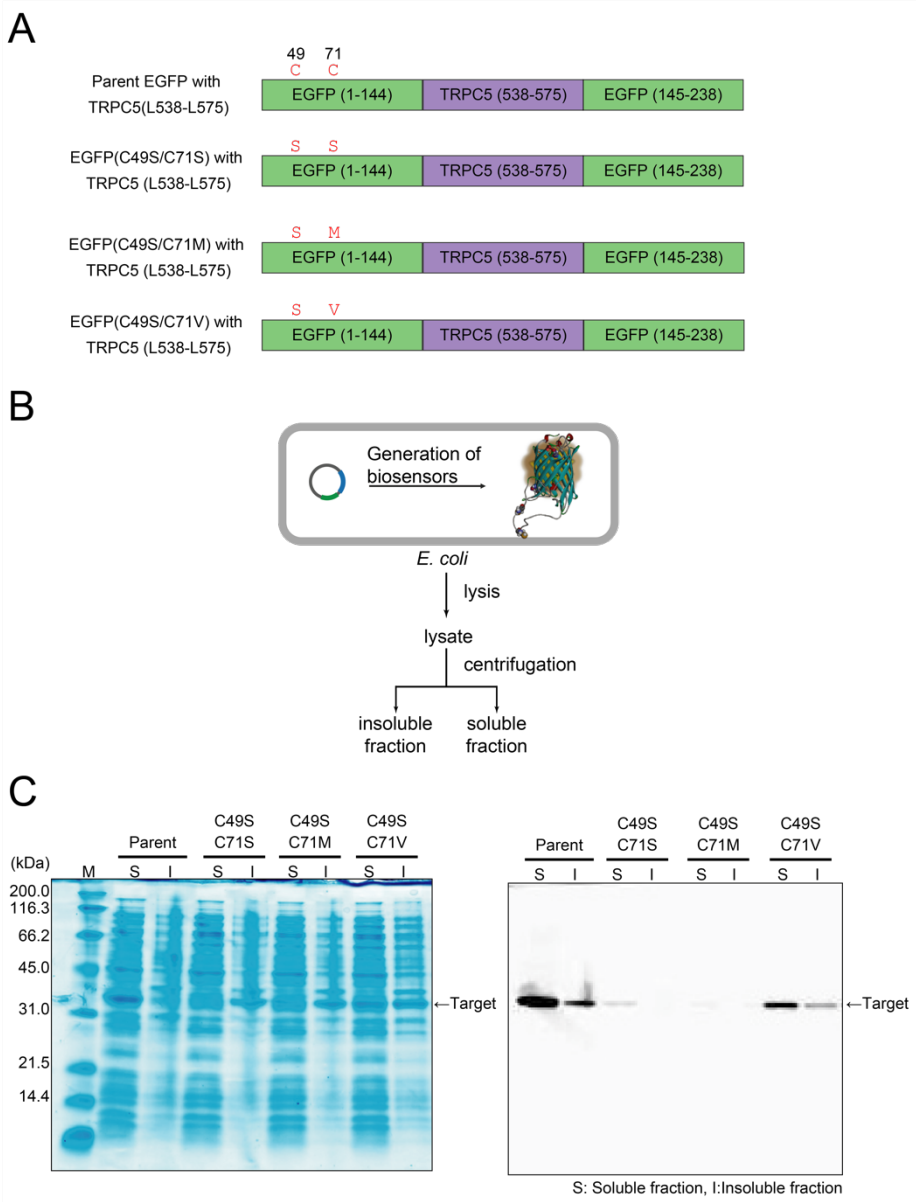

Figure 2.4. (A) An illustration of the EGFP derivatives fused to TRPC5 (L538-L575). (B) A scheme illustrates the procedure for comparing the solubility and the fluorescence properties of TRPC5 (L538-L575) fused EGFP derivatives in the *E. coli* lysate. The *E. coli* expressing each TRPC5 (L538-L575) fused EGFP derivative was lysed, and the lysate was centrifuged to separate the soluble and insoluble fractions. Each fraction was analyzed by means of SDS-PAGE and the fluorescence intensity of each band of TRPC5 (L538-L575) fused EGFP derivatives was analyzed by the fluorescence imager. (C) SDS-PAGE analysis of the soluble and insoluble fractions of each TRPC5 (L538-L575) fused EGFP derivatives (parent EGFP, C49S/C71S, C49S/C71M and C49S/C71V) in the lysate. The gel image was visualized by CBB (upper) or EGFP fluorescence (lower).

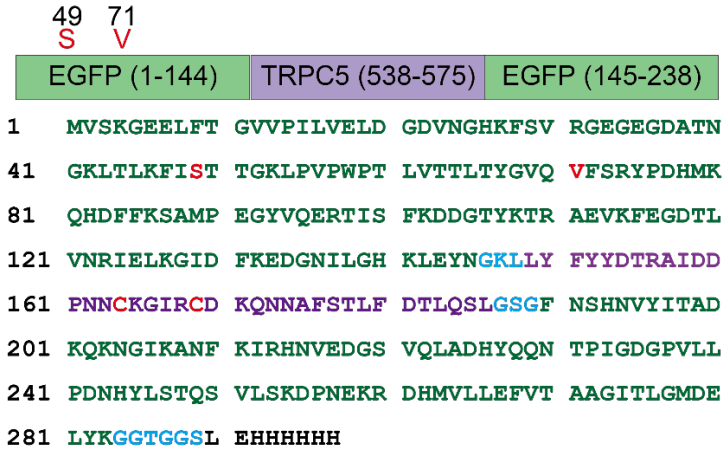

Figure 2.5. Illustration and amino acid sequence of EGFP-TRPC5. The partial segment of TRPC5 (Leu538-Leu575) was inserted into EGFP as indicated in the amino acid sequence. To prevent the pseudo-positive reaction to NO and perturbation of the quantitation of disulfide bond formation, C49 and C71 in EGFP were substituted to C49S and C71V, respectively, as indicated in the amino acid sequence.

2. 2. 3. Identification and the optical properties of EGFP-TRPC5

Further purification of EGFP-TRPC5 was conducted as described in the experimental section and the major band in SDS-PAGE corresponded to the calculated molecular weight of EGFP-TRPC5 (33,236) with the purity over 95% in SDS-PAGE (Figure 2.6 and 2.7A). The EGFP-TRPC5 was characterized by MALDI-TOF mass spectrometry as described in the experimental section. UV-Vis absorption spectrum of EGFP-TRPC5 indicated two absorption maxima around 395 nm and 490 nm (Figure 2.7B), corresponding to the protonated and deprotonated forms of the chromophore of EGFP, respectively.[10-12] Additionally, excitation spectrum of EGFP-TRPC5 at 509 nm (Figure 2.7C) showed two maxima around 395 nm (shoulder peak) and around 466 nm, which corresponded well to the two absorption maxima (Figure 2.7B). Emission spectra of EGFP- TRPC5 excited at 395 nm and 466 nm showed emission peak at 509 nm (Figure 2.7D).

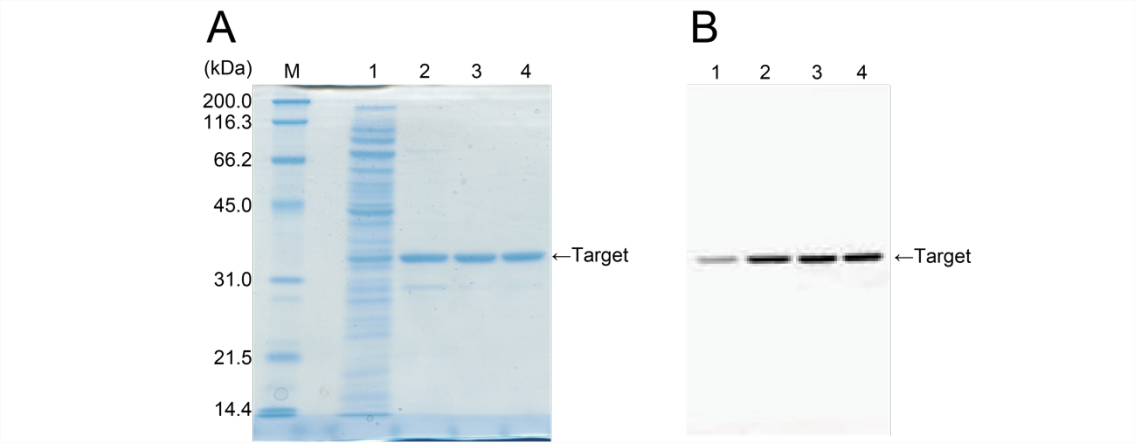

Figure 2.6. SDS-PAGE analysis of EGFP-TRPC5 at each purification step visualized by CBB (A) and fluorescence (B). M: protein marker (M.W. 6,500 -200,000), 1: soluble fraction of the *E. coli* lysate expressing EGFP-TRPC5, 2: after the His-tag affinity chromatography purification, 3: after the butyl column chromatography purification, 4: the stock solution in glycerol.

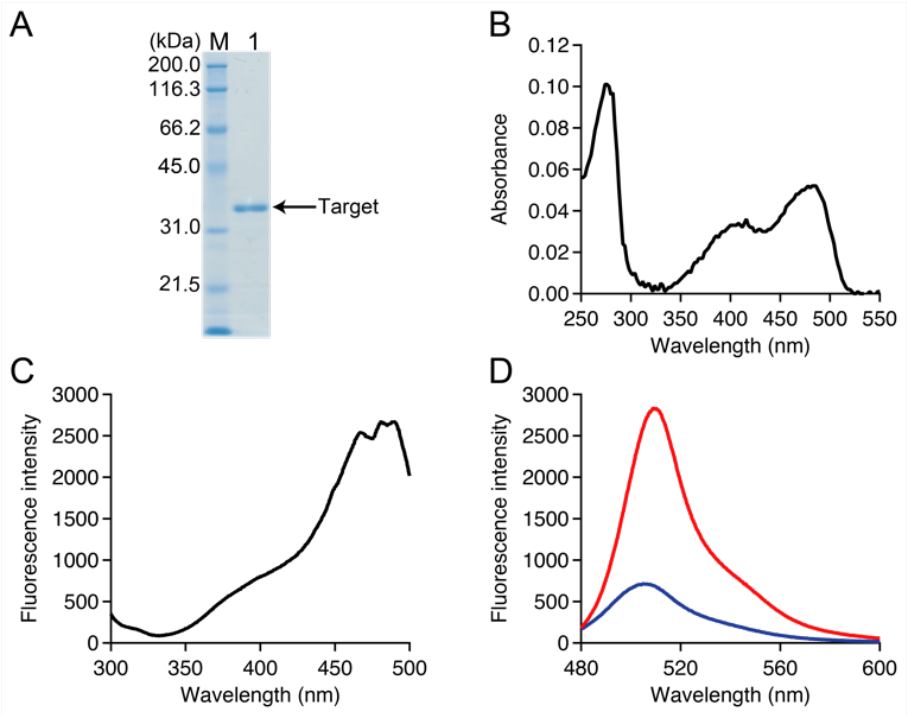

Figure 2.7. Gel electrophoretic and spectroscopic characterization of EGFP-TRPC5. (A) SDS-PAGE analysis of purified EGFP-TRPC5. M: marker (M.W. 6,500 - 200,000), lane 1: purified EGFP-TRPC5. An arrow indicates the main band with the expected molecular weight of 33,236. (B) UV-Vis absorption spectrum of EGFP-TRPC5. (C) Excitation

spectrum of EGFP-TRPC5 for the emission wavelength of 509 nm. (D) Emission spectra of EGFP-TRPC5 with excitation at 395 nm (blue) and 466 nm (red), respectively.

2. 2. 4. Fluorescence response of EGFP-TRPC5 upon the reduction of disulfide bond

The content of free thiol group in purified EGFP-TRPC5 evaluated by the conventional DTNB (5,5'-dithio-bis-(2-nitrobenzoic acid)) method (Figure 2.8) was less than 10% (Table 2.1 and Figure 2.9A), which indicated that most of the cysteine residue in purified EGFP-TRPC5 formed disulfide bond. After its reduction with dithiothreitol (DTT) followed by the removal of excess DTT by size exclusion chromatography, EGFP-TRPC5 in the reduced form contained 89% of free thiol group (Table 2.1 and Figure 2.9B).

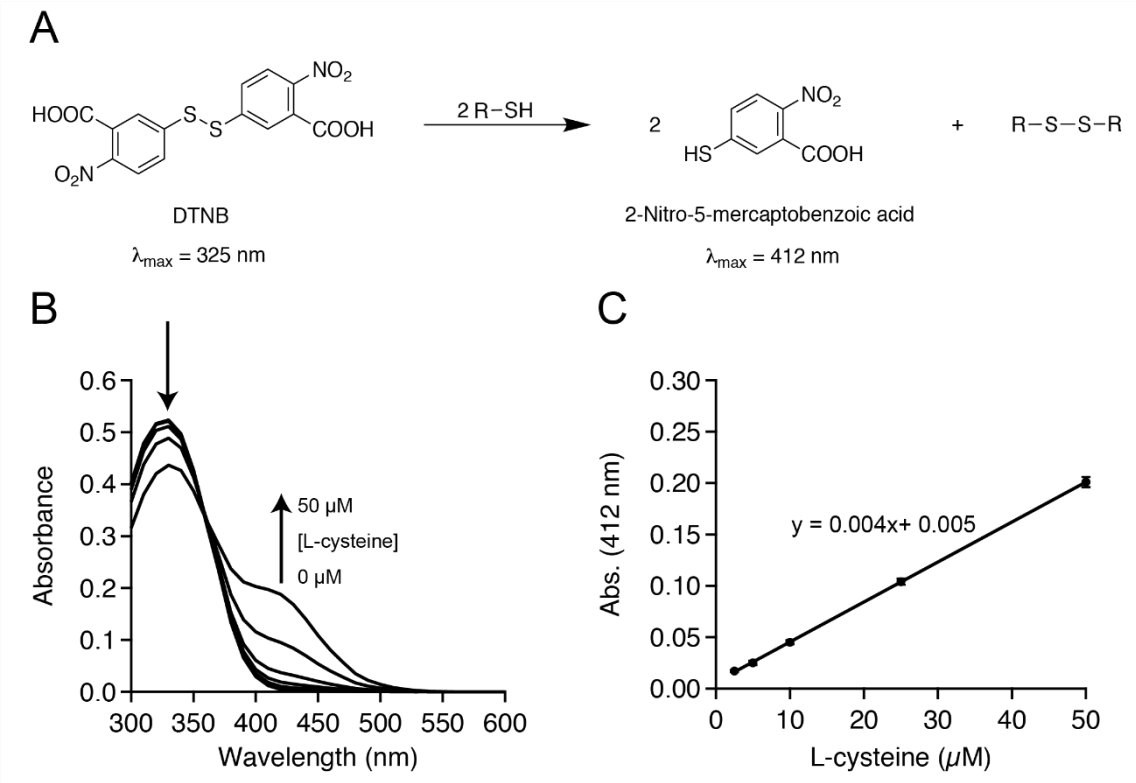

Figure 2.8. The DTNB method for quantitation of the free thiol group. (A) Reaction scheme of the DTNB method. DTNB was reduced by a free thiol group and then two molecules of 2-nitro-5-mercaptobenzoic acid (NTB) were produced. DTNB shows an absorption maximum at 325 nm and NTB shows maximum at 412 nm. (B) The absorption

spectral change of DTNB with increasing concentrations of L-cysteine (0, 2.5, 5, 10, 25, and 50 μM). (C) Calibration of the DTNB method by various L-cysteine concentrations (2.5, 5, 10, 25, and 50 μM). The detection limit of DTNB method was evaluated as 2.5 μM of L-cysteine in this condition.

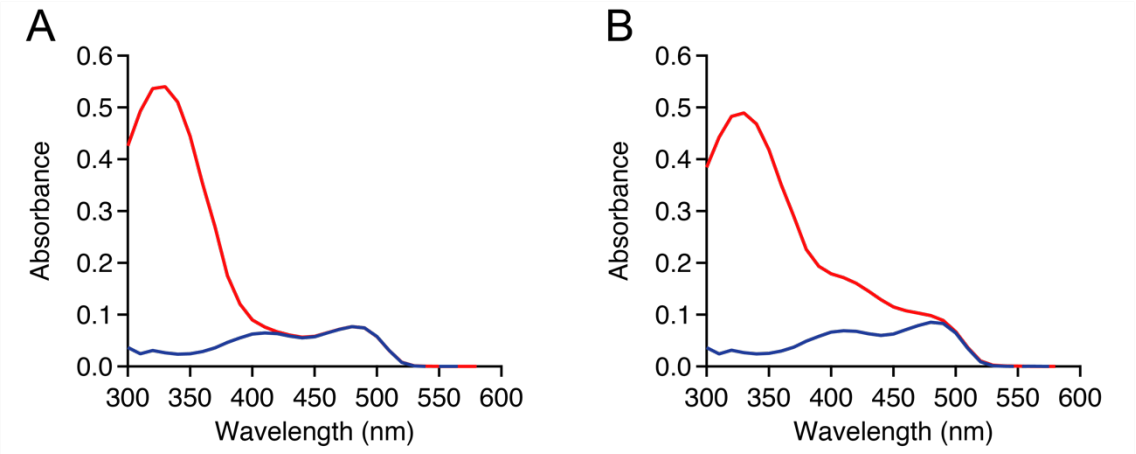

Figure 2.9. Absorption spectra of the DTNB reaction mixtures to quantitate the free thiol content of EGFP-TRPC5 (A) before or (B) after reduction with DTT (red line: EGFP-TRPC5 with DTNB; blue line: EGFP-TRPC5 without DTNB). To determine the absorption of 2-Nitro-5-mercaptobenzoic acid at 412 nm, the absorption of EGFP-TRPC5 itself was subtracted from that of EGFP-TRPC5 treated with DTNB at 412 nm.

Table 2.1. Change of the free thiol content upon disulfide bond cleavage

Conditions	Free thiol contents
Without DTT	< 10%
With 1 mM DTT	89%

The fluorescence emission change upon disulfide bond cleavage was analyzed by comparing the fluorescence spectra of EGFP-TRPC5 before and after the reduction with DTT. When excited at 395 nm, a measurable decrease in the emission intensity at 509 nm was observed for the reduced form of EGFP-TRPC5 as compared to that in the oxidized form (Figure 2.10A). The emission intensity at 509 nm slightly decreased for the reduced form of EGFP-TRPC5 when excited at 466 nm. The ratio for the emission intensity at 509 nm by excitation at 395 nm and 466 nm decreased from 0.248 to 0.230 upon the reduction of disulfide bond (Figure 2.10B). These results indicated that the conformation at the structural segment of TRPC5 was changed upon reduction of the disulfide bond cleavage. Further, the conformational change at the structural segment of TRPC5 could be quantitated as the ratiometric fluorescence response of EGFP.

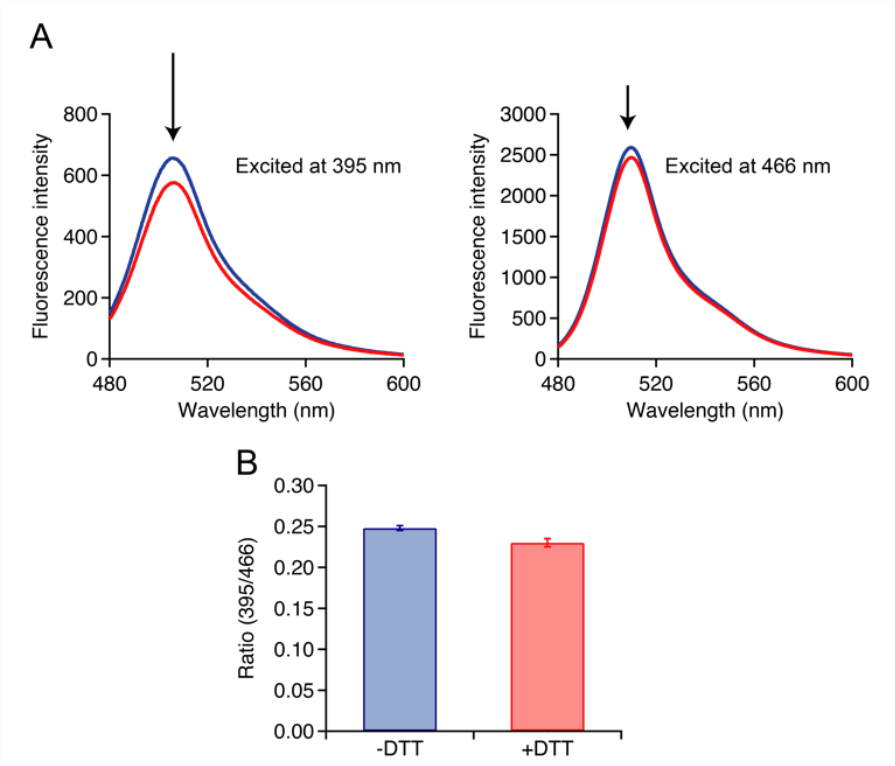

Figure 2.10. Reduction of the disulfide bond of EGFP-TRPC5 corresponding to the reverse process of NO-induced reaction with the cysteine residues. (A) Fluorescence spectra of EGFP-TRPC5 (left: excited at 395 nm, right: excited at 466 nm) in the oxidized form (blue) and reduced form (red). (B) Changes in the emission intensity ratio of fluorescence emission spectra of EGFP-TRPC5 (509 nm) excited at 395 nm versus at 466 nm for the oxidized (–DTT) and the reduced (+DTT) forms. The emission intensity ratios

(Ratio (395/466)) were calculated by dividing fluorescence intensity at 509 nm when excited at 395 nm by fluorescence intensity at 509 nm when excited at 466 nm.

2. 2. 5. Fluorescence responses of EGFP-TRPC5 to NO

In order to evaluate the response of TRPC5 segment to NO, EGFP-TRPC5 was treated with DTT, then purified by size exclusion chromatography. The free thiol content of reduced EGFP-TRPC5 was determined to be 93% by the DTNB method (Table 2.2). The reduced EGFP-TRPC5 was reacted with 1-Hydroxy-2-oxo-3-(N-methyl-3-aminopropyl)-3-methyl-1-triazene (NOC7) as the NO donor[20], which releases two NO with a half-life of 2.4 min in the reaction condition (Figure 2.11). The emission intensity ratio of the reduced EGFP-TRPC5 was lower than that of the non-reduced form (Figure 2.13). In the presence of NOC7 (500 μM), the ratio of fluorescence emission intensity for reduced EGFP-TRPC5 increased (Figure 2.13, line in red) from 0.183 to 0.188 to the value of non-reduced EGFP-TRPC5 (Figure 2.13, line in black) within 30 min. On the other hand, the ratio did not change significantly (within ± 0.001) in the absence of NOC7 (Figure 2.13, line in blue) at least for 30 min. The fluorescence emission of EGFP-TRPC5 responded to NO in the ratiometric manner to the opposite direction compared to the ratiometric change during the disulfide bond cleavage by DTT (Figure 2.10). The increase in the emission ratio of EGFP-TRPC5 in response to NO likely resulted from the formation of disulfide bond. The relationship between the disulfide bond formation and the increase in the emission ratio of EGFP-TRPC5 by NO was evaluated by quantitating the free thiol content in EGFP-TRPC5 after the reaction with NOC7. The free thiol content was drastically decreased from 93% to 17% after the reaction with NO (500 μM NOC7) (Table 2.2).

Table 2.2. Contents of free thiol group upon reduction with DTT and reaction with NO

Conditions	Free thiol contents
Without DTT	< 10%
With 1 mM DTT	93 ± 9%
With 500 μM NOC7	17 ± 4%
With 5 mM ascorbic acid	20 ± 4%

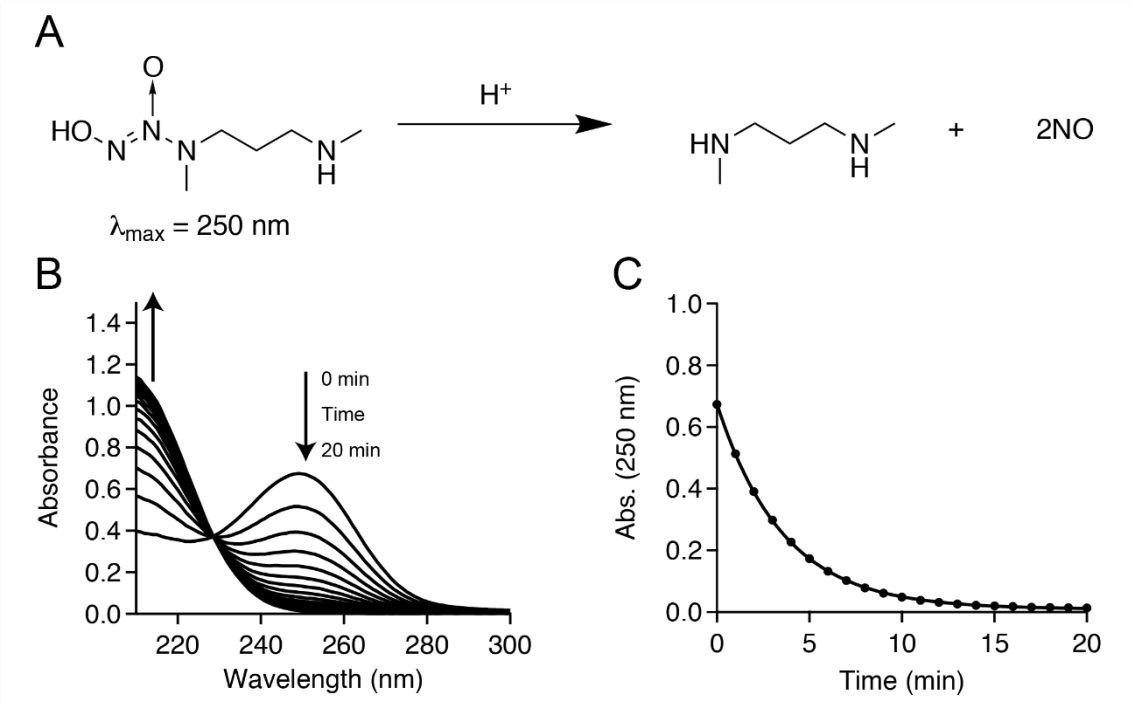

Figure 2.11. (A) Reaction scheme of NOC7. Two molecules of NO are released from one molecule of NOC7 in the presence of proton. (B) The absorption spectral change of NOC7 in a buffer containing 100 mM phosphate (pH 7.0), 500 mM NaCl, 0.005% Tween 20. (C) The time course change of absorbance at 250 nm in (B). The plots were fitted to a first-order kinetics. The half-life of NOC7 under the condition was determined as 2.4 min.

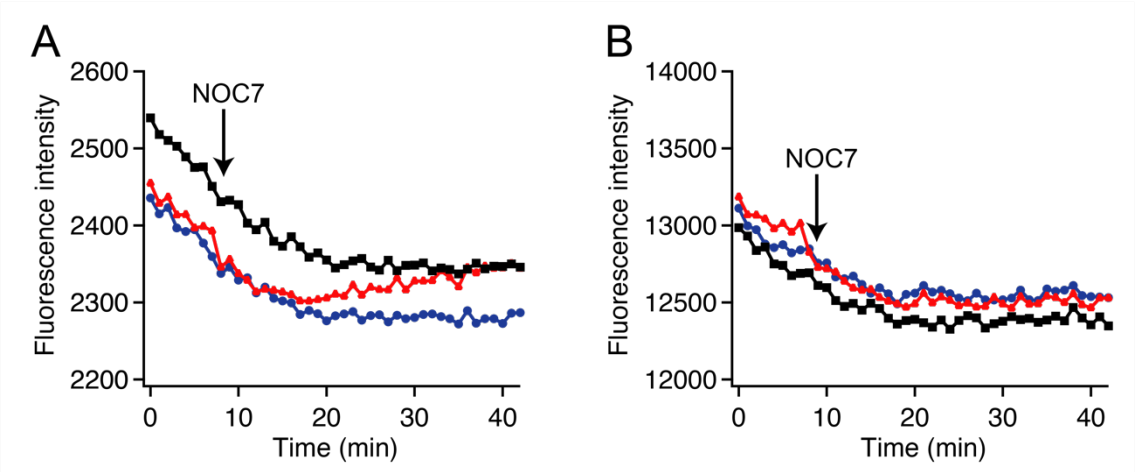

Figure 2.12. Time course change for the fluorescence emission intensity of EGFP-TRPC5 in the presence of NO. The fluorescence intensity at 535 nm excited at (A) 400 nm or (B) 485 nm, respectively. EGFP-TRPC5 in the reduced form (red and blue) and oxidized form (black) were treated with NOC7 (red and black). Reactions were started with the addition of NOC7 between 8-9 min. Only a solution (0.01 M NaOH) was added to EGFP-TRPC5 (blue). The emission intensity ratio was shown in Figure 2.11.

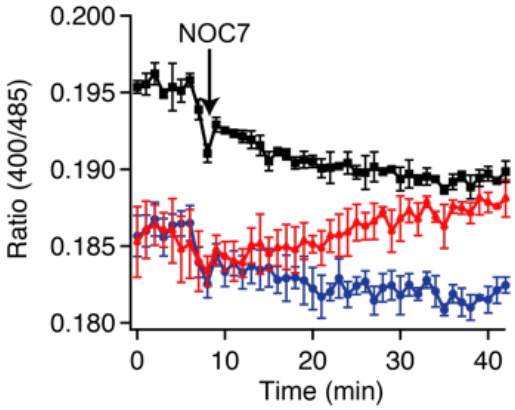

Figure 2.13. Time course changes for the emission intensity ratio of EGFP-TRPC5 in the presence of NO. EGFP-TRPC5 in the reduced form (line in red and line in blue) and oxidized form (line in black) were treated with (line in red and line in black) or without (line in blue) NOC7 (500 μM). Reactions were started with addition of NOC7 or a solution (0.01 M NaOH) between 8-9 min. Spikes in the ratio value were observed upon addition of NOC7. The emission intensity ratios (Ratio (400/485)) were calculated by dividing fluorescence intensity at 535 nm when excited at 400 nm by fluorescence intensity at 535 nm when excited at 485 nm.

To confirm the reaction pathway for the formation of disulfide bond by NO, the following experiment was conducted. Both the disulfide bond and the S-nitrosylated thiol group, the intermediate of disulfide bond formation by NO, show negative response to DTNB. The S-nitrosylated thiol group was selectively reduced in the presence of disulfide bond by the gentle reaction with ascorbic acid.[21] After the ascorbic acid treatment, NOC7-treated EGFP-TRPC5 contained 20% of free thiol residue, which was similar to that observed before the ascorbic acid treatment (17%) (Table 2.2). The result strongly indicated that little or no S-nitrosylated thiol group existed in EGFP-TRPC5 after the reaction with NOC7. EGFP-TRPC5 reacted with NO to form the S-nitrosylated thiol group, which instantly formed a disulfide bond in the segment (Leu538 to Leu575) of TRPC5. Therefore, the observed increase in the emission ratio is dominantly caused by the disulfide bond formation by Cys553 and Cys558. The disulfide bond formation by Cys553 and Cys558 causes the local structural change in the segment of TRPC5 that transduced to the N-terminal Leu538 and the C-terminal Leu575. Even in the absence of NOC7, the free thiol content of reduced EGFP-TRPC5 decreased from 93 to 49% after 30 min incubation possibly due to the air oxidation, which associated with a gradual decrease in the ratio of fluorescence emission of EGFP (Figure 2,13, line in blue) as the sum of increment of the ratio due to the air oxidation and decrement of the ratio due to the photo-bleaching (Figure 2.13, line in black). The air oxidation induced less amount of disulfide bond formation than the one with NOC7. These results indicated that conformational change of the structural segment of TRPC5 was induced by the disulfide bond formation in response to NO, and supported the notion that the open state of TRPC5 channel is stabilized by the disulfide bond formation.

2. 2. 6. Possible structural changes of TRPC5 upon the reaction with NO

Results in the section 2.2.4 and 2.2.5 supported the proposed model of TRPC5 activation that the gating was triggered by the structural change upon disulfide bond formation.[1] Although the degree to which TRPC5 changes its structure in response to NO is unknown, the observed modulation of EGFP emission indicates that the TRPC5 derived segment Leu538 to Leu575 in the loop configuration effectively perturbed the local structure proximal to the EGFP chromophore. Therefore, the structural change upon the cysteine modification transduced at least to Leu538 and Leu575 of TRPC5, extending

more than 15 amino acid residues away from the disulfide bond. The N-terminal of the structural segment (Leu538 to Leu541) resides in the S5 helix and the C-terminal (Leu568 to Leu575) locates in the part of pore helix of TRPC5 (Figure 2.14). It is likely that the structural changes induced upon the disulfide bond formation and reduction transduces to these helices. The reaction with NO induced a gradual increase in the ratio of fluorescence emission of EGFP-TRPC5 with drastic decrease in the free thiol content, while little or no S-nitrosylated group was detected in NO-treated EGFP-TRPC5. The fluorescence emission change of EGFP-TRPC5 is likely the outcome of the disulfide bond formation between Cys553 and Cys558, though a transient structural change could be induced by the seemingly short-lived S-nitrosylated group. The NO-induced disulfide bond formation between Cys553 and Cys558 would reasonably stabilize the structural change at the N-terminal side of pore-forming region of TRPC5. Changes in the ratios of emission intensity of EGFP upon the disulfide bond formation and reduction were the reversible process (Figure 2.10 and 2.13). These results are parallel with the finding that the gating of TRPC5 for Ca^{2+} uptake is reversible upon the reaction to NO and to the reducing condition

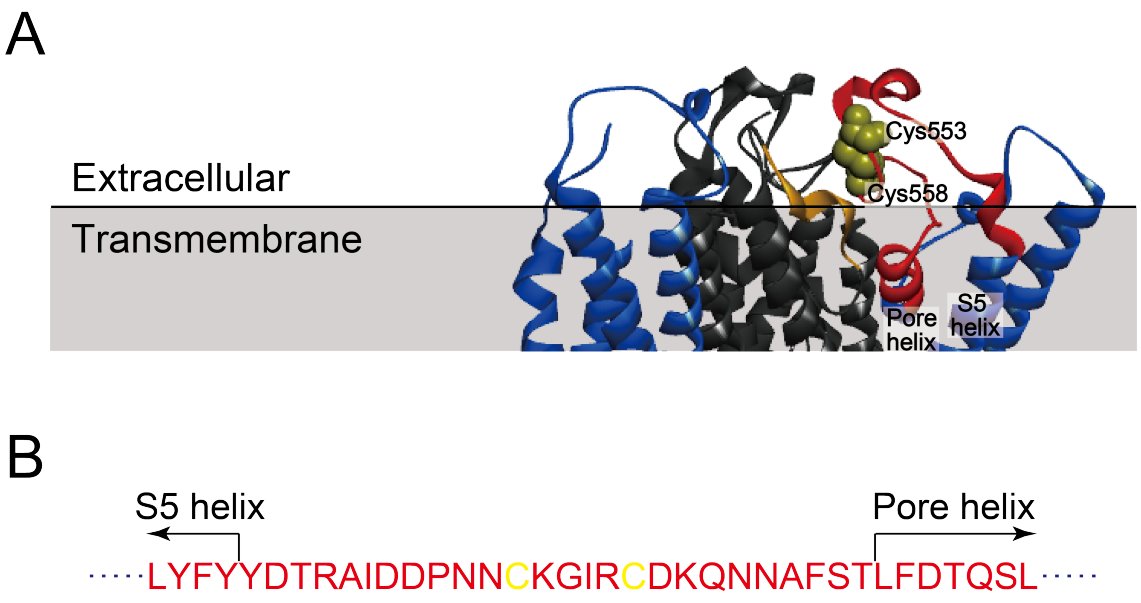

Figure 2.14. (A) Cryo-EM of TRPC5 homotetramer around the transmembrane. NO-sensing domain and two cysteines were represented in red and CPK representation in yellow, respectively. Two cysteines were located near but outside of the membrane. pore helix and S5 helix were embedded inside the transmembrane. (B) Amino acid sequence

of NO-sensing domain. The N-terminal of the structural segment (Leu538 to Leu541) resides in the S5 helix and the C-terminal (Leu568 to Leu575) locates in the part of pore helix of TRPC5.

2. 2. 7. Fluorescence responses of EGFP-TRPC5 in response to H_2O_2

TRPC5 expressed in human embryonic kidney (HEK) cells responded to 10 μM S-Nitroso-N-acetyl-DL-penicillamine (SNAP) as the NO donor, while at least 100 μM H_2O_2 was required to activate TRPC5[13], indicating that wild type TRPC5 specifically reacted with NO. Modulation of pKa and nucleophilicity of the target thiol by the interaction with hydrophilic residues in the hydrophobic environment was suggested[9,21], however, a question of whether the specificity of TRPC5 to NO is originated from the inherent character of amino acid residues near the cysteine or from the hydrophobic membrane surrounding TRPC5 has not been addressed yet.

Oxidant selectivity for the reaction of the TRPC5 structural segment containing the two cysteine residues was next evaluated by reacting with H_2O_2 (Figure 2.15A). In these experiments, the initial free thiol content of the sample was determined to be 76% by the DTNB method (Table 2.3). Upon incubation of the reduced EGFP-TRPC5 with H_2O_2 (100 μM), the emission ratio of EGFP-TRPC5 also increased (Figure 2.15A, line in red). The free thiol content after the incubation with H_2O_2 was determined to be less than 11% (Table 2.3). Additionally, the emission intensity change of EGFP-TRPC5 in response to H_2O_2 (100 μM) was faster than that to the same concentration of NOC7 (100 μM) (Figure 2.15). These results indicated that the disulfide bond formation at the TRPC5 segment (Leu538 to Leu575) embedded in EGFP showed no preferential reactivity to NO over H_2O_2.

Table 2.3. Contents of free thiol group upon reduction with DTT and reaction with H_2O_2

Conditions	Free thiol contents
Without DTT	< 11%
With 1 mM DTT	76 ± 4%
With 100 μM H_2O_2	< 11%

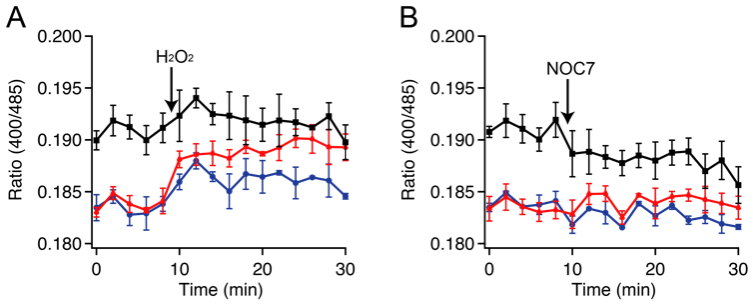

Figure 2.15. Time course changes for the emission intensity ratio of EGFP-TRPC5 in response to (A) H_2O_2 (100 μM H_2O_2) and (B) NO (100 μM NOC7). EGFP-TRPC5 in the reduced form (line in red and line in blue) and oxidized form (line in black) were treated with (line in red and line in black) or without (line in blue) H_2O_2 (A) or NO (B), respectively. Reactions were started with addition of (A) H_2O_2 (100 μM) or a buffer and (B) NOC7 (100 μM) or a solution (0.01 M NaOH) between 8-10 min, respectively. The emission intensity ratios (Ratio (400/485)) were calculated by dividing fluorescence intensity at 535 nm when excited at 400 nm by fluorescence intensity at 535 nm when excited at 485 nm.

The structural segment of TRPC5 (Leu538 to Leu575) by itself is insufficient to show the specific reactivity to NO as observed for wild type TRPC5. Difference in the NO releasing rate between NOC7 and SNAP, which was used in the previous study[13], cannot account for the lack of NO selectivity because NOC7 has faster NO releasing rate than SNAP, that is, the half-life of NOC7 is 2.4 min (Figure 2.11) and SNAP is 4.6 h in the aqueous condition.[22] From the cryo-EM structure of TRPC5, the structural segment containing two cysteine residues, Cys553 and Cys558, locate in the extracellular part near the cytoplasmic membrane (Figure 2.15). This suggests that the selectivity of TRPC5 to NO against H_2O_2 arises from the difference in hydrophobicity or polarity of NO and H_2O_2.

Because H_2O_2 is considered to be more hydrophilic than NO, NO would be more accessible to the transmembrane domain of TRPC5 in the cytoplasmic membrane.

2. 3. Conclusions

In this chapter, the putative NO-sensing segment of TRPC5 containing two cysteine residues was embedded in an EGFP to evaluate its structural changes in response to NO. EGFP-TRPC5 thus designed formed a disulfide bond and exerted emission intensity changes in response to NO. The structural change was maintained by the disulfide bond formation and affected the residues more than 15 residues away from the disulfide bond. The results support the proposed activation mechanism for the NO response of TRPC5 that the NO-induced disulfide bond formation would be transduced to the S5 helix and the pore helix that contribute to form pore of TRPC5 channel.[1] While TRPC5 triggers gating selectively in response to NO over H_2O_2, the isolated structural segment of TRPC5 encompassing from the S5 helix to the pore helix is not sufficient to show the specific reactivity to NO. Other factors, the difference in the hydrophobicity or the polarity between NO and H_2O_2 could influence the high selectivity of TRPC5 toward NO.

2. 4. Materials and methods

2. 4. 1. Materials

The restriction enzymes (*Nde*I, *Xho*I and *Dpn*I) were purchased from New England Biolabs. Purified oligonucleotide primers for gene construction were purchased from Thermo Fisher Scientific Inc. (Waltham, MA, USA). *E. coli* BL21 (DE3) competent cells were purchased from Invitrogen (Carlsbad, CA). Mini Elute Gel Extraction Kit was purchased from QIAGEN (Tokyo, Japan). HiTrap™ Butyl HP column (5 mL) and HisTrap™ HP column (5 mL) were purchased from GE Healthcare Japan Inc. (Tokyo, Japan). PrimeSTAR HS DNA polymerase, T4 DNA ligase, and *E. coli* DH5α competent

cells were purchased from TaKaRa Bio Inc. (Shiga, Japan). NOC7 was purchased from DOJINDO LABOLTORIES (Kumamoto, Japan). All the other chemicals were purchased from Wako Chemicals (Osaka, Japan), Tokyo Chemical Industry Co., Ltd (Tokyo, Japan), Sigma-Aldrich Japan (Tokyo, Japan) and Nacalai Tesque (Kyoto, Japan).

2. 4. 2. Construction of plasmids

The gene encoding EGFP in Btk-cpGFP[24] was sequentially amplified by PCR using primers listed in Table 2. 4. The PCR products were run on a 1% agarose gel (TAE) and purified with a Mini Elute Gel extraction Kit. The PCR products and pET29a were digested with *Nde*I and *Xho*I and were purified in the same manner. These products were incubated with T4-DNA-ligase. The mixture was transformed into *E. coli* DH5α competent cells for amplification. The vector encoding parent EGFP with TRPC5 (L538-L575) was purified and sequenced.

Table 2.4. Nucleotide sequences of primers for construction of an expression vector for the parent EGFP with TRPC5 (L538-575).

primer	from 5' to 3'
Primer 1 (F-EGFP)	AAAAAAAAAA CATATG GTGAGCAAGGGCGAGGAGCTG
Primer 2 (R-TRPC5-EGFP)	TGCCCTTGCAATTATTCGGATCATCAATGGCTCGGGTATCATAA TAGAAATACAGAAGCTTGCCGTTGTACTCCAGCTTG
Primer 3 (R-TRPC5)	GACTGGAGCGTATCGAACAGCGTCGAGAAGGCATTATTCTGCTT ATCGCATCGAATGCCCTTGCAATTATTCGGATCATC
Primer 4 (F-TRPC5-EGFP)	ATGCGATAAGCAGAATAATGCCTTCTCGACGCTGTTCGATACGCT CCAGTCGCTCGGATCCGGCTTTAACAGCCACAAC
Primer 5 (R-EGFP)	AAAAAACTCGAGTGATCCTCCGGTACCTCCCTTGTACAGCTCGT CCATGCCGAGAG

EGFP mutants, of which two cysteine residues (Cys49 and Cys71) were replaced with Ser49 and Ser71, Met71, or Val71, were sequentially constructed. The vector encoding parent EGFP with TRPC5 (L538-L575) was amplified by PCR using primers 6 and 7 (Table 2.5) for constructing the EGFP mutant (C49S). PCR product was treated with *Dpn*I and transformed into *E. coli* DH5α competent cells. The vector encoding EGFP (C49S) with TRPC5 (L538-L575) was purified and sequenced. The vector

encoding EGFP (C49S) with TRPC5 (L538-L575) was amplified by PCR using primers 8 and 9, primers 10 and 11, or primers 12 and 13 (Table 2.5) for mutating from Cys71 to Ser71, Met71 or Val71, respectively. Plasmids EGFP(C49S/C71S) with TRPC5 (L538-L575), EGFP (C49S/C71M) with TRPC5(L538-L575) and EGFP(C49S/C71V) with TRPC5 (L538-L575) were constructed by following the same procedure for constructing the plasmid EGFP (C49S) with TRPC5 (L538-L575).

Table 2.5. Nucleotide sequences of primer pairs for construction of an expression vector for cysteine mutated derivatives of the parent EGFP with TRPC5 (L538-L575).

primer	from 5' to 3'
Primer 6 (F-C49S)	TTCATCTCAACCACCGGCAAGCTGCCCGTG
Primer 7 (R-C49S)	GGTGGTTGAGATGAACTTCAGGGTCAG
Primer 8 (F-C71S)	GTGCAGTCATTCAGCCGCTACCCCGAC
Primer 9 (R- C71S)	GCTGAATGACTGCACGCCGTAGGTCAG
Primer 10 (F-C71M)	GTGCAGATGTTCAGCCGCTACCCCGAC
Primer 11 (R- C71M)	GCTGAACATCTGCACGCCGTAGGTCAG
Primer 12 (F- C71V)	GTGCAGGTGTTCAGCCGCTACCCCGAC
Primer 13 (R- C71V)	GCTGAACACCTGCACGCCGTAGGTCAG

2. 4. 3. Expression and purification of proteins

The plasmid EGFP-TRPC5 was transformed into *E. coli* BL21 (DE3) competent cells. The transformed cells were grown at 37 °C until OD_{600} reached 0.5, and the protein expression was induced with 1 mM IPTG for 24 h at 18 °C. The soluble fraction of the cell lysate containing the target protein was loaded to HisTrap^{TM} HP column with a linear gradient of 60–225 mM imidazole in 50 mM phosphate, 500 mM NaCl (pH 8.0). The fractions containing EGFP-TRPC5 were collected and diluted to the initial condition of next purification (50 mM phosphate, 500 mM $(NH_4)_2SO_4$ (pH 8.0)). The resultant was

loaded to HiTrap™ Butyl HP and eluted by $(NH_4)_2SO_4$ gradient (from 500 to 0 mM). Fractions containing EGFP-TRPC5 were collected and dialyzed against the solution containing 100 mM phosphate, 200 mM NaCl, 50%v glycerol (pH 8.0) and kept in -20 °C. Concentration of EGFP-TRPC5 in the glycerol stock was determined with the absorbance at 440 nm derived from the isosbestic point of chromophore in EGFP (the determined molecular coefficient of EGFP-TRPC at 440 nm: 15,000 $M^{-1}cm^{-1}$).

2. 4. 4. Characterization of EGFP-TRPC5 *in vitro*

EGFP-TRPC5 was characterized by MALDI-TOF mass spectrometry (AXIMA-LNR, SA matrix, Shimadzu, Kyoto, Japan). EGFP-TRPC5: m/z calcd 33,236; observed 33,179. Absorption spectra were measured with UV-2550 UV-Vis Spectrometer (SHIMADZU, Kyoto, Japan). Excitation and emission spectra were measured by F-7000 fluorescence spectrometer (HITACHI High-Tech Science, Tokyo, Japan) at 20 °C. Samples contained 2 μM EGFP-TRPC5 in a buffer containing 100 mM phosphate buffer, 500 mM NaCl, 0.005% Tween20 (pH 6.7). The emission spectra were measured by excitation at 395 nm and 466 nm and the excitation spectra were measured by the emission wavelength of 509 nm.

2. 4. 5. Reaction of EGFP-TRPC5 with NO or H_2O_2

The disulfide bond of EGFP-TRPC5 was reduced in a solution containing 20 μM EGFP-TRPC5, 100 mM phosphate (pH 8.0), 0.005% Tween 20, 1 mM DTT for 3 h at 25 °C. After reduction, the EGFP-TRPC5 solution was loaded to Micro Bio-Spin Chromatography Column P-6 (Bio-Rad) in a buffer containing 100 mM phosphate, 500 mM NaCl, 0.005% Tween20 (pH 6.75). Concentration of the free thiol group in EGFP-TRPC5 was measured by the DTNB method with Ellman's reagent (see next section). Reactions of EGFP-TRPC5 with NO were monitored by measuring the changes in fluorescence emission upon addition of NOC7 (dissolved in 0.01 M NaOH) to a solution of 13 μM EGFP-TRPC5 in the buffer containing 100 mM phosphate, 500 mM NaCl, 0.005 % Tween20 (pH 6.75) at 20 °C with Infinite F PLEX (TECAN, Zürich, Switzerland). Instead of the addition of NOC7, an equal amount of 0.01 M NaOH was added to the reaction solution. It should be noted that the pH value of the buffer did not

change between before and after the addition of NOC7 in 0.01 M NaOH. After the measurement, concentrations of the free thiol group of EGFP-TRPC5 in response to NO was measured by the DTNB method. In the case of H_2O_2, EGFP-TRPC5 was treated by H_2O_2 for 70 min.

2. 4. 6. Quantitation of the free thiol group

The concentration of free thiol group in EGFP-TRPC5 was measured by the DTNB method. Prior to the assay by the DTNB method, all the samples were purified by size exclusion chromatography to remove the thiol containing reagents such as DTT. An assay solution was prepared by mixing 100 μM DTNB in a solution containing 100 mM phosphate, 500 mM NaCl and 0.005% Tween20 (pH 6.75) with an aliquot of EGFP-TRPC5 solution. Absorption spectra of assay solution were measured by Infinite M200 PRO (TECAN, Zürich, Switzerland). The concentration of free thiol group in EGFP-TRPC5 was determined by the absorbance at 412 nm, which derived from 2-nitro-5-mercaptobenzoic acid (Figure 2.8). The concentration of EGFP-TRPC5 was also determined from the absorbance at 440 nm, the isosbestic point of chromophore in EGFP. The concentration of free thiol group was determined by the following equation:

$$y = 0.004x + 0.005$$

y and x represent the absorbance at 412 nm and concentration of L-cysteine [μM], respectively (Figure 2.8).

To the NOC7 treated EGFP-TRPC5, a solution containing ascorbic acid (final concentration: 5 mM) was added to specifically reduce the S-nitorsylated thiol. After 30 min, the reaction mixture was treated by the same procedure described above to quantitate the concentration of free thiol group by the DTNB method.

2. 5. References

1. Yoshida T, Inoue R, Morii T, Takahashi N, Yamamoto S, Hara Y, Tominaga M, Shimizu S, Sato Y, Mori Y. Nitric oxide activates TRP channels by cysteine S-nitrosylation. Nat. Chem. Biol. 2006;2:596-607.
2. Sakaguchi R, Mori Y. Transient receptor potential (TRP) channels: Biosensors for redox environmental stimuli and cellular status. Free Radical Biol. Med. 2020;146:36-44.
3. Gees M, Colsoul B, Nilius B. The Role of Transient Receptor Potential Cation Channels in Ca^{2+} Signaling. Cold Spring Harbor Perspect. Biol. 2010;2:a003962.
4. Hess DT, Matsumoto A, Kim SO, Marshall HE, Stamler JS. Protein S-nitrosylation: purview and parameters. Nat. Rev. Mol. Cell Biol. 2005;6:150-166.
5. Duan J, Li J, Chen GL, Ge Y, Liu J, Xie K, Peng X,Zhou W, Zhong J, Zhang Y, Xu J, Xue C, Liang B, Zhu L, Liu W, Zhang C, Tian XL, Wang J, Clapham DE, Zeng B, Li Z, Zhang J. Cryo-EM structure of TRPC5 at 2.8-Å resolution reveals unique and conserved structural elements essential for channel function. Sci. Adv. 2019;5:eaaw7935.
6. Tallini YN, Ohkura M, Choi BR, Ji G, Imoto K, Doran R, Lee J, Plan P, Wilson J, Xin HB, Sanbe A, Gulick J, Mathai J, Robbins J, Salama G, Nakai J, Kotlikoff MI. Imaging cellular signals in the heart *in vivo*: Cardiac expression of the high-signal Ca^{2+} indicator GCaMP2. Proc. Natl. Acad. Sci. U. S. A. 2006;103:4753-4758.
7. Zhang J, Campbell, Ting AY, Tsien RY. Creating new fluorescent probes for cell biology. Nat. Rev. Mol. Cell Biol. 2002;3:906-918.
8. Berg J, Hung YP, Yellen G. A genetically encoded fluorescent reporter of ATP:ADP ratio. Nat. aMethods. 2009;6:161-166.
9. Nakai J, Ohkura M, Imoto K. A high signal-to-noise Ca^{2+} probe composed of a single green fluorescent protein. Nat. Biotechnol. 2001;19:137-141.
10. Morise H, Shimomura O, Johnson FH, Winant J. Intermolecular Energy Transfer in the Bioluminescent System of Aequorea. Biochemistry. 1974;13:2656-2662.
11. Bejec K, Sixma TK, Kitts PA, Kain SR, Tsien RY, Ormö M, Remington SJ. Structural basis for dual excitation and photoisomerization of the Aequorea victoria green fluorescent protein. Proc. Natl. Acad. Sci. U. S. A. 1997;94:2306-2311.

12. Cormack BP, Valdivia RH, Falkow S. FACS-optimized mutants of the green fluorescent protein (GFP). Gene. 1996;173:33-38.
13. Ormo M, Cubitt AB, Kallio K, Gross LA, Tsien RY, Remington SJ, Crystal Structure of the Aquorea victoria Green Fluorsescent Protein. Science. 1996;273:1392-1395.
14. Wong PSY, Hyun J, Fukuto JM, Shirota FN, DeMaster EG, Shoeman DW, Nagasawa HT. Reaction between S-Nitrosothiols and Thiols: Generation of Nitroxyl (HNO) and Subsequent Chemistry. Biochemistry. 1998;37:5362-5371.
15. Percival MD, Ouellet M, Campagnolo C, Claveau D, Li C. Inhibition of Cathepsin K by Nitric Oxide Donors: Evidence for the Formation of Mixed Disulfides and a Sulfenic Acid. Biochemistry. 1999;38:13574-13583.
16. Pédelacq JD, Cabantous S, Tran T, Terwilliger TC, Waldo GS. Engineering and characterization of a superflolder green fluorescent protein. Nat. Biotechnol. 2006;24:79-88.
17. Jain RK, Joyce PB, Moliente M., Halban PA, Gorr SU. Oligomerization of green fluorescent protein in the secretory pathway of endocrine cells. Biochem. J. 2001;360:645-649.
18. Suzuki T, Arai S, Takeuchi M, Sakurai C, Ebana H, Higashi T, Hashimoto H, Hatsuzawa K, Wada I. Development of Cystein-Free Fluorescent Proteins for Oxidative Environment. PLoS ONE. 2012;7:e37551.
19. Costantini LM, Baloban M, Markwardt ML, Rizzo M, Guo F, Verkhusha VV, Snapp EL. A palette of fluorescent proteins optimized for diverse cellular environments. Nat. Commun. 2015;7670:6.
20. Hrabie JA, Klose JR, Wink DA, Keefer LK. New nitric oxide-releasing zwitterions derived from polyamines. J. Org. Chem. 1993;58:1472-1476.
21. Jaffrey SR, Erdjument-Bromage H, Ferris CD, Tempst P, Snyder SH. Protein S-nitrosylation: a physiological signal for neuronal nitric oxide. Nat. Cell Biol. 2001;3:193-197.
22. Ignarro LJ, Lippton H, Edwards JC, Baricos WH, Hyman AL, Kadowitz PJ, Gruetter CA. Mechanism of Vascular Smooth Muscle Relaxation by Organic Nitrates, Nitrites, Nitroprusside and Nitiric Oxide: Evidence for the Involvement of S-Nitrosothiols as Active Intermediates. *J. Pharmacol. Exp. Ther.* 1981;218:739-749.

Chapter 3

A two-step screening to optimize the signal response of autofluorescence protein-based biosensor

3. 1. Introduction

As described in chapter 1, genetically encoded biosensors constructed from the AFP are especially useful because they are easy to localize at specific area in the cells and suitable for the long-time imaging.[1,2] In general, AFP-based fluorescent biosensor is designed by conjugating an appropriate recognition or reaction module for a given target to the transducing module AFP. [3-5] Structural changes of the recognition module induced by the recognition/reaction event are transduced to AFP, which eventually results in fluorescence signal changes of AFP.[6,7] The structurally well-characterized native proteins, such as those analyzed by X-ray crystallography, NMR spectroscopy or Cryo-EM, are suitable for conjugating the recognition module to AFP by means of structure-based design.[5-12] However, the information on the structural change of recognition module for a target of interest is not always available. While AFP-based sensors were constructed by conjugating protein domains without the structural information, lack of the detailed information often caused difficulty in the optimization of biosensors.[13-16]

As described in chapter 2, to evaluate this putative NO-induced structural change of TRPC5[17], EGFP-TRPC5 was constructed by fusing a segment of the putative NO-sensing module of TRPC5 channel containing Cys553 and Cys558 residues as a loop structure to near chromophore of EGFP by means of the structure-based design.[18] EGFP-TRPC5 successfully detected the putative structural change upon the disulfide bond

formation induced with the reaction to NO as the change of fluorescence intensity ratio. The fact that the NO-induced disulfide bond formation was detected by EGFP-TRPC5 implied an application of EGFP-TRPC5 as NO biosensor in the mammalian cells by enhancing its ratiometric signal of only 8% increment.

In this chapter, a facile two-step screening method was applied to enhance the ratiometric signal of AFP-based biosensor. It was considered that the ratiometric signal of EGFP-TRPC5 was low because the disulfide bond formation site was located quite far from the EGFP chromophore to effectively transduce the structural change upon oxidation. The amino acid residues in the NO-sensing module were deleted from the N- and/or C- terminal to bring the disulfide bond more proximal to the EGFP chromophore in the mutants of EGFP-TRPC5. The first candidates were selected based on the *in silico* simulation with estimating the structural changes of the NO-sensing segment upon the disulfide bond formation as the root means square deviation (RMSD). Out of the 47 simulated mutants, 10 candidates were selected for the second screening, where the candidates were expressed in *E.coli* and assayed upon partial purification. The measurement of the signal response upon the disulfide bond cleavage, reverse process of disulfide bond formation, in the second screening indicated that five mutants showed larger changes of the ratiometric signal. Especially, one of them, 551-575, showed 4 times enhancement of the ratiometric signal over EGFP-TRPC5.

3. 2. Results and discussions

3. 2. 1. Strategy of enhancement of the signal response of EGFP-TRPC5

As described in chapter 2, in EGFP-TRPC5, a partial segment of the putative NO-sensing region ranging from Leu538 to Leu575 of TRPC5 was incorporated into EGFP to monitor its putative structural change upon disulfide bond formation in response to NO. This segment was inserted between Asn144 and Phe145 of EGFP to form a loop-like structure with Cys553 and Cys558 locating around its center (Figure 3.1A). Based on the general action mechanism of single AFP-based biosensor, structural changes of this segment upon the disulfide bond formation of two cysteines were transduced to the

structural perturbation around the chromophore of EGFP to modify its emission properties. The chromophore of EGFP exists in equilibrium between the protonated and deprotonated forms, showing absorption peak around 400 nm and 470 nm, respectively. Structural changes in this segment upon disulfide bond formation were successfully detected as the changes in fluorescence emission ratio between the protonated and deprotonated states of EGFP chromophore, albeit to a small degree.

To design a fluorescent NO biosensor based on EGFP-TRPC5, the structural change associated with the disulfide bond formation should be transduced more efficiently to cause the structural perturbation near the EGFP chromophore. The structure of EGFP-TRPC5 was predicted based on the crystal structure of EGFP and amino acid sequence applied with Discovery Studio (version 3.1 Client), inserting the amino acid sequence of the linker and the segment of TRPC5 into the crystal structure of EGFP (Figure 3.1B). It was considered that the rartiometric signal of EGFP-TRPC5 was low because the disulfide bond formation site was located quite far from the EGFP chromophore to effectively transduce the structural change upon oxidation. One of the strategies to efficiently transduce structural changes upon disulfide bond formation in the EGFP chromophore, is the deletion of amino acid residues between the site of disulfide bond formation and EGFP. The amino acid residues in the NO-sensing module were deleted from the N- and/or C- terminal to bring the disulfide bond site more proximal to the EGFP chromophore in the mutants of EGFP-TRPC5 (Figure 3.1B).

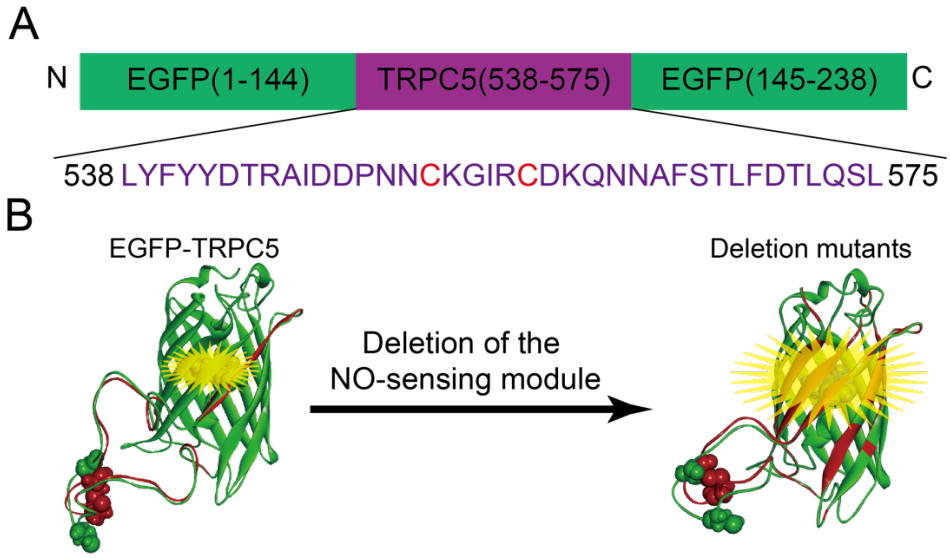

Figure 3.1 (A) NO-sensing segment of TRPC5, L538 to L575, was introduced between

Asn144 and Phe145 of EGFP. (B) Schematic illustration of the EGFP-TRPC5 construct and its mutants. Molecular models of reduced (green) and oxidized (red) forms are shown. Images were superimposed by matching the coordinates of Cα atoms of residues from L119 to I128, which were opposite to the NO-sensing segment. The chromophore, Cys553, and Cys558 are shown as CPK representations.

3. 2. 2. *In silico* simulation of segment structures embedded into EGFP

even with the simplest one-by-one deletion of amino acid residues from the N- and/or C-terminal, a total of 47 mutants were identified as candidate deletion mutants (Figure 3.2).

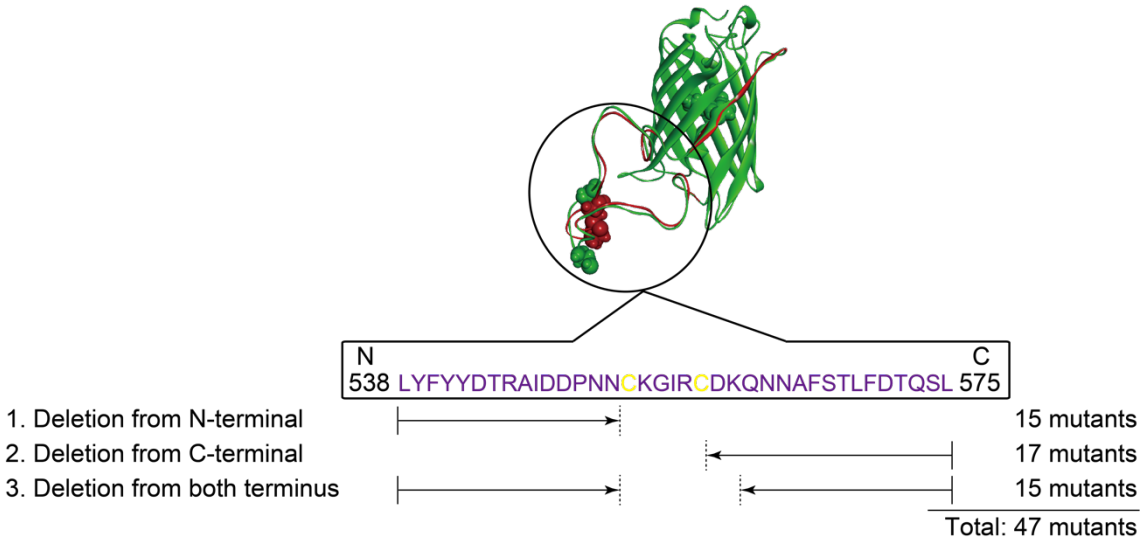

Figure 3.2. NO-sensing segment of TRPC5 (from Leu538 to Leu575) was inserted by splitting EGFP (between 144 and 145).[18] EGFP-TRPC5 mutants were designed to delete the NO-sensing segment from the N- and/or C-terminus.

Instead of performing bacterial expression, purification, and evaluation of all 47 mutants, we first screened mutants based on *in silico* simulations of the structures of the 47 deletion mutants in their reduced and oxidized forms (Figure 3.3, 3.4, and 3.5).

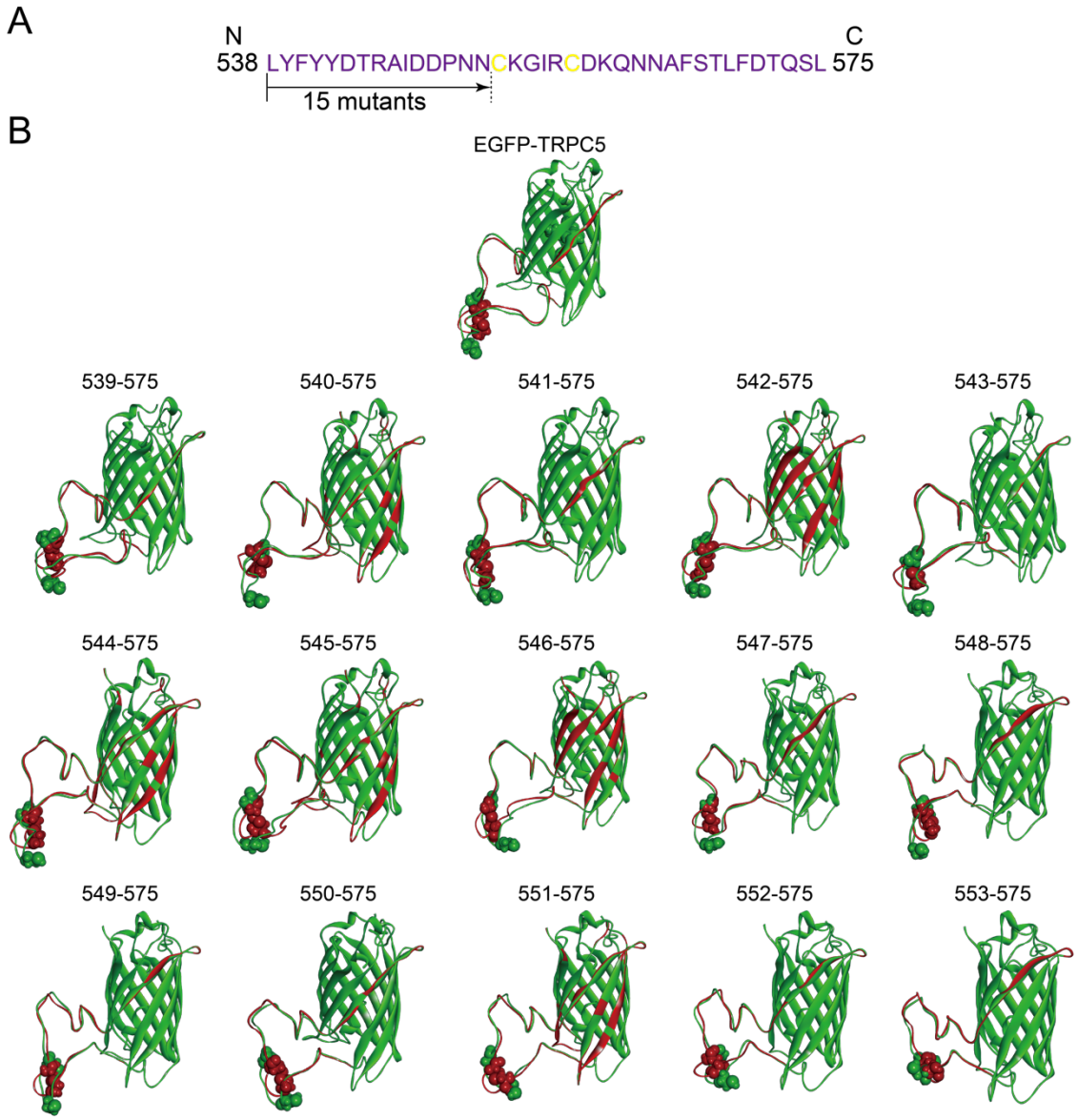

Figure 3.3. The simulation results of the mutants deleted from N-terminal side of recognition module. (A) Amino acid sequence of the structural change domain extracted from TRPC5, L538-L575, in parent EGFP-TRPC5. Deletion mutants deleted from Leu538 to N552 (15 mutants) were simulated. (B) The molecular models of 15 N-terminal side deleted-mutants. Numbers shown above the structures corresponded to the number of amino acids in TRPC5 used in each structure. The structures of mutants in reduced (green) and oxidized (red) forms were superimposed by matching the coordinates of Cα atoms of residues from L119 to I128, which were opposite side of conformational change domain.

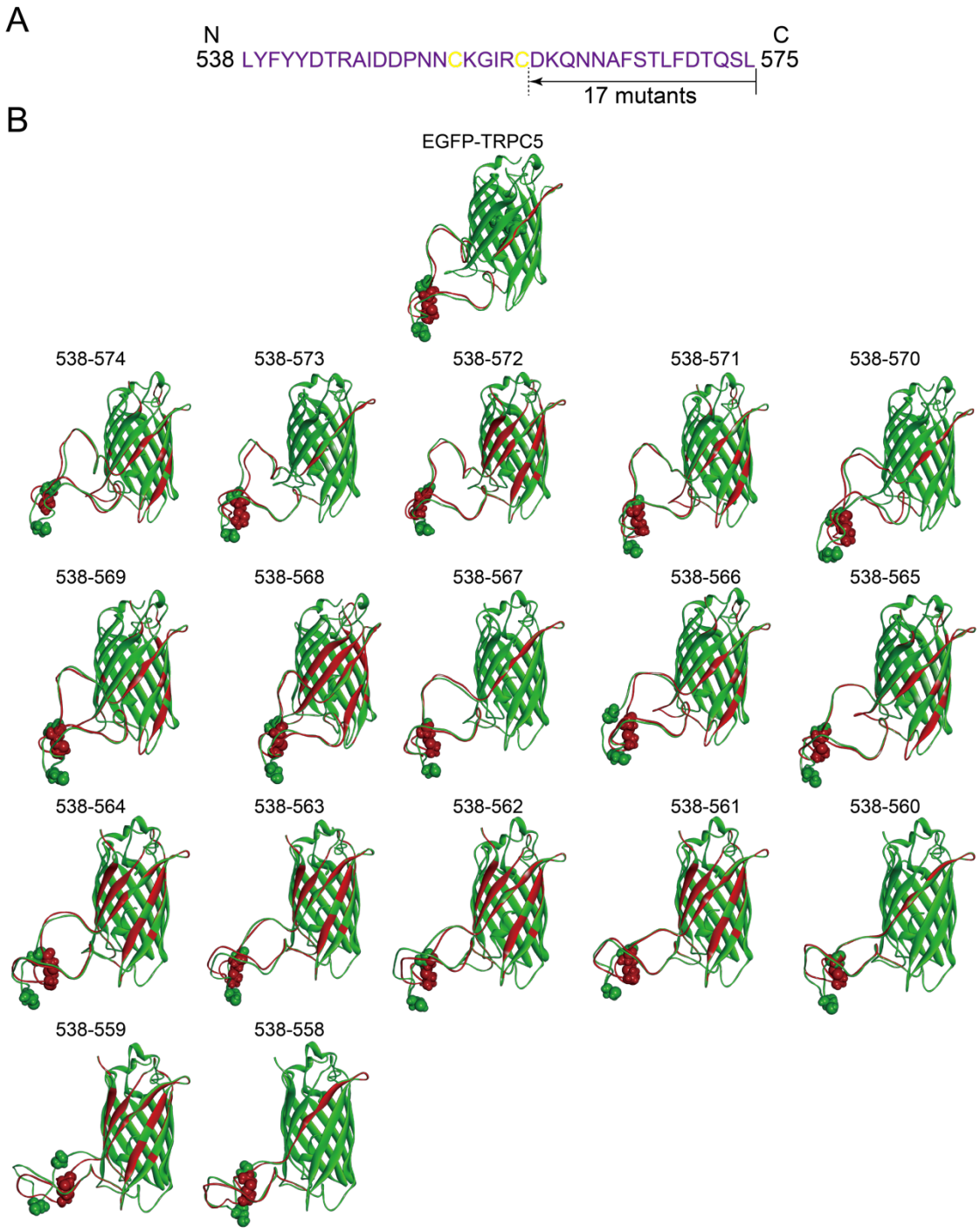

Figure 3.4. The simulation results of the mutants deleted from C-terminal of recognition module. (A) Amino acid sequence of the structural change domain extracted from TRPC5, L538-L575 in parent EGFP-TRPC5. Deletion mutants deleted from Leu575 to D559 (17 mutants) were simulated. (B) The molecular models of 17 C-terminal side deleted-mutants. Numbers shown above the structures corresponded to the number of amino acids in TRPC5 used in each structure. The structures of mutants in reduced (green) and

oxidized (red) forms were superimposed by matching the coordinates of Cα atoms of residues from L119 to I128, which were opposite side of conformational change domain.

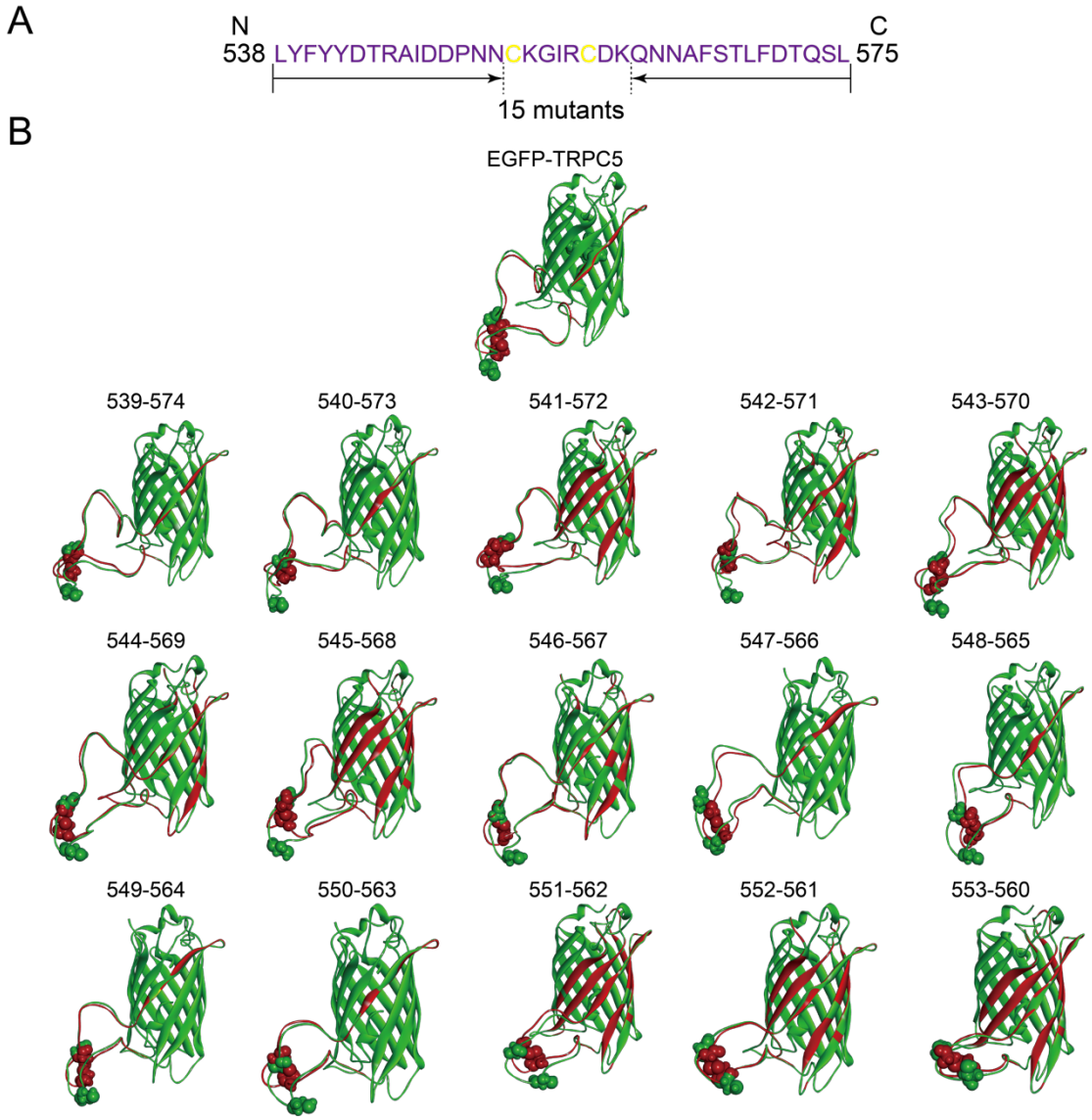

Figure 3.5. The simulation of the mutants deleted from both terminals of recognition module. (A) Amino acid sequence of the structural change domain extracted from TRPC5, L538-L575 in parent EGFP-TRPC5. Deletion mutants deleted from both Leu538 to N552 and Leu575 to D559 (15 mutants) were simulated. (B) The molecular models of 15 both terminus side deleted-mutants. Numbers shown above the structures corresponded to the number of amino acids in TRPC5 used in each structure. The structures of mutants in reduced (green) and oxidized (red) forms were superimposed by matching the coordinates of Cα atoms of residues from L119 to I128, which were opposite side of conformational change domain.

3. 2. 3. First screening: *in silico* root-mean-square-deviation (RMSD) evaluation of segment structural change induced by disulfide bond formation

The folded structure of EGFP was fixed during the simulation to avoid an unnecessary deformation from its proper folding. The structural change in the appended TRPC5 partial segment would be crucial to evaluate the structural perturbation of the EGFP. Therefore, the degrees of structural change in the appended TRPC5 partial segment upon disulfide bond formation were evaluated using the RMSD of the coordinates of the backbone of amino acid residues in the NO-sensing segment region between that of the reduced (Figure 3.3, 3.4, and 3.5, structure in green) and oxidized (Figure 3.3, 3.4, and 3.5, structure in red) forms superimposed on the EGFP domain. The RMSD values for the N-terminal residues of Cys553 and the C-terminal residues of C558 were calculated separately, that is, GKL-L538-N552 and D559-L575-GSG, where GKL and GSG were the linkers on each side in the case of EGFP-TRPC5 (Table 3.1). RMSD values on the N-terminal side were plotted against the C-terminal side for all simulated mutants (Figure 3.6). RMSD values in the N-terminal side were distributed from 1.2 Å to 4.5 Å and those in the C-terminal side from 0.5 Å to 3.9 Å. EGFP-TRPC5 showed small RMSD values compared to those of the other deletion mutants (Figure 3.6, black filled circles). Among these, 10 mutants showing large RMSD values were chosen for subsequent screening (Figures 3.6, and 3.7, plotted in red filled circles or shown in red boxes). Three mutants with small RMSD values, 538-567, 538-565, and 538-560, were also selected for comparison (Figures 3.6 and 3.7, plotted in blue filled circles or shown in blue boxes).

Table 3.6. RMSD values in N- versus C-terminal side of TRPC5 segment of the parent EGFP-TRPC5 and 47 deletion mutants. The color was consistent with Figure 3.5.

	RMSD (Å)	
Constructs	N-terminal	C-terminal
EGFP-TRPC5	**1.2**	**1.2**
553-560	1.2	1.3
538-567	1.3	1.1
544-569	1.3	1.3
538-565	1.4	0.8
538-568	1.4	0.9
541-575	1.4	1.0
538-569	1.4	1.1
538-565	1.4	1.6
542-575	1.5	1.1
552-561	1.5	1.3
549-575	1.6	1.2
538-571	1.6	1.4
545-568	1.6	2.1
545-575	1.7	1.0
549-564	1.7	1.2
552-575	1.7	1.9
538-560	1.8	0.4
544-575	1.8	0.7
538-561	1.8	1.3
539-574	1.8	1.3
553-575	1.9	1.3
540-575	2.0	0.5
539-575	2.0	1.1
538-574	2.1	1.3
538-558	2.1	1.5
538-563	2.1	1.5
538-564	2.1	1.6
538-573	2.1	1.7
540-573	2.1	1.9
543-575	2.2	0.8
551-575	2.2	1.7
545-575	2.3	1.1
542-571	2.3	1.6
538-570	2.3	1.9
548-575	2.4	0.8
538-562	2.5	1.6
546-575	2.6	0.6
550-563	2.6	1.7
551-562	2.6	2.5
546-567	2.7	0.8
550-575	2.7	1.0
543-570	2.8	1.7
547-566	2.8	2.2
541-572	2.9	1.0
538-572	2.9	1.5
548-565	3.3	2.0
538-559	4.4	3.9

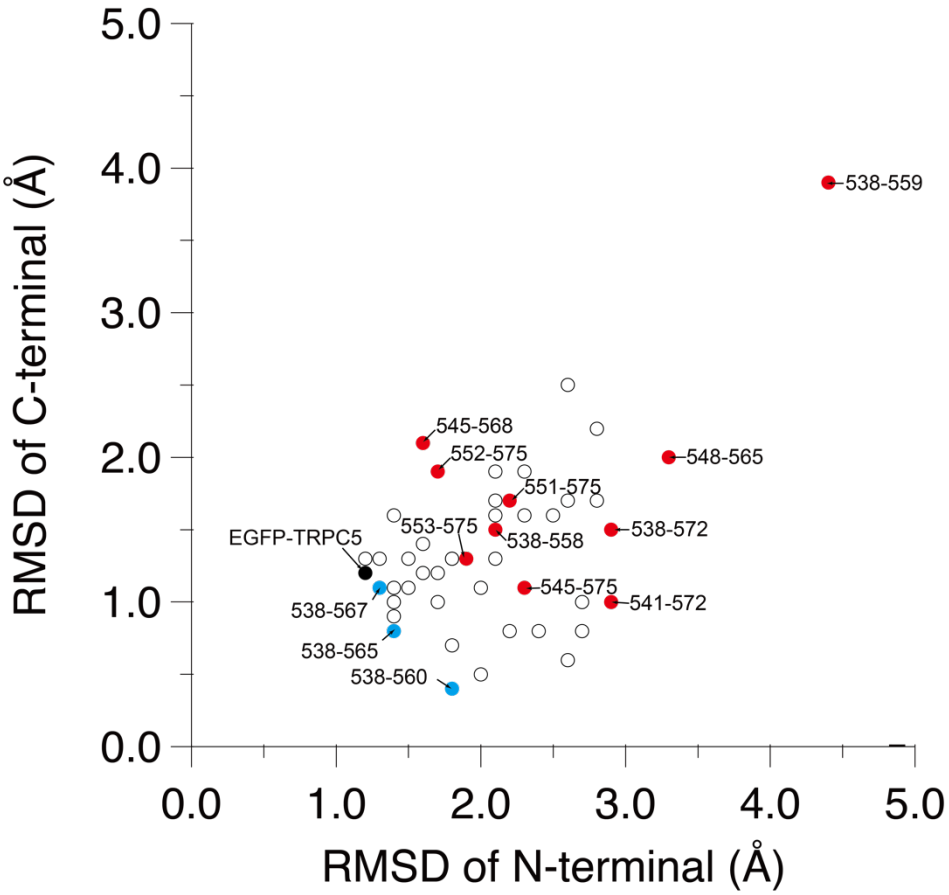

Figure 3.6. The plots of RMSD values in N-terminal side versus C-terminal side of TRPC5 segment of the parent EGFP-TRPC5 and 47 simulated deletion mutants. The RMSD values were calculated with the difference of coordinate of TRPC5 segment between reduced and oxidized forms as shown in Figure S2-S4. The parent EGFP-TRPPC5 was plotted in black filled circle. From 47 mutants, 10 mutants showing large RMSD values were chosen for the next screening (plotted in red filled circle). Three mutants with small RMSD values were also selected for comparison (plotted in blue filled circle).

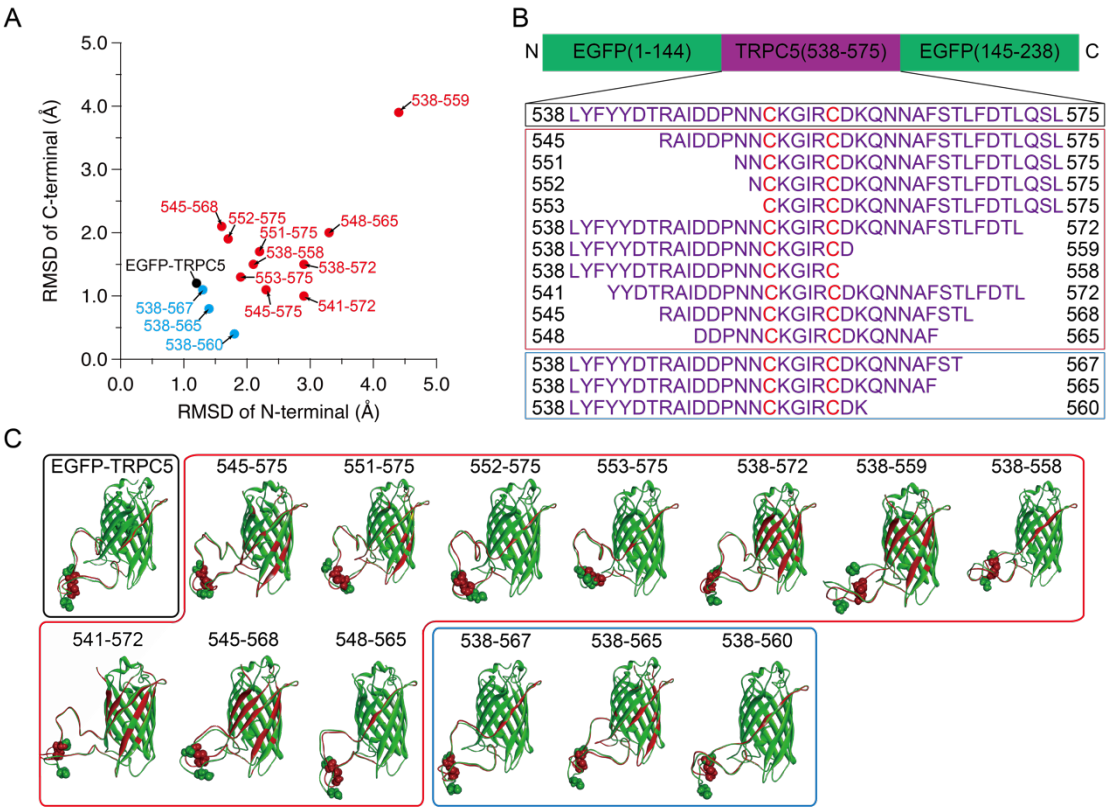

Figure 3.7. (A) Plots of RMSD values of N-terminal versus C-terminal sides of the TRPC5 segment of the parent EGFP-TRPC5 and its mutants selected from the first screening (those of all mutants were shown in Figure 3.6). Black circle: parent EGFP-TRPC5; red circles: 10 mutants showing large RMSD values; blue circles: three mutants showing low RMSD values. (B) Amino acid sequences of the NO-sensing segment of the EGFP-TRPC5 mutants selected after the first screening and (C) their molecular models. Black box: parent EGFP-TRPC5; red box: 10 mutants showing large RMSD values; blue box: three mutants showing low RMSD values. Cys553 and Cys558 are shown in CPK representation.

3. 2. 4. Rough purification of chosen mutants for second screening

Genes encoding 13 mutants of EGFP-TRP5 deleted at TRPC5 (L538-L575) were constructed (Table 3.3) and expressed in *Escherichia coli* (*E.coli*). For high-throughput screening, the expressed mutant proteins were partially purified by omitting several purification steps as described in chapter 2 (Figure 3.8) (see Materials and Methods).

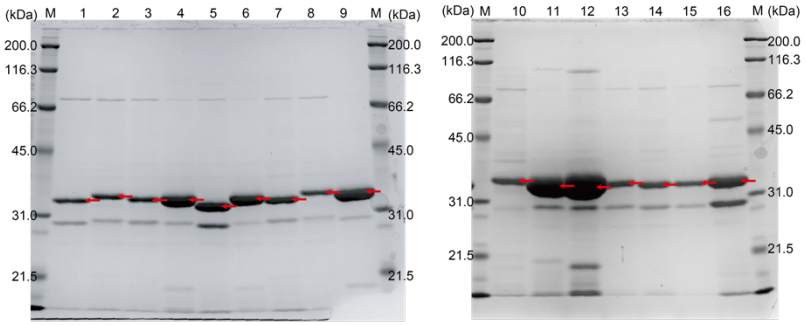

Figure 3.8. SDS-PAGE analysis of partially purified parent EGFP-TRPC5 and mutants for *in vitro* screening. M: molecular marker (6,500-200,000), lane 1: 538-559, lane 2: 538-572, lane 3: 538-565, lane 4: 553-575, lane 5: 548-565, lane 6: 552-575, lane 7: 541-572, lane 8: 538-575, lane 9: 551-575, lane 10: parent EGFP-TRPC5 lane 11: 545-575, lane 12: 551-575, lane 13: 538-567, lane 14: 538-560, lane 15: 538-558, lane 16: 545-568

3. 2. 5. Second screening: Construction and screening of the crude deletion mutants

As described in chapter 2, the parent EGFP-TRPC5 mostly formed a disulfide bond upon purification as evaluated by the conventional DTNB (5,5'-dithio-bis-(2-nitrobenzoic acid)) method with a purity of over 95% by SDS-PAGE analysis.[18] By assuming that the parent EGFP-TRPC5 mutants also formed a disulfide bond through partial purification, changes in the fluorescence emission ratio (ΔR) upon reduction of the disulfide bond would provide opposite signal changes in the responses to NO.

First, the ΔR value of the parent EGFP-TRPC5, defined as the change in the fluorescence emission ratio (R) without or with DTT, was measured at pH 6.9 (Table 3.2). The partially purified parent EGFP-TRPC5 showed a -0.013 change in ΔR upon reduction of the disulfide bond, which is consistent with the value determined using highly purified

original EGFP-TRPC5 (-0.010) as described in chapter2. This result indicates that the parent EGFP-TRPC5 mainly formed disulfide bonds after partial purification. Next, ΔR of all the constructed mutants was determined using the same procedure (Table 3.2). Among the 10 mutants with greater RMSD, five mutants, 545-575, 551-575, 552-575, 553-575, and 548-565 showed larger ΔR values than that of the parent EGFP-TRPC5. However, a comparison of $\Delta R/R_{oxi}$, which is the ratio of ΔR compared to the R of the oxidized form, should be used to evaluate the enhancement of the signal response. Four mutants, 545-575 (-14%), 551-575 (-31%), 552-575 (-22%) and 553-575 (-17%) showed larger $\Delta R/R_{oxi}$ than that of the parent EGFP-TRPC5 (-9%), whereas 548-565 (-8%) showed a similar $\Delta R/R_{oxi}$ to that of the parent EGFP-TRPC5. The signal response was enhanced in these four mutants; in particular, mutants 551-575, 552-575, and 553-575 showed a 2 to 4 times larger signal response compared to that of the parent EGFP-TRPC5. In contrast, no mutant showed larger $\Delta R/R_{oxi}$ values among the mutants with the three smaller RMSD. Therefore, *in silico* screening provided candidates for enhanced signal response.

It should be mentioned that the large RMSD did not always correspond to a large signal response. This result could be explained by the fact that the *in silico* simulation applied in this study was a quite simple structural optimization, where the steric clashes between the atoms were eliminated and the bond angles and lengths were adjusted within the defined structure.

Table 3.2. Changes in fluorescence emission ratios upon reduction for all constructs at pH 6.9.

Constructs	R		ΔR	ΔR/R_{oxi}
	w/o DTT (R_{oxi}[1)])	w/ DTT (R_{red}[2)])	(R_{red} - R_{oxi})	(R_{red} - R_{oxi})/R_{oxi} *100(%)
EGFP-TRPC5	0.147	0.134	-0.013	-9%
545-575	0.143	0.123	-0.020	-14%
551-575	0.258	0.177	-0.081	-31%
552-575	0.179	0.140	-0.039	-22%
553-575	0.234	0.195	-0.039	-17%
538-572	0.178	0.182	0.004	3%
538-559	0.240	0.251	0.011	5%
538-558	0.204	0.201	-0.003	-1%
541-572	0.144	0.136	-0.008	-5%
545-568	0.189	0.187	-0.002	-1%
548-565	0.331	0.305	-0.026	-8%
538-567	0.210	0.209	-0.001	0%
538-565	0.215	0.221	0.006	3%
538-560	0.232	0.229	-0.003	-1%

[1)] Fluorescence emission ratio (R) in oxidized form.

[2)] Fluorescence emission ratio (R) in reduced form.

3. 2. 6. Investigation of pH dependency of fluorescence emission changes upon reduction in the second screening

The dependency of ΔR values on the solution pH from 6.0 to 8.0 were also measured for all the constructs because the R values of the protonation or deprotonation state of chromophore depends on pH resulted from the shift of the equilibrium of them.[6,20] Except for 545-575, 551-575, 552-575, 553-575, the other constructs showed smaller ΔR values than the parent EGFP-TRPC5 at all the pH conditions (Figure 3.9). On the other hand, 545-575, 551-575, 552-575, 553-575, which showed larger ΔR values in pH 6.9, showed larger ΔR values in acidic pH than the basic pH due to the increase of ratio values

(Figure 3.10). Based on these results, the mutants 551-575, 552-575 and 553-575 showing larger ΔR values than the parent EGFP-TRPC5 at all the tested pH conditions, were further investigated as NO biosensors.

The dependency of fluorescence intensity on pH was different among the constructs. In 538-575, the fluorescence intensity excited at 395 nm was decreased with the increase of pH. On the other hand, the fluorescence intensity excited at 466 nm increased with the shifting to basic pH. The fluorescence intensity of 545-575 in the protonation state showed larger change than of the deprotonation state (Figure 3.10B), but the R value of 545-575 showed only moderate changes even in the acidic pH, in which the population of the protonation state increased. Other constructs, 551-575, 552-575, and 553-575 showed larger sensitivity to pH in the R value, which resulted from the increase in sensitivity to pH for the fluorescence emission derived from the protonated state. The higher sensitivity of fluorescence emission intensity to the solution pH implies that the chromophores of these mutants are more sensitive to the environment. Therefore, chromophore itself was more sensitive to the structural change of EGFP itself, even the similar structural change, not to larger structural change of EGFP resulted from efficiently transduction of the structural change of NO-sensing segment upon cleavage of disulfide bond. These effects could partially contribute to the enhancement of signal response. However, although some constructs, like 545-575 and 552-575, the sensitivity to pH is similar with other constructs which did not show the enhancement of the signal response, these constructs showed the enhancement of the signal response, these results indicated that deletion mutation certainly contributed to the efficiently transduction of structural change of NO-sensing segment.

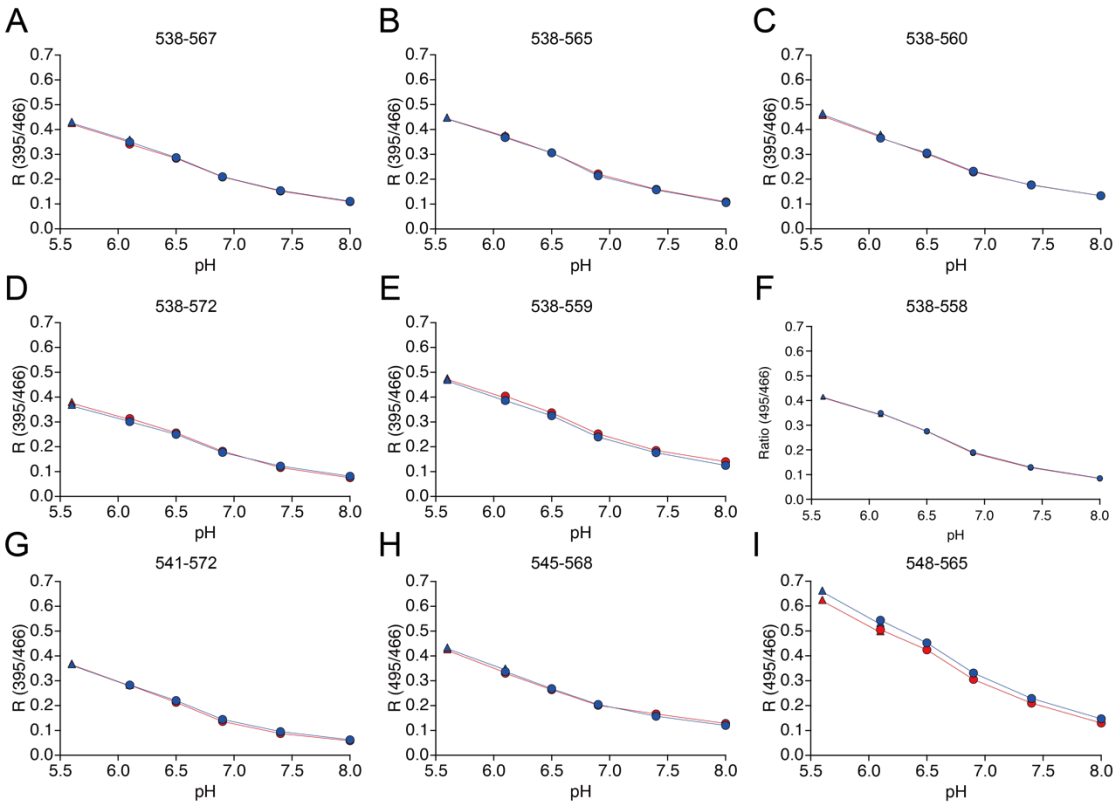

Figure 3.9. The changes of the R values upon reduction in different pH. Mutants (A) 538-567. (B) 538-565. (C) 538-560. (D) 538-572. (E) 538-559. (F) 538-558. (G) 541-572. (H) 545-568 (I) 548-565 in reduced (blue plot) and oxidized (red plot) forms. Reduced forms were prepared by the treatment with DTT at pH 8.0, then 6 times diluted by each buffer. Oxidized forms were also prepared with same procedure without DTT. pH 5.6 or 6.1: 100 mM citrate, 500 mM NaCl, 0.005% Tween-20 (plots in triangle), pH 6.1, 6.5, 6.9, 7.4, or 8.0: 100 mM phosphate, 500 mM NaCl, 0.005% Tween-20 (plots in circle).

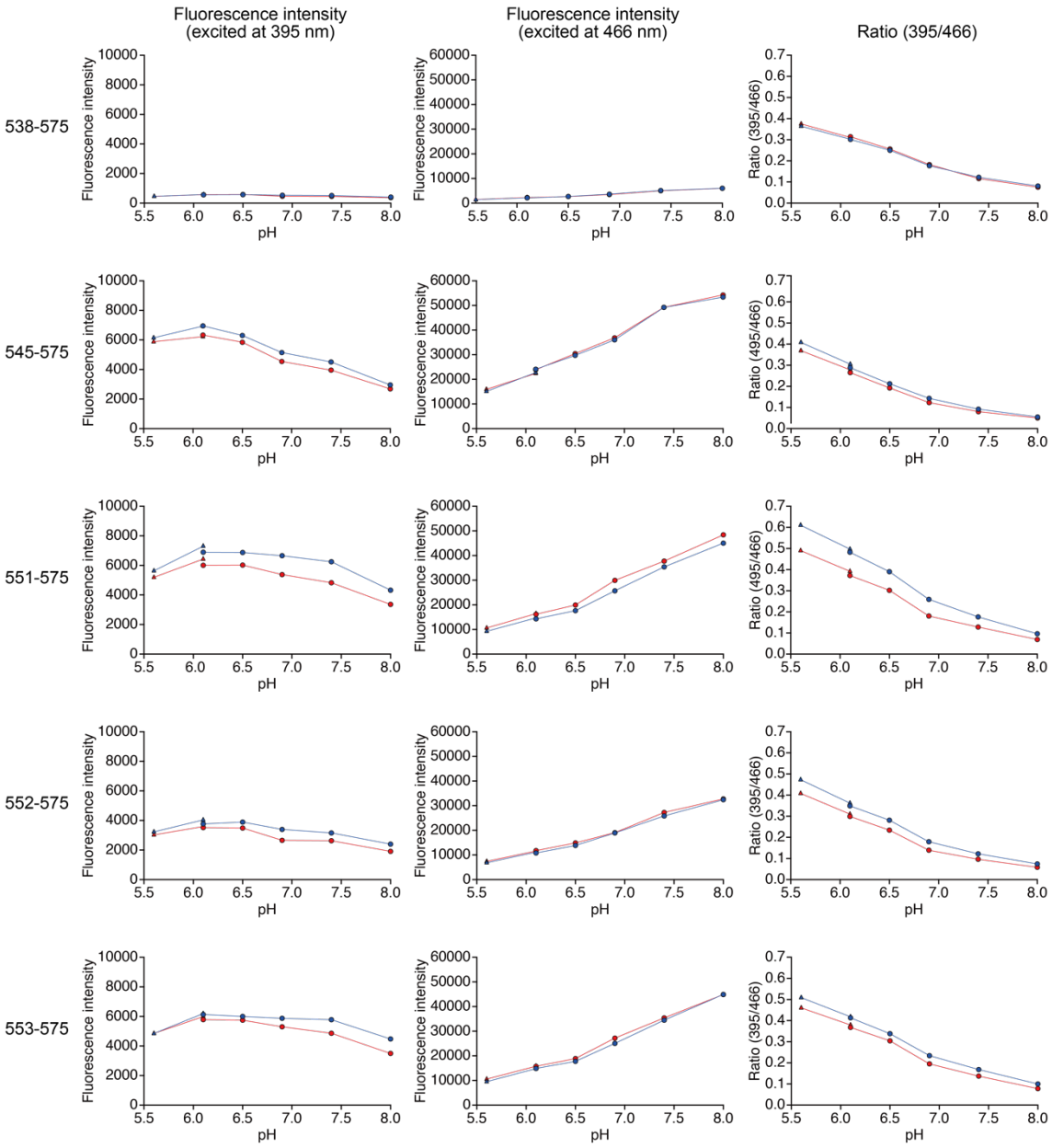

Figure 3.10. Changes of the fluorescence intensity and fluorescence emission ratio upon reduction at pH 5.6 or 6.1 in the buffer containing 100 mM citrate, 500 mM NaCl, 0.005% Tween-20 (plots in triangle) or pH 6.1, 6.5, 6.9, 7.4, or 8.0 in the buffer containing 100 mM phosphate, 500 mM NaCl, 0.005% Tween-20 (plots in circle) of the parent 538-575 and the mutants 545-575, 551-575, 552-575, 553-575, and 548-565 which showed the larger ΔR than 538-575 (left: fluorescence intensity at 510 nm when excited at 395 nm, center: fluorescence intensity at 510 nm when excited at 466 nm, right: the ratios of fluorescence emission intensity excited at 395 nm versus 466nm) in the reduced form (plots on blue) and oxidized form (plots in red). Reduced forms (plots in red) were

prepared by the treatment with DTT at pH 8.0, then diluted 6 times to adjust to each pH value. Oxidized forms (plots in blue) were also prepared with same procedure without DTT. At pH 6.1, two independent data sets with different buffer compositions were shown.

3. 2. 7. The effect of deletion mutation for the NO-sensing segment

The effect of amino acid residues deleted in the mutants on ΔR values were investigated by plotting each ΔR values of mutant against the deleted position at the N-terminal side of C553 (L538 to C553) and the C-terminal side of C558 (L575 to C558) (Figure 3.11). In the N-terminal side of C553, ΔR values seemed to increase with deleting the amino acid residues from the N-terminal to Cys553 with showing the largest ΔR values at N551. Further deletion from N551 caused decrease in ΔR values. On the other hand, deletion from the C-terminal side did not show an obvious tendency on ΔR values. These results indicate that N-terminal side of the segment of TRPC5 is more prone to change the structure of segment than the C-terminal side. Therefore, a simple *in silico* structural optimization alone, such as the one applied in the first screening, is not enough for designing NO sensors exhibiting high ΔR values. The above consideration clearly indicates the necessity of the second *in vitro* screening step to effectively select the mutants that show the high signal response in response to NO.

Interestingly, the mutants 538-558 and 553-575 possessing the shortest segments for the N-terminal side and the C-terminal side showed only moderate ΔR values. Simple deletion of the amino acid residues between the Cys residue and EGFP did not always result an effective transduction of the structural change associated with the disulfide bond formation by C553 and C558. The amino acid sequences between C553 or C558 and EGFP certainly played important roles in transducing the structural change associated with the disulfide bond formation.

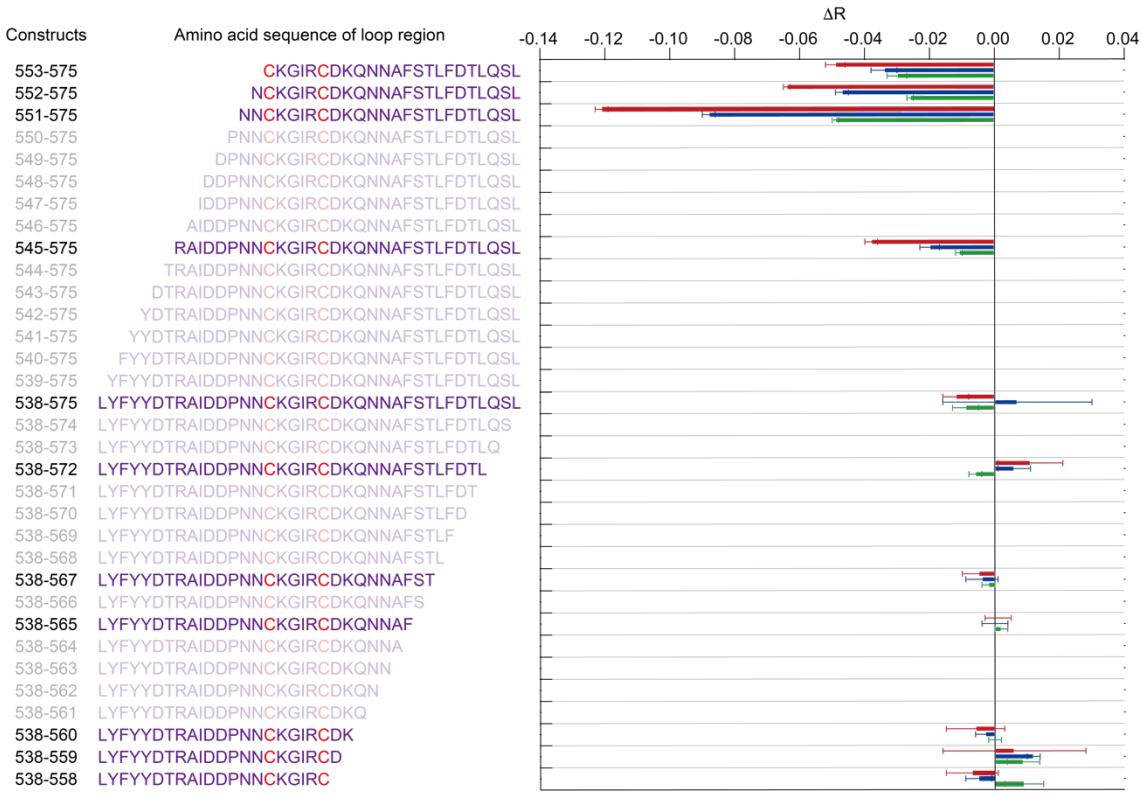

Figure 3.11. ΔR values of the constructed mutants on pH 5, 6, or 7 in the second. *in vitro*, screening were summarized on the same graph. Amino acid sequences of the segment of TRPC5 of deletion mutants from N-terminal to Cys553 and C-terminal from Cys558 were shown, constructed and unconstructed mutants were shown in the deepen and light characters, respectively. Red, blue, and green bars indicated ΔR values on pH 5, 6, and 7, respectively.

3. 3. Conclusions

Deletion of the recognition module of EGFP-TRPC5 enhanced the signal response by efficiently transducing the structural change in the recognition module associated with disulfide bond formation to the structural perturbation of the EGFP chromophore. A two-step screening strategy, *in silico* first and *in vitro* second, was developed to obtain deletion mutants that enhanced the signal response of EGFP-TRPC5. In the first screening, although evaluation of the structural change of recognition module based on RMSD with *in silico* simulations did not always correspond to large signal response, this evaluation

provided 10 candidates from 47 possible mutants. Finally, this screening strategy successfully provided four mutants that enhanced ratiometric signal response than that of the parent EGFP-TRPC5 upon reduction.

3. 4. Materials and methods

3. 4. 1. Materials

Purified oligonucleotide primers for gene construction were purchased from Thermo Fisher Scientific Inc. (Waltham, MA, USA). *E. coli* BL21 (DE3) competent cells were purchased from Invitrogen (Carlsbad, CA). QIAprep Spin Miniprep Kit was purchased from QIAGEN (Tokyo, Japan). His GraviTrap™ column, PD-10 column, HiTrap™ Butyl HP column (5 mL) and HisTrap™ HP column (5 mL) were purchased from GE Healthcare Japan Inc. (Tokyo, Japan). PrimeSTAR HS DNA polymerase, and *E. coli* DH5α competent cells were purchased from TaKaRa Bio Inc. (Shiga, Japan). NOC7 was purchased from DOJINDO LABOLTORIES (Kumamoto, Japan). All the other chemicals were purchased from Wako Chemicals (Osaka, Japan), Tokyo Chemical Industry Co., Ltd (Tokyo, Japan), Sigma-Aldrich Japan (Tokyo, Japan) and Nacalai Tesque (Kyoto, Japan).

3. 4. 2. In silico design of deletion mutants in the first in silico screening

Discovery Studio (version 3.1, Accelrys) was used for *in silico* simulations. EGFP-TRPC5 in the reduced form was designed by embedding the amino acid sequence of Leu538 to Leu575 into EGFP (PDB ID: 2B3P) between Asn144 and Phe145, as described in a previous report.[32] All deletion mutants were simulated based on the structure of EGFP-TRPC5 in the reduced form. Fixed-atom constraints were applied to the EGFP structure. Amino acids in the recognition module were deleted from the structure of EGFP-TRPC5 in the reduced form. Sketches tool was applied to create new peptide bonds between the carbon atom in the N-terminal side and the nitrogen atom at the C-terminal side of the deleted amino acids. Clean geometry tool was applied to each

deletion mutant 10 times to predict sterically acceptable structures just after creating the connection between the carbon and nitrogen atoms. A standard dynamic cascade tool was applied to perform MM and MD calculations on the structures after the application of the clean geometry tool. the structures of the mutants in oxidized form were obtained with same procedure after creating disulfide bonds between the thiols of Cys553 and Cys558.

To compare the structural changes upon formation of disulfide bonds, the obtained structures of each mutant in the reduced and oxidized forms were superimposed by matching the coordinates of the Cα atoms in each residue from L119 to I128, whose residues were opposite to the conformational change domain. RMSD tool was applied to the N-terminal side of Cys553 and the C-terminal side from Cys558 of the loop region containing linker sequences to calculate the RMSD of the differences in coordinates of the backbone of amino acids of each region between the reduced and oxidized forms and estimate the structural changes upon quantitatively forming disulfide bonds. RMSD values of the N-terminal side were plotted against RMSD values of the C-terminal side for each mutant.

3. 4. 3. Construction of plasmids

Plasmids encoding mutants, selected from the *in silico* screening, in which the NO-sensing segment of TRPC5 (L538-L575) was shortened to R545-L575, N551-L575, N552-L575, C553-L575, L538-L572, L538-T567, L538-F565, L538-K560, L538-D559, L538-C558, Y541-L572, R545-L568, or D548-F565 were sequentially constructed. First, the vector encoding EGFP-TRPC5 (L538-L575) was amplified by PCR using primers 1 and 2, 3 and 4, 5 and 6, 7 and 8, 9 and 10, 11 and 12, 13 and 14, 15 and 16, 17 and 18, or 19 and 20 (Table 3.3) to generate deletion mutants, EGFP-TRPC5 (R545-L575), N551-L575, N552-L575, C553-L575, Y538-L572, L538-T567, L538-F565, L538-K560, L538-D559, or L538-C558, respectively, in which one side was deleted from the parent EGFP-TRPC5. The PCR product was treated with *Dpn*I (New England Biolabs Japan) and transformed into *E. coli* DH5α competent cells. Vectors encoding EGFP-TRPC5 (R545-L575), N551-L575, N552-L575, C553-L575, L538-L572, L538-T567, L538-F565, L538-K560, L538-D559, or L538-C558 were purified and sequenced. Plasmids EGFP-TRPC5 (Y541-L572), TRPC5 (R545-L568), and TRPC5 (D548-F565) were constructed using primers 21 and 22, 23 and 24, or 25 and 26 (Table 3.3) to EGFP-TRPC5 (L538-

L572), EGFP-TRPC5 (R545-L575), or EGFP-TRPC5 (L538-F565), respectively, with following the same procedure.

Table 3.3. Nucleotide sequences of primer pairs for construction of an expression vector for deletion mutated derivatives of the structural change domain, TRPC5 (L538-L575).

Primers	from 5' to 3'
Primer 1(F_545-575)	CAAGCTTCGAGCCATTGATGATCCG
Primer 2 (R_545-575)	TGGCTCGAAGCTTGCCGTTGTACTC
Primer 3 (F_551-575)	CAAGCTTAATAATTGCAAGGGCATT
Primer 4 (R_551-575)	AATTATTAAGCTTGCCGTTGTACTC
Primer 5 (F_552-575)	CAAGCTTAATTGCAAGGGCATTCGA
Primer 6 (R_552-575)	TGCAATTAAGCTTGCCGTTGTACTC
Primer 7 (F_553-575)	CAAGCTTTGCAAGGGCATTCGATGC
Primer 8 (R_553-575)	CCTTGCAAAGCTTGCCGTTGTACTC
Primer 9 (F_538-572)	TACGCTCGGATCCGGCTTTAACAGC
Primer 10 (R_538-572)	CGGATCCGAGCGTATCGAACAGCGT
Primer 11 (F_538-567)	CTCGACGGGATCCGGCTTTAACAGC
Primer 12 (R_538-567)	CGGATCCCGTCGAGAAGGCATTATT
Primer 13 (F_538-565)	TGCCTTCGGATCCGGCTTTAACAGC
Primer 14 (R_538-565)	CGGATCCGAAGGCATTATTCTGCTT
Primer 15 (F_538-560)	CGATAAGGGATCCGGCTTTAACAGC
Primer 16 (R_538-560)	CGGATCCCTTATCGCATCGAATGCC
Primer 17 (F_538-559)	ATGCGATGGATCCGGCTTTAACAGC
Primer 18 (R_538-559)	CGGATCCATCGCATCGAATGCCCTT
Primer 19 (F_538-558)	TCGATGCGGATCCGGCTTTAACAGC
Primer 20 (R_538-558)	CGGATCCGCATCGAATGCCCTTGCA
Primer 21 (F_541-575)	CAAGCTTTATTATGATACCCGAGCC
Primer 22 (R_541-575)	CATAATAAAGCTTGCCGTTGTACTC
Primer 23 (F_538-568)	GACGCTGGGATCCGGCTTTAACAGC
Primer 24 (R_538-568)	CGGATCCCAGCGTCGAGAAGGCATT
Primer 25 (F_548-575)	CAAGCTTGATGATCCGAATAATTGC

Primer 26 (R_548-575)	GATCATCAAGCTTGCCGTTGTACTC

3. 4. 4. Expression and purification of proteins

Plasmids encoding the 13 mutants were transformed into *E. coli* BL21 (DE3) competent cells.

For partial purification for *in vitro* screening, the transformed cells were grown at 37 °C until the OD_{600} reached 0.6-0.8, and protein expression was induced with 1 mM IPTG for 24 h at 25 °C. The soluble fractions of the cell lysates containing the target proteins were loaded onto a His GraviTrap^{TM} column with 60 mM imidazole in 50 mM phosphate and 500 mM NaCl (pH 8.0) and eluted with 100 mM imidazole, 50 mM phosphate, and 500 mM NaCl (pH 8.0). Each elution sample containing each target protein was collected and loaded onto a PD-10 column equilibrated with 100 mM phosphate and 0.005% Tween-20 (pH 8.0).

3. 4. 5. Measurement of the fluorescence intensity change upon reduction in the second *in vitro* screening

After PD-10 treatment, mutants were reduced in a solution containing 100 mM phosphate, 0.005% Tween 20, and 1 mM DTT (pH 8.0) for 2 h at 25 °C. The reduced solutions were diluted six times to shift the pH to 5.6 or 6.1 with buffer containing 100 mM citrate, 500 mM NaCl, and 0.005% Tween20 (pH 5.5 or 5.9) or to 6.1, 6.5, 6.9, 7.4, or 8 with buffer containing 100 mM phosphate, 500 mM NaCl, and 0.005% Tween20 (pH 5.8, 6.3, 7.0, 7.3, or 8.0). Oxidized solutions were prepared using the same procedure but without DTT treatment. The emission spectra of the reduced and oxidized solutions were measured by excitation at 395 nm and 466 nm with an Infinite M200 PRO (TECAN, Zürich, Switzerland) at 20 °C. The fluorescence emission ratios were calculated by dividing the fluorescence intensity at 510 nm, excited at 395 nm, and 466 nm.

3. 5. References

1. Palmer AE, Qin Y, Park JG, McCombs JE. Design and application of genetically encoded biosensors. Trends Biotechnol. 2011;29:144-152.
2. Wenfeng L, Deng M, Yang C, Liu F, Guan X, Du Y, Wang L, Chu J. Genetically encoded single circularly permuted fluorescent protein-based intensity sensors. J. Phys. D: Appl. Phys. 2020;53:113001
3. Tallini YN, Ohkura M, Choi BR, Ji G, Imoto K, Doran R, Lee J, Plan P, Wilson J, Xin HB, Sanbe A, Gulick J, Mathai J, Robbins J, Salama G, Nakai J, Kotlikoff MI. Imaging cellular signals in the heart *in vivo*: Cardiac expression of the high-signal Ca^{2+} indicator GCaMP2. Proc. Natl. Acad. Sci. U. S. A. 2006;103:4753-4758.
4. Zhang J, Campbell RE, Ting AY, Tsien RY. Creating new fluorescent probes for cell biology. Nat. Rev. Mol. Cell Biol. 2002;3:906-918.
5. Berg J, Hung YP, Yellen G. A genetically encoded fluorescent reporter of ATP:ADP ratio. Nat. Methods. 2009;6:161-166.
6. Nakai J, Ohkura M, Imoto K. A high signal-to-noise Ca^{2+} probe composed of a single green fluorescent protein. Nat. Biotechnol. 2001;19:137-141.
7. Nagai T, Sawano A, Park ES, Miyawaki A. Circulary permutated green fluorescent proteins engineered to sense Ca^{2+}. Proc. Natl. Acad. Sci. U. S. A. 2001;98:3197-3202.
8. Kitaguchi T, Oya M, Wada Y, Tsuboi T, Miyawaki A. Extracellular calcium influx activates adenylate cyclase 1 and potentiates insulin secretion in MIN6 cells. Biochem. J. 2013;450:365-373.
9. Qin Y, Sammond DW, Braselmann E, Carpenter MC, Palmer AM. Development of an Optical Zn^{2+} Probe Based on a Single Fluorescent protein. ACS Chem. Biol. 2016;11:2744-2751.
10. Matsuda S, Harada K, Ito M, Takizawa M, Wongso D, Tsuboi T, Kitaguchi T. Generation of cGMP indicator with an Expanded Dynamic Range by Optimization of Amino Acid Linkers between a Fluorescent Protein and PDE5α. ACS Sens. 2017;2:46-51.
11. Tainaka K, Sakaguchi R, Hayashi H, Nakano S, Liew FF, Morii T. Design strategies of fluorescent biosensors based on biological macromolecular receptors. Sensors 2010;10:1355-1376.

12. Nakata E, Liew FF, Nakano S, Morii T. Recent Progress in the construction methodology of fluorescent biosensors based on biomolecules. Biosensors-Emerging materials and Applications. Serra, P. A. Ed. pp. 123-140 (2011)
13. Marvin JS, Borghuis BG, Tian L, Cichon J, Harnett MT, Akerboom J, Gordus A, Renninger SL, Chen TW, Bargmann CI, Orger MB, Schreiter ER, Demb JB, Gan WB, Hires SA, Looger LL. An optimized fluorescent probe for visualizing glutamate neurotransmission. Nat. Methods 2013;10:162-170.
14. Patriarchi T, Cho JR, Merten K, Howe MW, Marley A, Xiong WH, Folk RW, Broussard GJ, Liang R, Jang MJ, Zhong H, Dombeck D, von Zastrow M, Nimmerjahn A, Gradinaru V, Williams JT, Tian L. Ultrafast neuronal imaging of dopamine dynamics with designed genetically encoded sensors. Science 2018;360:eaat4422.
15. Jing M, Zhang P, Wang G, Feng J, Mesik L, Zeng J, Jiang H, Wang S, Looby JC, Guagliardo NA, Langma LW, Lu J, Zuo Y, Talmage DA, Role LW, Barrett PQ, Zhang LI, Luo M, Song Y, Zhu JJ, Li Y. A genetically encoded fluorescent acetylcholine indicator for *in vitro* and *in vivo* studies. Nat. Biotechnol. 2018;36:726-737.
16. Marvin JS, Shimoda Y, Magloire V, Leite M, Kawashima T, Jensen TP, Kolb I, Knott EL, Novak O, Podgorski K, Leidenheimer NJ, Rusakov DA, Ahrens MB, Kullman DM, Looger L. L. A genetically encoded fluorescent sensor for *in vivo* imaging of GABA. Nat. Methods 2019;16:763-770.
17. Yoshida T, Inoue R, Morii T, Takahashi N, Yamamoto S, Hara Y, Tominaga M, Shimizu S, Sato Y, Mori Y. Nitric oxide activates TRP channels by cysteine S-nitrosylation. Nat. Chem. Biol. 2006;2:596-607.
18. Tajima S, Nakata E, Sakaguchi R, Saimura M, Mori Y, Morii T. Fluorescence detection of the nitric oxide-induced structural change at the putative nitric oxide sensing segment of TRPC5. Bioorg. Med. Chem. 2020;28:115430.
19. Pédelacq JD, Cabantous S, Tran T, Terwilliger TC, Waldo GS. Engineering and characterization of a superflolder green fluorescent protein. Nat. Biotechnol. 2006;24:79-88.
20. Elsliger MA, Wachter RM, Hanson GT, Kallio K, Remington J. Structural and Spectral Response of Green Fluorescent Protein Variants to Changes in pH. Biochemistry 1999;38:5296-5301.

Chapter 4
Evaluation of selectivity and kinetics of the putative fluorescence NO sensors

4. 1. Introduction

Nitric oxide (NO) is the cell signaling molecule that controls diverse biological functions, such as cardio vascular[1,2], nervous[3,4] and immune systems.[5] The tumor cell signaling[6], plant physiology, such as stomatal closure, growth, and development[7], and cellular morphology[8] are also found to be controlled by cellular NO dynamics. Because of its high reactivity, NO regulates the functions of many proteins via post-translational modifications, such as S-nitrosylation of the side-chain of cysteine[3,8,9] or by regulating the metal ion binding of metalloproteins.[10-12] The genetically encoded biosensors based on the AFP are a useful tool to explore the cellular behavior of biomolecules because it is autonomously expressed in the cell by simple transfection of a plasmid encoding the fluorescent sensor and maintained upon cell growth or cell division.[13-15] Due to the biological importance of cellular NO dynamics, there are increasing demands on the development of genetically encoded NO sensors. The first example of AFP based genetically encoded NO sensor detected endogenous NO production in living cells, but it required the addition of relatively high concentration of iron (II) that could cause toxicity in the cell.[16]

As described in chapter 2, EGFP-TRPC5 was designed to evaluate the structural change of the putative NO-sensing segment of TRPC5, Leu538-Leu575, associated with the S-nitrosylation and successive disulfide bond formation. EGFP-TRPC5 shows characteristic response to NO that (1) forms disulfide bond to show increasing ratio of emission intensity, and (2) requires no additive cofactor to exert an expected fluorescence

emission change upon reaction to NO. Thus EGFP-TRPC5 provides a promising prototype of the genetically encoded NO sensors albeit only slightly signal response. As described in chapter 3, a facile two-step screening was conducted for the enhancement of the signal responses of EGFP-TRPC5. As a result, three mutants, 551-575, 552-575, and 553-575, successfully showed 2-4 times enhancement of fluorescence emission ratio (ΔR) upon the disulfide bond cleavage compared to the parent EGFP-TRPC5. Therefore, further investigation of these three mutants 551-575, 552-575, or 553-575 had possibility to show that they are applicable as genetically encoded NO biosensors requiring no additives.

In this chapter, further investigation of the properties of NO sensor candidates 551-575, 552-575, and 553-575 were conducted to confirm whether three NO sensor candidates 551-575, 552-575, or 553-575 could work as the NO biosensor. It was confirmed that these NO candidates were potentially applicable as a genetically encoded NO sensor, its lack of the specificity to NO and H_2O_2 has to be compensated by a simultaneous usage of specific H_2O_2 sensor.

4. 2. Results and discussions

4. 2. 1. Purification and identification of the NO sensor candidates 551-575, 552-575, and 553-575

As described in chapter 3, three NO sensor candidates 551-575, 552-575, and 553-575 showed 2 to 4 times larger signal change than the parent EGFP-TRPC5. To investigate whether the NO sensor candidates 551-575, 552-575, and 553-575 could detect NO by forming disulfide bonds, the R values and contents of the free thiol group of these three NO sensor candidates upon reaction with NO were evaluated.

These NO sensor candidates 551-575, 552-575, and 553-575 were purified in the same manner as that described in the chapter 2 for the parent EGFP-TRPC5 (Figure 4.1).[17] These NO sensor candidates showed over 95% purity in SDS-PAGE analyses (Figure 4.1A). The samples were characterized by MALDI-TOF mass spectroscopy (see the experimental section). The UV-Vis absorption spectra indicated two absorption maxima

at approximately 395 nm and 490 nm (Figure 4.1B). The excitation spectra showed two excitation maxima at approximately 395 nm and 466 nm when emitted at 509 nm (Figure 4.1C). The emission spectra of these NO sensor candidates excited at 395 nm and 466 nm showed an emission peak at 509 nm (Figure 4.1D and 4.1E). These optical properties of the NO sensor candidates were comparable to those of the parent EGFP-TRPC5. [17]

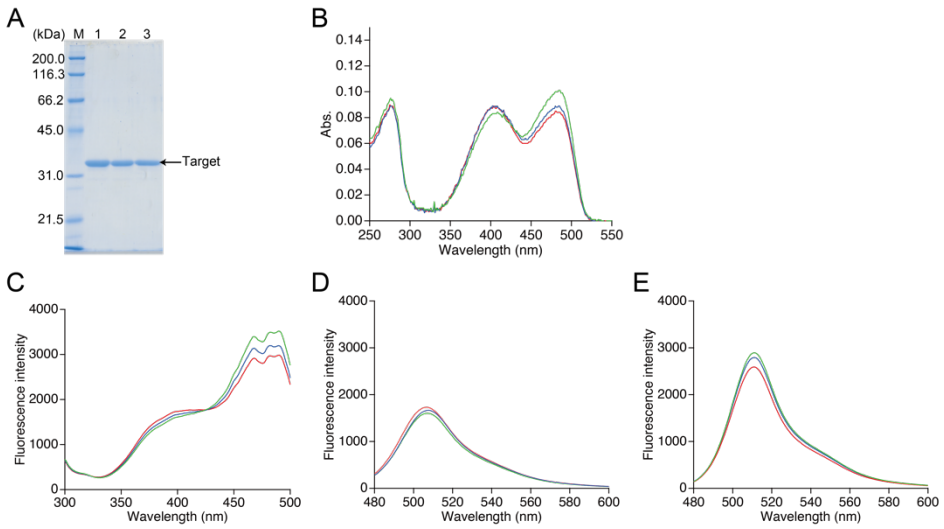

Figure 4.1. Gel electrophoresis and spectroscopic characterization of the purified NO sensor candidates 551-575, 552-575, and 553-575. (A) SDS-PAGE analysis of purified NO sensor candidates. M: molecular marker (6,500-200,000), lane 1: purified 551-575, lane 2: purified 552-575, lane 3: purified 553-575. (B) UV-Vis absorption spectra, (C) excitation spectra emitted at 509 nm and (D, E) emission spectra excited at (D) 395 nm or (E) 466 nm of the NO sensor candidates 551-575 (red line), 552-575 (blue line), and 553-575 (green line).

4. 2. 2. Changes of the fluorescence emission ratios upon reduction of the NO sensor candidates

The free thiol group contents in purified 551-575, 552-575, and 553-575 evaluated using the DTNB method were less than 10%, 13%, and 11%, respectively. It should be noted that the two cysteine residues, Cys49 and Cys71, in the original EGFP were substituted with Ser49 and Val71, respectively, as described in a chapter 2 (Figure 4.2).[17] Thus, these results indicate that most Cys553 and Cys558 residues in the TRPC5 partial segment of the purified NO sensor candidates formed disulfide bonds. Next, correlations between the fluorescence emission ratio (R) and the contents of free thiol groups were investigated. These NO sensor candidates were reduced with DTT, and excess DTT was removed using size exclusion chromatography. The free thiol group contents of the NO sensor candidates 551-575, 552-575, and 553-575 were then determined to be 100% in the reduced form (Table 4.1). The change in fluorescence emission upon disulfide bond cleavage was analyzed by comparing the fluorescence spectra of the reduced and oxidized forms (Figure 4.3). When excited at 395 nm, the fluorescence emission intensity at 509 nm of the NO sensor candidates 551-575 and 552-575 decreased for the reduced form compared to that in the oxidized form, and that of the NO sensor candidate 553-575 did not change upon disulfide bond cleavage. The emission intensity at 509 nm increased for the reduced form of all NO sensor candidates when excited at 466 nm. The R values decreased to 31%, 20%, and 14% for NO sensor candidates 551-575, 552-575, and 553-575, respectively, which were slightly lower than those observed during the *in vitro* screening as described in a chapter 3. Among them, the NO sensor candidate 551-575 showed four times larger change in the fluorescence emission ratio compared to that of the parent EGFP-TRPC5 (a decrease of 8%).

551-575

EGFP(1-144) TRPC5(551-575) EGFP(145-238)

```
1       MVSKGEELFT GVVPILVELD GDVNGHKFSV RGEGEGDATN GKLTLKFIST
51      TGKLPVPWPT LVTTLTYGVQ VFSRYPDHMK QHDFFKSAMP EGYVQERTIS
101     FKDDGTYKTR AEVKFEGDTL VNRIELKGID FKEDGNILGH KLEYNGKLNN
151     CKGIRCDKQN NAFSTLFDTL QSLGSGFNSH NVYITADKQK NGIKANFKIR
201     HNVEDGSVQL ADHYQQNTPI GDGPVLLPDN HYLSTQSVLS KDPNEKRDHM
251     VLLEFVTAAG ITLGMDELYK GGTGGSLEHH HHHH
```

552-575

EGFP(1-144) TRPC5(552-575) EGFP(145-238)

```
1       MVSKGEELFT GVVPILVELD GDVNGHKFSV RGEGEGDATN GKLTLKFIST
51      TGKLPVPWPT LVTTLTYGVQ VFSRYPDHMK QHDFFKSAMP EGYVQERTIS
101     FKDDGTYKTR AEVKFEGDTL VNRIELKGID FKEDGNILGH KLEYNGKLNC
151     KGIRCDKQNN AFSTLFDTLQ SLGSGFNSHN VYITADKQKN GIKANFKIRH
201     NVEDGSVQLA DHYQQNTPIG DGPVLLPDNH YLSTQSVLSK DPNEKRDHMV
251     LLEFVTAAGI TLGMDELYKG GTGGSLEHHH HHH
```

553-575

EGFP(1-144) TRPC5(553-575) EGFP(145-238)

```
1       MVSKGEELFT GVVPILVELD GDVNGHKFSV RGEGEGDATN GKLTLKFIST
51      TGKLPVPWPT LVTTLTYGVQ VFSRYPDHMK QHDFFKSAMP EGYVQERTIS
101     FKDDGTYKTR AEVKFEGDTL VNRIELKGID FKEDGNILGH KLEYNGKLCK
151     GIRCDKQNNA FSTLFDTLQS LGSGFNSHNV YITADKQKNG IKANFKIRHN
201     VEDGSVQLAD HYQQNTPIGD GPVLLPDNHY LSTQSVLSKD PNEKRDHMVL
251     LEFVTAAGIT LGMDELYKGG TGGSLEHHHH HH
```

Figure 4.2. Illustrations and amino acid sequences of NO sensor candidates 551-575, 552-575, and 553-575. Green, purple, blue, and red colors indicated the amino acid sequences derived from EGFP, the segments of TRPC5, linker, and cysteine residues of the segments of TRPC5, respectively.

Table 4.1. Free thiol content of mutants 551-575, 552-575, and 553-575 upon reduction.

Conditions	Constructs		
	551-575	552-575	553-575
Without DTT	< 10%	< 13%	< 11%
With 1 mM DTT	100%	100%	100%

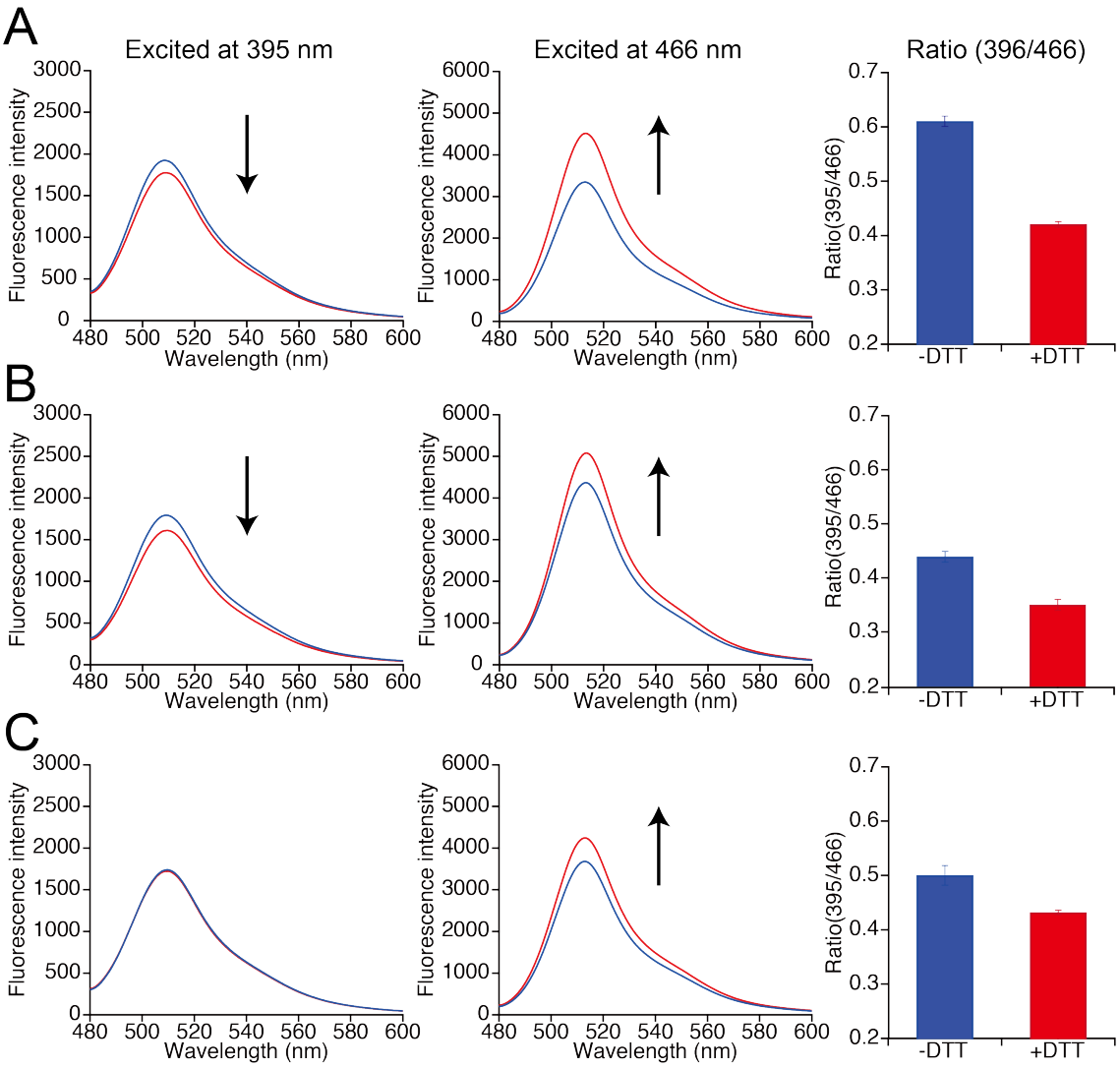

Figure 4.3. Spectral changes upon reduction of disulfide bonds in NO sensor candidates (A) 551-575, (B) 552-575, and (C) 553-575 with DTT. Left: emission spectra when excited at 395 nm; center: emission spectra when excited at 466 nm; right: R values in reduced (blue) and oxidized (red) forms. R values were calculated by dividing the fluorescence intensity at 535 nm excited at 395 nm with that excited at 466 nm.

4. 2. 3. NO sensing of the NO sensor candidates obtained from a two-step screening

Next, the responses of the NO sensor candidates 551-575, 552-575, and 553-575 in reduced form to NO were evaluated. Upon the DTT reduction, the free thiol contents of the NO sensor candidates 551-575, 552-575, and 553-575 were determined to be 100%, 71%, and 74%, respectively, using DTNB quantitation (Table 4.2). The R values of the reduced NO sensor candidates were lower than those of their respective oxidized forms (Figure 4.4). The reduced NO sensor candidates were treated with the NOC7 as a NO donor.[18] In the presence of NOC7 (500 μM), all the NO sensor candidates showed higher R values than the respective reduced form (Figure 4.4). The free thiol contents of the NO sensor candidates were drastically decreased to 11% or less than 10% after the reaction with NO (500 μM NOC7) (Table 4.2). These results indicate that the NO sensor candidates 551-575, 552-575, and 553-575 show higher signal responses than the parent EGFP-TRPC5 to NO with the reaction of their thiol groups in a ratiometric manner. To confirm the reaction pathway for disulfide bond formation upon reaction with NO, the presence of an S-nitrosylated thiol group as an intermediate of disulfide bond formation was evaluated by treatment with ascorbic acid that selectively reduces the S-nitrosylated thiol group in the presence of disulfide bond, as described in chapter 2.[17,19] The free thiol contents of these NO sensor candidates after the 4.5 h reaction in 551-575 and 2.5 h reaction in 552-575 and 553-575 with NO were similar or did not change upon treatment with ascorbic acid (5 mM) (Table 4.2). This result indicates that almost all cysteine residues in these NO sensor candidates reacted with NO, forming a disulfide bond without preserving the S-nitrosylated form. The reaction of NO sensor candidate 551-575 with NO was also analyzed at an early stage to verify the formation of S-nitrosyl cysteine. After reaction with NO for 30 min, the free thiol content of NO sensor candidate 551-575 was 43%, which was increased to 52% upon treatment with ascorbic acid (5 mM) (Table 4.1). Although the results suggest the presence of S-nitrosylated cysteine (9%), almost all the S-nitrosylated cysteine residues in 551-575 were converted to the disulfide bond form after 30 min, suggesting that disulfide bond formation was faster than the S-nitrosylation reaction. These results indicate that the increase in the signal response of these NO sensor candidates was the outcome of disulfide bond formation upon reaction with NO (500 μM NOC7), with little contribution from the S-nitrosyl cysteine group to detect NO in a ratiometric manner.

Table 4.2.

Contents of free thiol of the NO sensor candidates 551-575, 552-575, and 553-575 upon reduction and reaction to NO

Conditions	Constructs			
	551-575		552-575	553-575
	30 min	230 min	150 min	150 min
Without DTT	< 10%		< 13%	< 11%
With 1 mM DTT	100%		71 ± 2%	74 ± 2%
With 500 μM NOC7	43 ± 3%	11 ± 1%	< 10%	< 10%
With 5 mM ascorbic acid	52 ± 3%	15 ± 3%	< 10%	< 10%

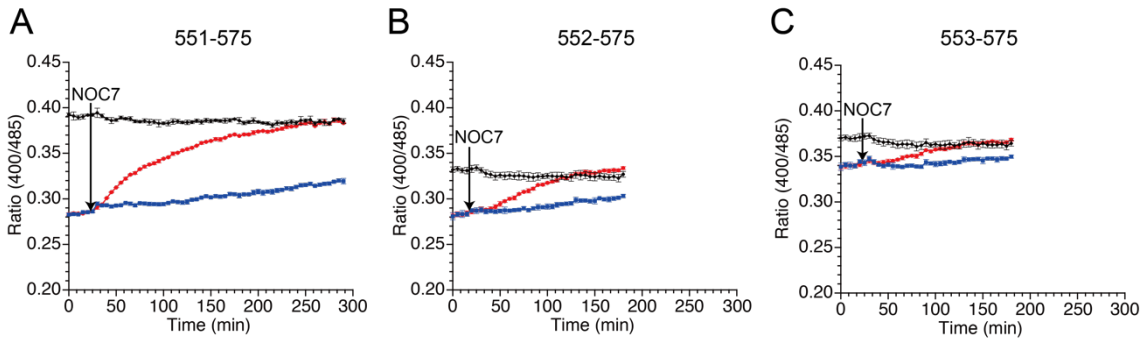

Figure 4.4. Time course changes in R values of NO sensor candidates (A) 551-575, (B) 552-575, and (C) 553-575 in the presence of NO (500 μM NOC7). R values were calculated by dividing the fluorescence intensity at 535 nm excited at 400 nm with that excited at 485 nm. Reduced (blue and red) and oxidized (black) forms were treated with (red and black) or without (blue) NOC7 (500 μM) between 25 to 30 min.

4. 2. 4. The selectivity of the NO sensor candidates 551-575, 552-575, and 553-575

The wild-type TRPC5 responds more rapidly to NO over H_2O_2[20], but the parent EGFP-TRPC5 reacted to H_2O_2 as well.[17] The responses of the NO sensor candidates 551-575, 552-575 and 553-575 to H_2O_2 were also evaluated. After preparation of the reduced form of these NO sensor candidates in the same manner, fluorescence emission in the presence of H_2O_2 (500 μM) was measured (Figure 4.5). The R values of all NO sensor candidates in the reduced forms increased to those of the respective oxidized forms

(Figure 4.5), and the free thiol group content decreased to less than 11% for all NO sensor candidates (Table 4.3). These results indicate that NO sensor candidates 551-575, 552-575, and 553-575 also detected H_2O_2 in a ratiometric manner by forming disulfide bonds. These results are consistent with those of the parent EGFP-TRPC5.

Table 4.3.

Contents of free thiol of the NO sensor candidates 551-575, 552-575, and 553-575 upon reduction and reaction to H_2O_2

Conditions	Constructs		
	551-575	552-575	553-575
Without DTT	< 10%	< 13%	< 11%
With 1 mM DTT	100%	100%	100%
With 500 μM H_2O_2	< 11%	< 10%	< 10%

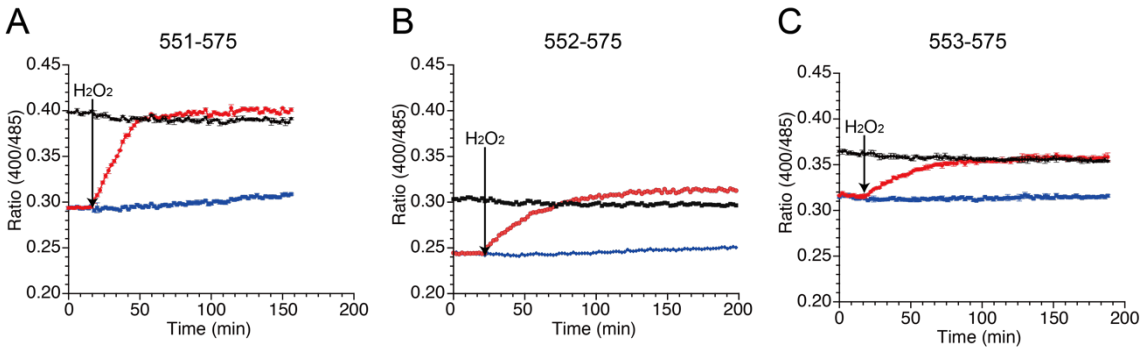

Figure 4.5. Time course changes in R values of NO sensor candidates (A) 551-575, (B) 552-575, and (C) 553-575 in the presence of H_2O_2 (500 μM). R values were calculated by dividing the fluorescence intensity at 535 nm excited at 400 nm with that excited at 485 nm. Reduced (blue and red) and oxidized (black) forms were treated with (red and black) or without (blue) H_2O_2 (500 μM) between 16 to 18 min.

4. 2. 5. Estimation of the kinetics of the NO sensor candidates 551-575, 552-575, and 553-575

To compare the kinetics and the specificity of the NO sensor candidates 551-575, 552-575, and 553-575, and the parent EGFP-TRPC5 for the reaction with NO and H_2O_2[17], the half-maximum times of the reactions, defined as the time when R values reach half their maximum values, were estimated (Table 4.4 and Figure 4.6, 4.7, and 4.8). Comparison of the half-maximum times upon reaction with NO and H_2O_2 within the same construct shows that the one to 500 μM H_2O_2 was faster than that to NO (500 μM NOC7) for all constructs, indicating that they were more prone to react with H_2O_2 than the original TRPC5. Furthermore, the half-maximum times of NO sensor candidates 551-575, 552-575, and 553-575 were three to five times larger than that of the parent EGFP-TRPC5. Based on the fact that the S-nitrosylation step was slower than the disulfide bond formation step (Table 4.2), the S-nitrosylation step, not the disulfide bond formation step, in these NO sensor candidates was slower than that in the parent EGFP-TRPC5. A shift in the pKa of cysteines to a basic pH in these NO sensor candidates could decrease the S-nitrosylation rate of the thiolate group.

Table 4.4.

The half-maximum times (min) of each construct upon reaction to NO and H_2O_2.

Constructs	[NOC7]	[H_2O_2]		
	500 μM	100 μM	250 μM	500 μM
538-575	8 ± 1	19 ±1	11 ± 1	4 ± 1
551-575	33 ± 2	54 ± 2	N.D.[1)]	13 ± 1
552-575	38 ± 3	>48	30 ± 1	17 ± 1
553-575	44 ± 5	>58	37 ± 3	19 1

[1)]No data.

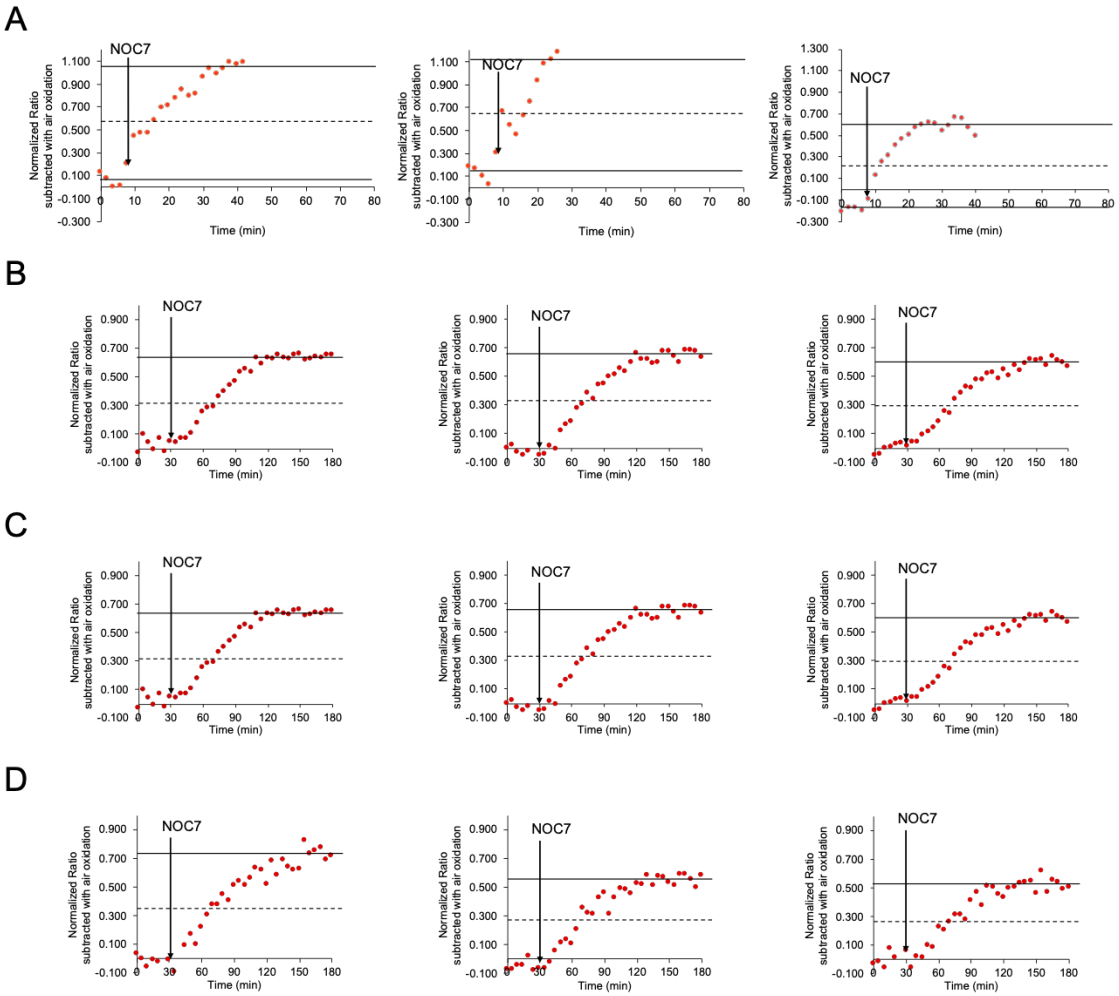

Figure 4. 6. Time course changes of the normalized ratios subtracted with air oxidation in addition of 500 μM NOC7 of (A) EGFP-TRPC5. (B) 551-575. (C) 552-575. (D) 553-575. Solid lines indicated the maximum or minimum values upon reaction. Dot lines indicated the half values of the maximum values. Each graph indicates result of each sample.

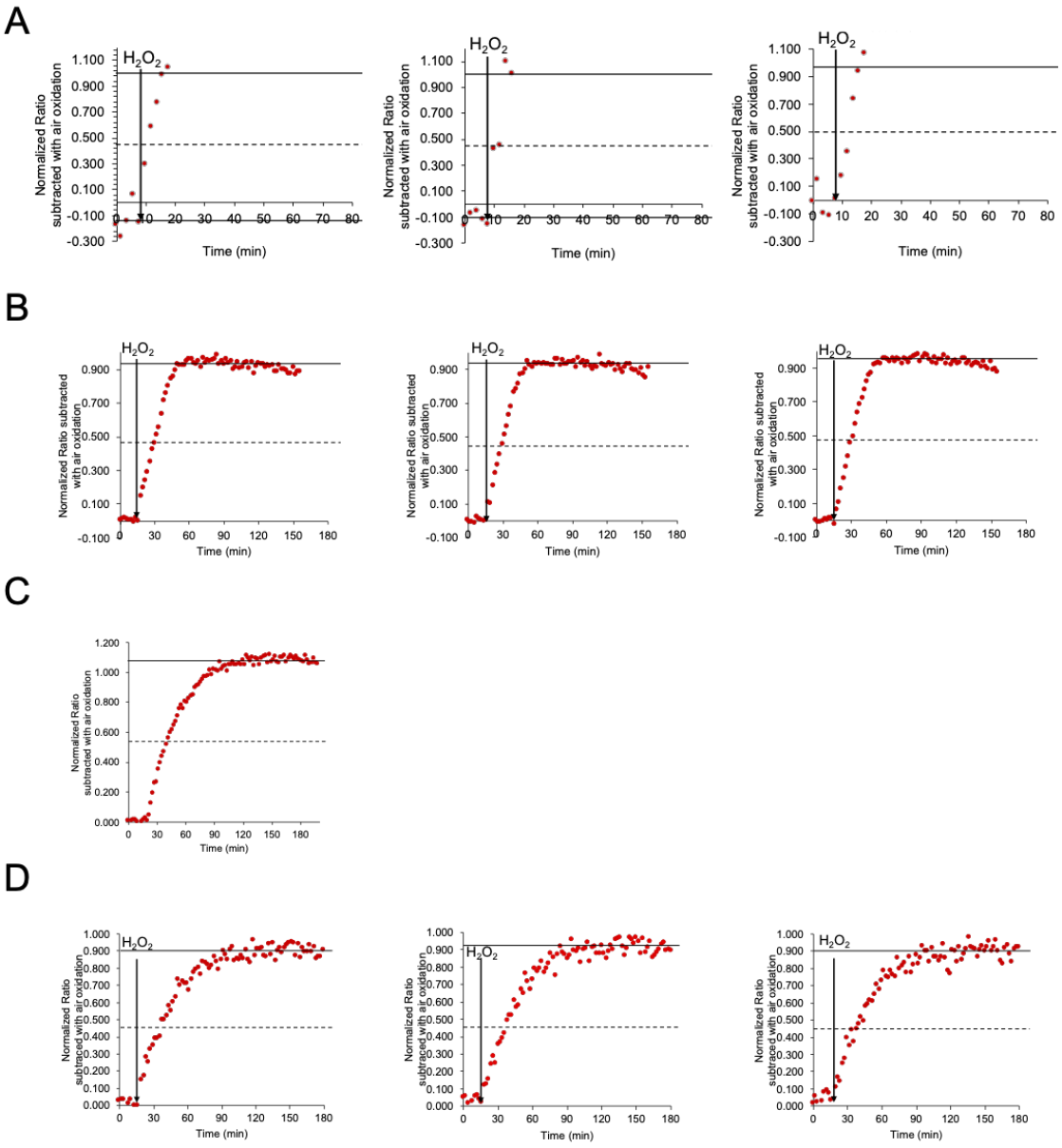

Figure 4. 7. Time course changes of the normalized ratio subtracted with air oxidation in addition of 500 μM H_2O_2 of (A) EGFP-TRPC5. (B) 551-575. (C) 552-575. (D) 553-575. Solid lines indicated the maximum and minimum values upon reaction. Dot lines indicated the half values of the maximum values. Each graph indicates result of each sample.

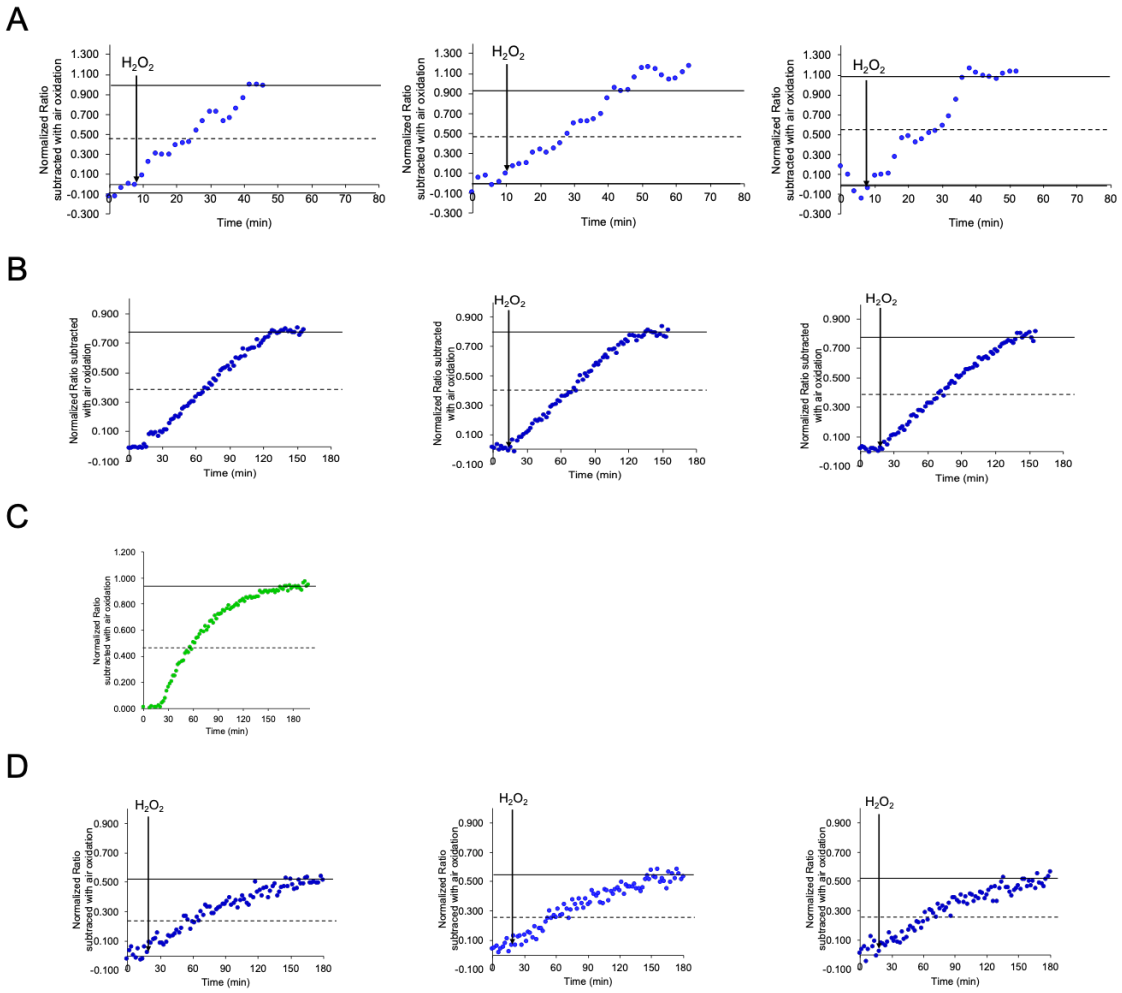

Figure 4. 8. Time course changes of the normalized ratio subtracted with air oxidation in addition of 100 μM H_2O_2 of (A) EGFP-TRPC5. (B) 551-575. (C) 552-575. (D) 553-575. Solid lines indicated the maximum and minimum values upon reaction. Dot lines indicated the half values of the maximum values. Each graph indicates result of each sample.

4. 2. 6. Structural investigation of the NO-sensing segment of TRPC5

Wild-type TRPC5 expressed in human embryonic kidney (HEK) cells showed specific reaction to NO (10 μM SNAP as an NO donor) over 100 μM H_2O_2.[20] As described in the chapter 2, the parent EGFP-TRPC5 containing the putative NO sensing segment did not show the specificity to NO over H_2O_2. The NO sensor candidates 551-575, 552-575, and 553-575, which contained the partial segments of TRPC5, N551-L575, N552-L575, and C553-L575, as the sensing module, respectively, also reacted almost equally to H_2O_2 and NOC7 at the same concentration. The kinetics characteristics of the NO sensor candidates 551-575, 552-575, and 553-575 to NO or H_2O_2 (Table 4.4) were similar to those of the parent EGFP-TRPC5, indicating that the N-terminal side of the TRPC5 partial segment L538-N552 is not crucial for the TRPC5 specificity to NO. The Cryo-EM structure[21] shows the partial segment L538-L575 is located in the extracellular region near the plasma membrane (Figure 4.9, represented in purple). The C-terminal side of this segment is likely buried in the plasma membrane. In contrast, the N-terminal side of the partial segment resides on TRPC5, exposing most of its part outside the plasma membrane. Further information on the surface charge and surface hydrophobicity of the TRPC5 partial segment L538-N575 were obtained from the Cryo-EM structure (Figure 4.9B and 4.9C). In the side view, the transmembrane region shows lower charge density and higher hydrophobicity than those of the extracellular region corresponding to the N-terminal side of partial segment L538-N552. In the top view, the surface charge density and hydrophilicity around the partial segment L538-L575 seemed to decrease from the top of the partial segment, corresponding to the N-terminal side, to the bottom of the partial segment, corresponding to the C-terminal side in the transmembrane domain. The hydrophilicity and charge density of N-terminal side of the partial segment, L538-N552, would play small role in accumulation of NO. Although the C-terminal side of the partial segment partly showed hydrophobicity and charged characteristics compared to those of the N-terminal side, the hydrophobic transmembrane domain would reinforce the accessibility of NO over H_2O_2 to the NO-sensing region.

The larger half-maximum times of the NO sensor candidates 551-575, 552-575, 553-575 compared to that of the parent EGFP-TRPC5 suggest that the pKa of thiol group in Cys553 or Cys558 would shift to the acidic side upon the deletion of the N-terminal side of the partial segment, L538-N552. The pKa of the thiol group is modulated by the

interaction with positive amino acid residues.[19] However, because of the presence of both positively and negatively charged residues surround Cys553 and Cys558. as observed in the surface charge distribution of L538-L575 (Figure 4.10), a clear insight into the effect of amino acid residue(s) on the shift of pKa remained to be obtained. Alternatively, the pKa shift of the cysteine thiol groups would not reflect the effect of amino acid residue(s) of TRPC5 in nature, but take place only in constructs where extracted NO-sensing segment of TRPC5 was embedded to EGFP and exposed to the solution.

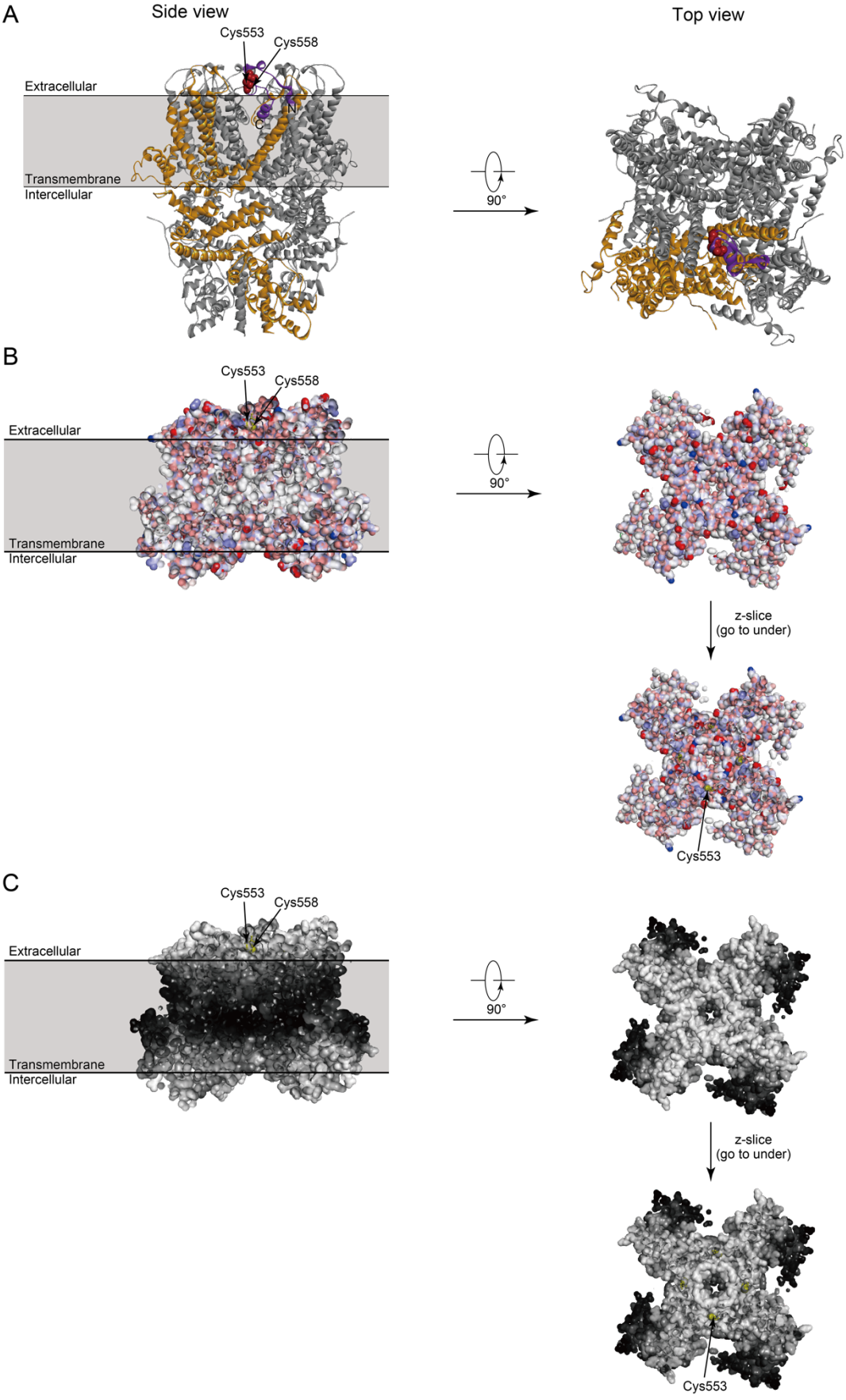
A
Side view
Top view
Cys553
Cys558
Extracellular
Transmembrane
Intercellular
N
C
90°
B
Cys553
Cys558
Extracellular
Transmembrane
Intercellular
90°
z-slice
(go to under)
Cys553
C
Cys553
Cys558
Extracellular
Transmembrane
Intercellular
90°
z-slice
(go to under)
Cys553

Figure 4.9. (A) A Side view (left) and top view (right) of Cryo-EM structure of TRPC5 homotetramer (PDB ID: 6AEI).[21] One monomer of TRPC5 homotetramer is represented in orange and the partial segment, L538-L575, is represented in purple. Cys553 and Cys558 is represented in CPK representation. The N-terminal side of the partial segment was exposed to the extracellular. (B-C) (B) The surface charge density and (C) hydrophobicity of TRPC5 homotetramer in side view (left) and top view (right). In the side view, surface was vertically sliced to show the surface charge around Cys553 and Cys558. In the top view, surface charge in the top of TRPC5 and around Cys553 and Cys558 were shown. (B) Blue, red, and white color indicated positive, negative, and no charge, respectively. As each color showed more vivid, each charge was possessed stronger. (C) White and black colors indicated hydrophilic and hydrophobic surface, respectively.

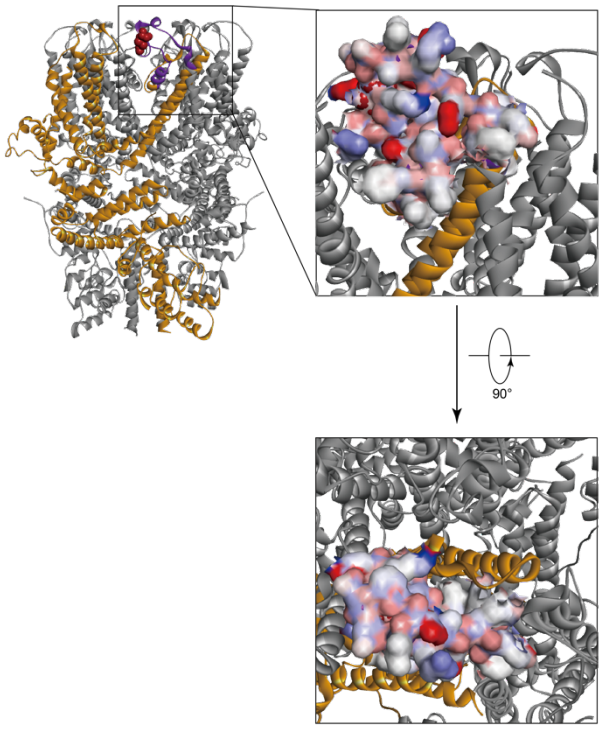

Figure 4.10. The surface charge of the partial segment of NO-sensing domain, L538-L575 in TRPC5 (PDB ID: 6AEI).[21] One monomer of TRPC5 homotetramer and the partial segment, L538-L575, are shown in orange and purple, respectively. Cys553 and Cys558 is showed as CPK representation. In the zoomed up view, the surface charge around L538-L575 is shown as blue, red, and white colors indicated positive, negative, and no charge, respectively.

4. 3. Conclusions

Further purifications and investigations of the NO sensor candidates 551-575, 552-575, and 553-575 obtained from the chapter 3 were conducted to confirm the they could work as the NO biosensor. NO sensor candidates showed larger ΔR values upon cleavage of disulfide bond than that of the parent EGFP-TRPC5. Additionally, NO sensor candidates showed the increment of the ratios upon disulfide bond formation with reaction to NO and H_2O_2. Three NO sensor candidates would be applicable as redox biosensors. Additionally, their lack of the specificity to NO and H_2O_2 has to be compensated by a simultaneous usage of specific H_2O_2 sensor. Therefore, Three NO sensor candidates would be applicable NO biosensor without requiring any additive upon simultaneous usage of specific H_2O_2 sensor. On the other hand, structural investigation with surface charge density and hydrophobicity of the Cryo-EM structure of TRPC5 indicated that the hydrophobic transmembrane domain would reinforce the accessibility of NO over H_2O_2 to the NO-sensing region.

NO sensor candidate 551-575 showed four times larger signal response than that of the parent EGFP-TRPC5 in reaction with NO. While the two-step screening revealed a limitation to optimize the specificity of the sensor to NO over H_2O_2, the strategy successfully enhanced the signal response of parent AFP-based biosensor.

4. 4. Materials and methods

4. 4. 1. Materials

Purified oligonucleotide primers for gene construction were purchased from Thermo Fisher Scientific Inc. (Waltham, MA, USA). *E. coli* BL21 (DE3) competent cells were purchased from Invitrogen (Carlsbad, CA). QIAprep Spin Miniprep Kit was purchased from QIAGEN (Tokyo, Japan). His GraviTrap™ column, PD-10 column, HiTrap™ Butyl HP column (5 mL) and HisTrap™ HP column (5 mL) were purchased from GE Healthcare Japan Inc. (Tokyo, Japan). PrimeSTAR HS DNA polymerase, and *E. coli* DH5α competent cells were purchased from TaKaRa Bio Inc. (Shiga, Japan). NOC7 was

purchased from DOJINDO LABOLTORIES (Kumamoto, Japan). All the other chemicals were purchased from Wako Chemicals (Osaka, Japan), Tokyo Chemical Industry Co., Ltd (Tokyo, Japan), Sigma-Aldrich Japan (Tokyo, Japan) and Nacalai Tesque (Kyoto, Japan).

4. 4. 2. Expression and purification of proteins

For further investigation of NO sensor candidates 551-575, 552-575, or 553-575, cells were grown at 37 °C until the OD_{600} reached 0.5-0.7, and protein expression was induced with 1 mM IPTG for 24 h at 18 °C. The soluble fractions of cell lysates containing the target proteins were loaded onto a HisTrap™ HP column with a linear gradient of 60–225 mM imidazole in 50 mM phosphate and 500 mM NaCl (pH 8.0). Fractions containing NO sensor candidates 551-575, 552-575, or 553-575 were collected and diluted to the initial condition of the next purification step (50 mM phosphate, 900 mM $(NH_4)_2SO_4$ (pH 8.0)). The resultant products were loaded onto HiTrap™ Butyl HP and eluted using an $(NH_4)_2SO_4$ gradient (from 900 to 0 mM). Fractions containing 551-575, 552-575, or 553-575 were collected and dialyzed against a solution containing 100 mM phosphate, 200 mM NaCl, and 50% glycerol (pH 8.0), and stored at -20 °C. Concentrations of NO sensor candidates 551-575, 552-575, or 553-575 in the glycerol stocks were determined using absorbance at 440 nm derived from the isosbestic point of the EGFP chromophore (molecular coefficient of EGFP-TRPC at 440 nm: 15,000 M^{-1} cm^{-1}).

4. 4. 3. Characterizations of the NO sensor candidates 551-575, 552-575, and 553-575 *in vitro*

NO sensor candidates 551-575, 552-575, and 553-575 were characterized using MALDI-TOF mass spectrometry (AXIMA-LNR, SA matrix, Shimadzu, Kyoto, Japan). NO sensor candidate 551-575: m/z calcd 31,602; observed 31,586. NO sensor candidate 552-575: m/z calcd 31,488; observed 31,475. NO sensor candidate 553-575: m/z calcd 31,374; observed 31,356. Absorption spectra were measured using a UV-2550 UV-Vis spectrometer (Shimadzu, Kyoto, Japan). The excitation and emission spectra were measured using an F-7000 fluorescence spectrometer (Hitachi High-Tech Science, Tokyo, Japan) at 20 °C. Samples contained 4 μM 551-575, 552-575, or 553-575 in a buffer

containing 100 mM phosphate buffer, 500 mM NaCl, and 0.005％ Tween20 (pH 6.8). The emission spectra were measured by excitation at 395 and 466 nm, and the excitation spectra were measured at an emission wavelength of 509 nm.

4. 4. 4. Change of the fluorescence intensities of the NO sensor candidates 551-575, 552-575, and 553-575 to NO upon reduction *in vitro*

The disulfide bonds of NO sensor candidates 551-575, 552-575, or 553-575 were reduced in a solution containing 70 μM 551-575, 552-575, or 553-575, 100 mM phosphate (pH 8.0), 0.005% Tween 20, and 3.5 mM DTT for 2-3 h at 25 °C. After reduction, the solutions containing NO sensor candidates 551-575, 552-575, or 553-575 were loaded onto a Micro Bio-Spin Chromatography Column P-6 (Bio-Rad) equilibrated with a buffer containing 100 mM phosphate, 500 mM NaCl, and 0.005% Tween20 (pH 6.8). Concentrations of free thiol groups in NO sensor candidates 551-575, 552-575, or 553-575 were measured using the DTNB method with Ellman's reagent (see section 4.4.6). Concentrations of NO sensor candidates 551-575, 552-575, or 553-575 were determined with absorbance at 425 nm derived from the isosbestic point of the EGFP chromophore from pH 5.0 to 7.0 (molecular coefficient of EGFP-TRPC at 425 nm: 21,000 M^{-1} cm^{-1}). The excitation and emission spectra were measured using an F-7000 fluorescence spectrometer at 20 °C. Samples contained 4 μM 551-575, 552-575, or 553-575 in a buffer containing 100 mM phosphate buffer, 500 mM NaCl, and 0.005% Tween20 (pH 6.8). Oxidized solutions were prepared using the same procedure without DTT treatment. The emission spectra were measured by excitation at 395 and 466 nm, and the excitation spectra were measured at an emission wavelength of 509 nm.

4. 4. 5. Reaction of the NO sensor candidates 551-575, 552-575, and 553-575 to NO and H_2O_2

The disulfide bonds of NO sensor candidates 551-575, 552-575, or 553-575 were reduced in a solution containing 100 μM 551-575, 552-575, or 553-575, 100 mM phosphate, 0.005％ Tween 20, 5 mM DTT (pH 8.0) for 3 h at 25 °C. After reduction, the solutions containing NO sensor candidates 551-575, 552-575, or 553-575 were loaded to Micro Bio-Spin Chromatography Column P-6 (Bio-Rad) equilibrate with a buffer

containing 20 mM citrate, 500 mM NaCl, 0.005％ Tween20 (pH 5.5). Concentrations of the free thiol groups in NO sensor candidates 551-575, 552-575, or 553-575 were measured by the DTNB method with Ellman's reagent (see section 4.4.6). Concentrations of NO sensor candidates 551-575, 552-575, or 553-575 were determined with the absorbance at 425 nm derived from the isosbestic point of chromophore in EGFP from pH 5.0 to 7.0 (the determined molecular coefficient of EGFP-TRPC at 425 nm: 21,000 $M^{-1}cm^{-1}$). Reactions of NO sensor candidates 551-575, 552-575, or 553-575 with NO were monitored by measuring the changes in fluorescence emission upon addition of NOC7 (dissolved in 0.01 M NaOH) to a solution, which were diluted to 12 μM 551-575, 552-575, or 553-575 with the buffer containing 100 mM phosphate, 500 mM NaCl, 0.005 % Tween20 (pH 6.8), at 20 °C with Infinite F PLEX (TECAN, Zürich, Switzerland). Instead of the addition of NOC7, an equal amount of 0.01 M NaOH was added to the reaction solutions. It should be noted that the pH value of the buffer did not change between before and after the addition of NOC7 in 0.01 M NaOH. After the measurement, concentrations of the free thiol groups of NO sensor candidates 551-575, 552-575, or 553-575 in response to NO was measured by the DTNB method (see section 4.4.6). In the case of H_2O_2, 551-575, 552-575, or 553-575 were treated by H_2O_2 for 70 min.

4. 4. 6. Quantitation of the free thiol group

The concentrations of free thiol groups in NO sensor candidates 551-575, 552-575, or 553-575 were measured by the DTNB method. Prior to the assay by the DTNB method, all the samples were purified by size exclusion chromatography to remove the thiol containing reagents such as DTT. An assay solution was prepared by mixing 100 μM DTNB in a solution containing 100 mM phosphate, 500 mM NaCl and 0.005％ Tween20 (pH 6.8) with an aliquot of NO sensor candidates 551-575, 552-575, or 553-575 solutions. Absorption spectra of assay solutions were measured by Infinite M200 PRO (TECAN, Zürich, Switzerland). The concentrations of free thiol groups in NO sensor candidates 551-575, 552-575, or 553-575 were determined by the absorbance at 412 nm, which derived from 2-nitro-5-mercaptobenzoic acid. The concentrations of NO sensor candidates 551-575, 552-575, or 553-575 were also determined from the absorbance at 425 nm, the isosbestic point of chromophore in EGFP. The concentrations

of free thiol groups were determined by the following equation:

$$y = 0.004x + 0.005$$

y and x represent the absorbance at 412 nm and concentration of L-cysteine [μM], respectively, as described in the previous report.[12]

To the NOC7 treated 551-575, 552-575, or 553-575, solutions containing ascorbic acid (final concentration: 5 mM) were added to specifically reduce the S-nitorsylated thiol. After 30 min, the reaction mixture was treated by the same procedure described above to quantitate the concentration of free thiol group by the DTNB method.

4. 4. 7. Determination of the half-maximum times of the NO sensor candidates for the reaction of oxidants

The R values of NO sensor candidates 551-575, 552-575, or 553-575 upon reaction with NO or H_2O_2 (500 μM NOC7, 100 μM, or 500 μM H_2O_2) were subtracted from the R values under air oxidation conditions (0 M NOC7 or H_2O_2) to remove the air oxidation effects. The subtracted R values were normalized by dividing by ΔR upon reduction, which is called the normalized R. The minimum and maximum R values were determined as the average values of normalized R values before the addition of NOC7 or H_2O_2 and after saturation of the reactions, respectively. The half-maximum values were determined as the mean of the minimum and maximum R values. The average values of the half-maximum times were determined as the mean times of the measurement times before and after the normalized R reached the half-maximum R values, and intervals of measurement points were determined as error bars of the half-maximum times. In the parent EGFP-TRPC5, the normalized R values were smoothed with a linear weighted moving average of three points to remove the fluctuation of the normalized R values resulting from slight ΔR.

4. 5. References

1. Loscalzo J, Welch G. Nitric Oxide and Its Role in the Cardiovascular System. Prog. Cardiovasc. Dis. 1995;38:87-104.

2. Lei J, Vodovotz Y, Tzeng E, Billiar TR. Nitric oxide, a protective molecule in the cardiovascular system, Nitric Oxide. 2013;35:175-185.
3. Bradley SA, Steinert JR. Nitric Oxide-Mediated Posttranslational Modifications: Impacts at the Synapse. Oxid. Med. Cell. Longevity. 2016;2016:5681036.
4. Steinert JR, Robinson SW, Tong H, Haustein MD, Kopp-Scheinpflug C, Forsythe LD. Nitic Oxide Is an Activity-Dependent Regulator of Target Neuron Intrinsic Excitability. Neuron. 2011;71:291-305.
5. Hirst DG, Robson T. Nitric oxide physiology and pathology. Methods Mol. Biol. 2011;704:1-13.
6. Xu W, Liu LZ, Loizidou M, Ahmed M, Charles IG. The role of nitric oxide in cancer. Cell Res. 2002;12:311-320.
7. Wendehenne D, Durner J, Klessig DF. Nitric Oxide: a new player in plat signaling and defense responses. Curr. Opin. Plant Biol. 2004;7:449-455.
8. Horenberg AL, Houghton AM, Pandey S, Seshadri V, Guilford WH. S-nitrosylation of cytoskeletal proteins. Cytoskeleton. 2019;76:243-252.
9. Hess DT, Matsumoto A, Kim SO, Marshall HE, Stamler JS. Protein S-nitrosylation: purview and parameters. Nat. Rev. Mol. Cell Biol. 2005;6:150-166.
10. Johnson DC, Dean DR, Smith AD, Johnson MK. STRUCTURE, FUNCTION, AND FORMATION OF BIOLOGICAL IRON-SULFUR CLUSTERS. Annu. Rev. Biochem. 2005;74:247-281.
11. Radi R. Reaction of Nitric Oxide with Metalloproteins. Chem. Res. Toxicol. 1996;9:828-835.
12. Serrano PN, Wang H, Crack JC, Prior C, Hutchings MI, Thomson AJ, Kamali S, Yoda Y, Zhao J, Hu MY, Alp EE, Oganesyan VS, Le Brun NE. Nitrosylation of Nitiric-Oxide-Sensing Regulatory Proteins Containing [4Fe-4S] Clusters Gives Rise to Multiple Iron-Nitrosyl Complexes. Angew. Chem. Int. Ed. 2016;55:14575-14579.
13. Tallini YN, Ohkura M, Choi BR, Ji G, Imoto K, Doran R, Lee J, Plan P, Wilson J, Xin HB, Sanbe A, Gulick J, Mathai J, Robbins J, Salama G, Nakai J, Kotlikoff MI. Imaging cellular signals in the heart *in vivo*: Cardiac expression of the high-signal Ca^{2+} indicator GCaMP2. Proc. Natl. Acad. Sci. U. S. A. 2006;103:4753-4758.
14. Zhang J, Campbell RE, Ting AY, Tsien RY. Creating new fluorescent probes for cell biology. Nat. Rev. Mol. Cell Biol. 2002;3:906-918.

15. Berg J, Hung YP, Yellen G. A genetically encoded fluorescent reporter of ATP:ADP ratio. Nat. Methods. 2009;6:161-166.
16. Eroglu E, Gottschalk B, Charoensin S, Blass S, Bischof H, Rost R, Madreiter-Sokolowski CT, Pelzmann B, Bernhart E, Sattler W, Hallström S, Malinski T, Waldeck-Weiermair M, Graier WF, Malli R. Development of novel FP-based probes for live-cell imaging of nitric oxide dynamics. Nat. Commun. 2016;7:10623.
17. Tajima S, Nakata E, Sakaguchi R, Saimura M, Mori Y, Morii T. Fluorescence detection of the nitric oxide-induced structural change at the putative nitric oxide sensing segment of TRPC5. Bioorg. Med. Chem. 2020;28:115430.
18. Hrabie JA, Klose JR, Wink DA, Keefer LK. New nitric oxide-releasing zwitterions derived from polyamines. J. Org. Chem. 1993;58:1472-1476.
19. Hess DT, Matsumoto A, Kim SO, Marshall HE, Stamler JS. Protein S-nitrosylation: purview and parameters. Nat. Rev. Mol. Cell Biol. 2005;6:150-166.
20. Yoshida T, Inoue R, Morii T, Takahashi N, Yamamoto S, Hara Y, Tominaga M, Shimizu S, Sato Y, Mori Y. Nitric oxide activates TRP channels by cysteine S-nitrosylation. Nat. Chem. Biol. 2006;2:596-607.
21. Duan J, Li J, Chen GL, Ge Y, Liu J, Xie K, Peng X, Zhou W, Zhong J, Zhang Y, Xu J, Xue C, Liang B, Zhu L, Liu W, Zhang C, Tian XL, Wang J, Clapham DE, Zeng B, Li Z, Zhang J. Cryo-EM structure of TRPC5 at 2.8-Å resolution reveals unique and conserved structural elements essential for channel function. Sci. Adv. 2019;5:eaaw7935.

Chapter 5
Cellular application for confirming the ability as a redox sensor

5. 1. Introduction

For exploring signal transduction, many methods for detecting the biomolecules or proteins were developed. Some methods which requires fixation of the cell[1,2] just provide a static, snapshot view of cells. In signal transduction of living organisms, various biomolecules and proteins were related sophistically in the parallel multi-step reaction processes and regulated in the appropriate time and location.[3,4] Therefore, to explore the signal transduction, real-time visualization of biomolecules or proteins in living cells are necessary.[4-6] Furthermore, to understand their relationship, visualizing several biomolecules of the time of appearance and localization simultaneously are important. Fluorescence detection is the most useful method for real-time visualization because of its advantage of property of high sensitivity and selectivity, high spatial and temporal resolution, low cost for use, and good tissue penetration.[7-11] Especially, in auto-fluorescent protein (AFP) based biosensors, the localization could be controlled to the sites of interest within cell by introducing a certain organelle-specific targeting signal.[12] Additionally, various color palettes of AFPs, ranging from blue to red[13-16], contribute the simultaneous imaging within the same cells. Therefore, AFP-based biosensors were suitable for exploring signal transduction.

In the chapter 2, EGFP-TRPC5, a segment of the putative NO-sensing module of TRPC5 channel was fused to EGFP, successfully detected NO as the change of fluorescence emission ratio with the disulfide bond formation.[17,18] The successful detection of NO-induced disulfide bond formation by EGFP-TRPC5 implied an

application of EGFP-TRPC5 as a biosensor in the mammalian cells, by enhancing its ratiometric signal response of only 8% increment. As described in chapter 3, a facile two-step screening was conducted for the enhancement of the ratiometric signal respnonse of EGFP-TRPC5. As a result, three NO sensor candidates, 551-575, 552-575, and 553-575, successfully showed 2-4 times enhancement of the ratiometric signal respnonse. Further investigation as described in chapter 4 indicated that three NO sensor candidates, 551-575, 552-575, and 553-575, showed change of the ratio upon reaction to NO and H_2O_2. Therefore, these NO sensor candidates showed the sufficient signal change for working as the genetically encoded redox biosensors in the living cells.

In this chapter, it was confirmed whether redox sensor 551-575 could function as the biosensors in living cells. It was confirmed that redox sensors 551-575 could show the change of ratios in the living cells upon the addition of extracellular H_2O_2, indicating that 551-575 could be applicable for *in vivo* measurement as a redox sensor.

5. 2. Results and discussions

5. 2. 1. Construction of the plasmids for expression in mammalian cells

For expression of 551-575, 552-575, and 553-575 in mammalian cells, encoding regions were transferred from peT29a to pCI-neo, which include cytomegalovirus promotor for expression in mammalian cells. pCI-neo contains CMV promotor for expressing the protein of interest in mammalian cells. CMV enhancer and β-globin/IgG chimera intron promote a transcription and protein expression, respectively. SV Late poly(A) signal stabilizes the mRNA and increases the translation efficiency (Figure 5.1).

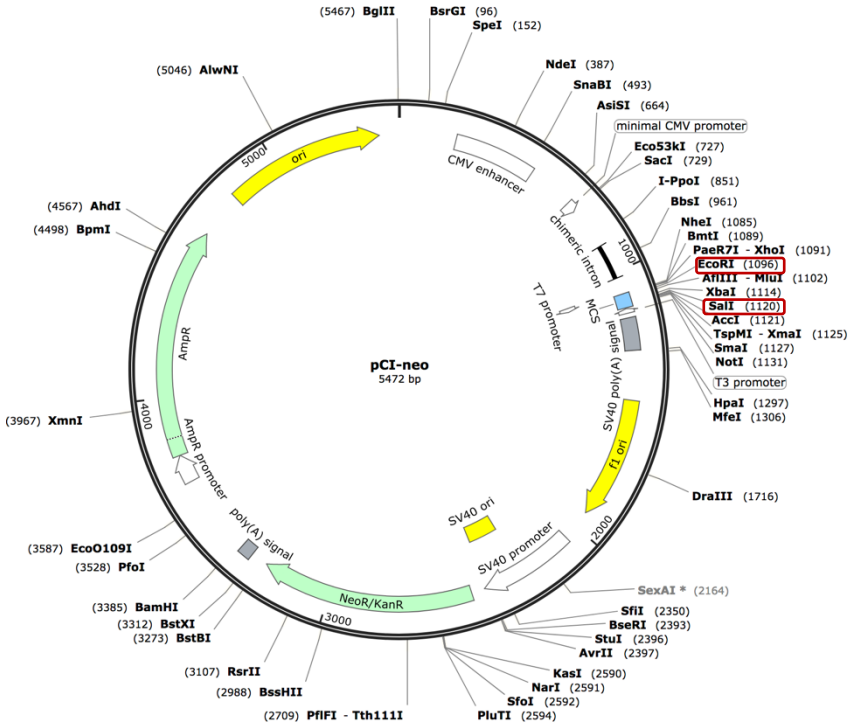

Figure 5.1. pCI-neo. pCI-neo eoncode CMV promotor. nucleic acid sequences encoding 551-575, 552-575, or 553-575 were inserted between EcoRI and SalI.

5. 2. 2. Expression of the redox sensors in mammalian HEK293 cells

It was confirmed whether redox sensors 551-575, 552-575, or 553-575 could show fluorescence in the mammalian cells. The constructed vectors as described in the previous section were transfected into the mammalian HEK293 cells with lipofectamine 2000, the cationic-lipid transfection reagent. Autofluorescence of mammalian cells which derived from intracellular molecules, such as NADH, flavin,[19,20] should overlap the fluorescence which derived from EGFP. Therefore, to measure the autofluorescence as the blank of fluorescence, pCI-neo vector template which did not encode any redox sensor were transfected into the cells with the same manner. The measurement with fluorescent microscope indicated that cells showed slight autofluorescence at 535 nm when excited at 403 nm and 480 nm, which cause overestimation of the fluorescence of redox sensors at the phenol and phenolate state of EGFP, respectively. Intensities of autofluorescence at 535 nm when excited at 403 nm and 480 nm, was analyzed. The distributions of the intensities of the autofluorescence showed that fluorescence intensity at 535 nm when

excited at 403 nm and 480 nm were calculated as 25 ± 33 and 82 ± 98, respectively (Figure 5. 2).

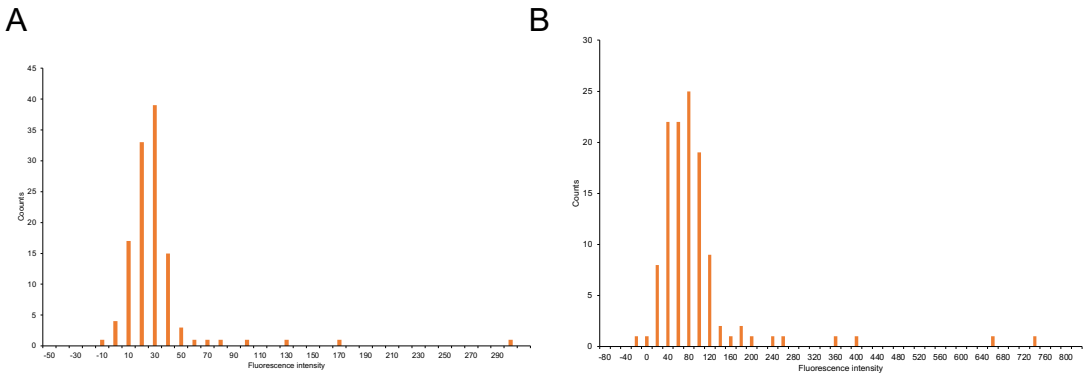

Figure 5.2. The fluorescence intensity distributions of autofluorescence deriving form HEK293 cells (119 cells were counted). Intensity of the background where cells did not exist was subtracted from the fluorescence intensity of each cell. (A) Fluorescence intensity emitted at 535 nm when excited at 403 nm was estimated as 25 ± 33. (B) Fluorescence intensity emitted at 535 nm when excited at 480 nm was estimated as 82 ± 98.

Next, each redox sensor, 551-575, 552-575, or 553-575 was expressed inside the HEK293 cells, respectively. Each redox sensor expressed in some cells showed obviously larger fluorescence than autofluorescence (Figure 5.3-5.6) on the measurement with fluorescent microscope. Analysis of the fluorescence intensity at 535 nm when excited at 403 nm and 480 nm of the cells into which each vector was transfected also indicted the existence of the cells which showed larger fluorescence intensity than autofluorescence (Figure 5.7 and 5.8). The thresholds of autofluorescence at 535 nm when excited at 403 nm and 480 nm were determined as 191 and 574, which were five times of standard distribution larger than average values, respectively. The values of 9%, 11%, 10% of cells into which vector encoding 551-575, 552-575, or 553-575, showed larger fluorescence than both thresholds of fluorescence intensity when excited at 403 nm and 480 nm. These results indicated than each redox sensor could expressed and showed the fluorescence in the mammalian HEK293 cells. Although fluorescence intensities showed various values depending on the cells (Figure 5.3-5.8), R values were independent values on cells, 0.135 ± 0.012 in 551-575, 0.134 ± 0.023 in 552-575, or 0.127 ± 0.015 in 553-575, respectively. These results came from the advantage of the ratio type biosensors and indicated that

these redox sensors could be used for the quantitative measurement.

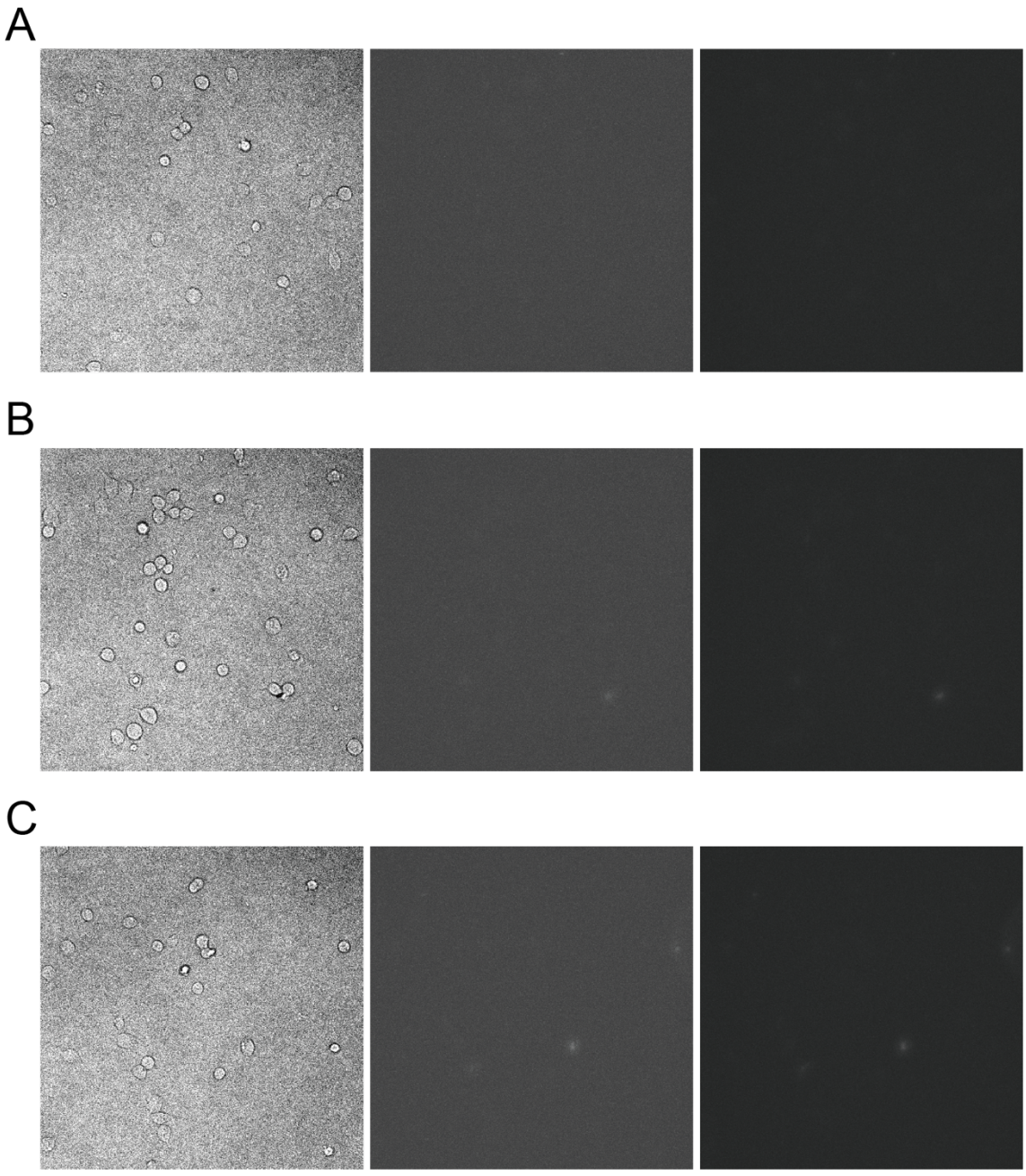

Figure 5.3. Fluorescence microscope images of the HEK293 into which template pCI-neo vector was transfected. (A) Area 1. (B) Area 2. (C) Area 3. Left: blight field images Center: fluorescence images at 535 nm excited at 403nm (linear contrast from 1000 to 5000), Right: fluorescence images at 535 nm excited at 480 nm (linear contrast from 0 to 15000).

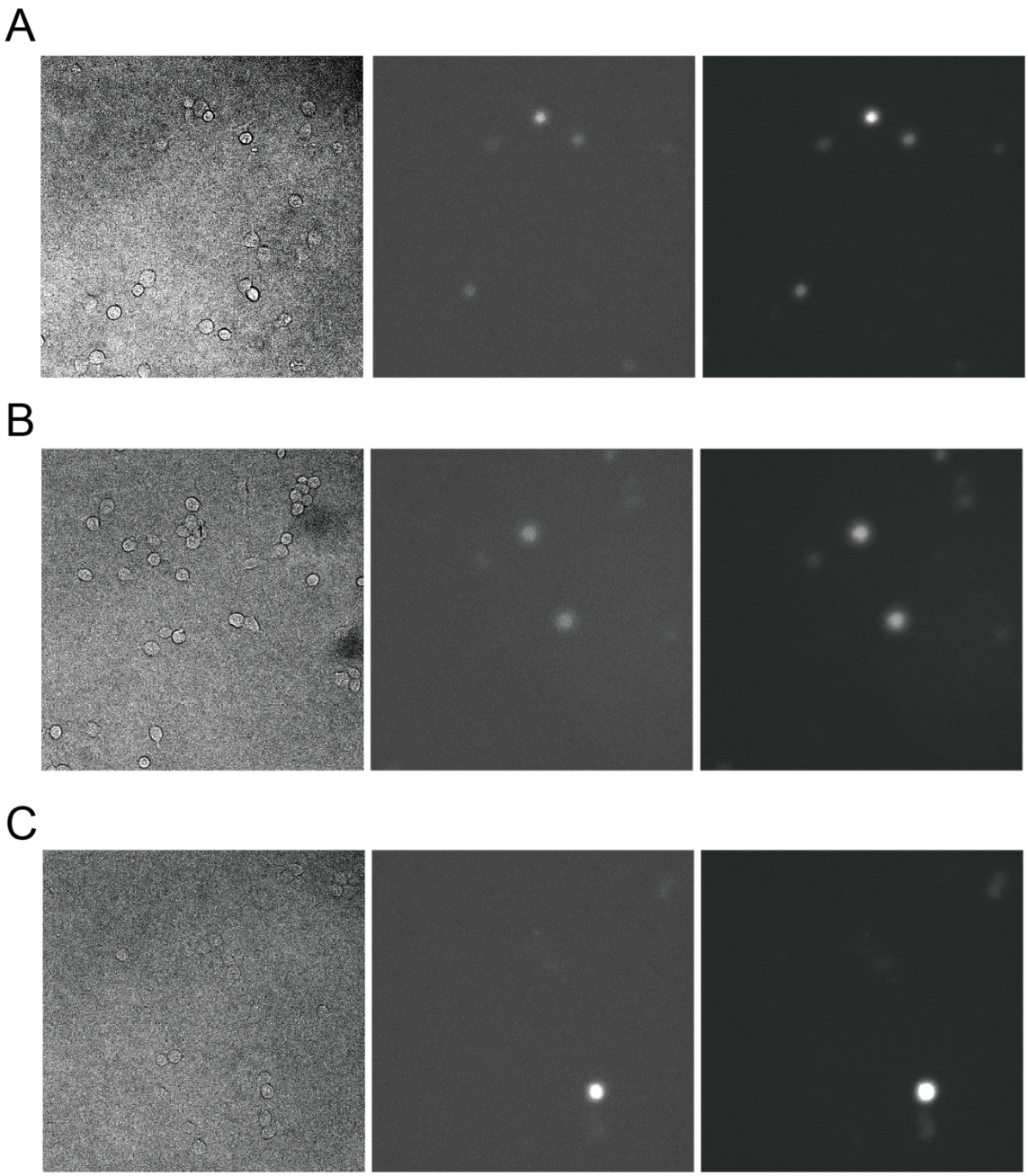

Figure 5.4. Fluorescence microscope images of the HEK293 into which vector encoding 551-575 was transfected. (A) Area 1. (B) Area 2. (C) Area 3. Left: blight field images Center: fluorescence images at 535 nm excited at 403nm (linear contrast from 1000 to 5000), Right: fluorescence images at 535 nm excited at 480 nm (linear contrast from 0 to 15000).

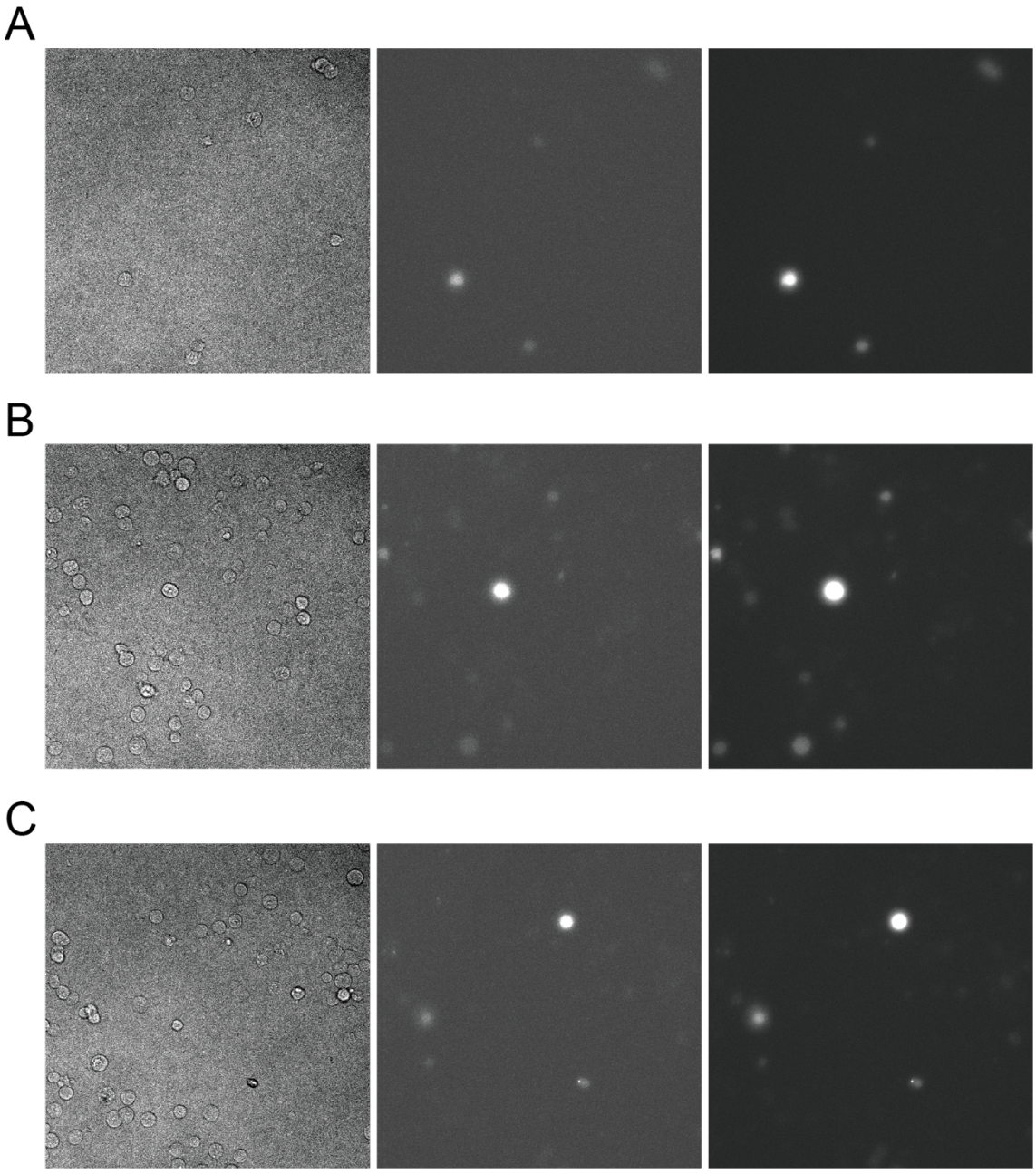

Figure 5.5. Fluorescence microscope images of the HEK293 into which vector encoding 552-575 was transfected. (A) Area 1. (B) Area 2. (C) Area 3. Left: blight field images Center: fluorescence images at 535 nm excited at 403nm (linear contrast from 1000 to 5000), Right: fluorescence images at 535 nm excited at 480 nm (linear contrast from 0 to 15000).

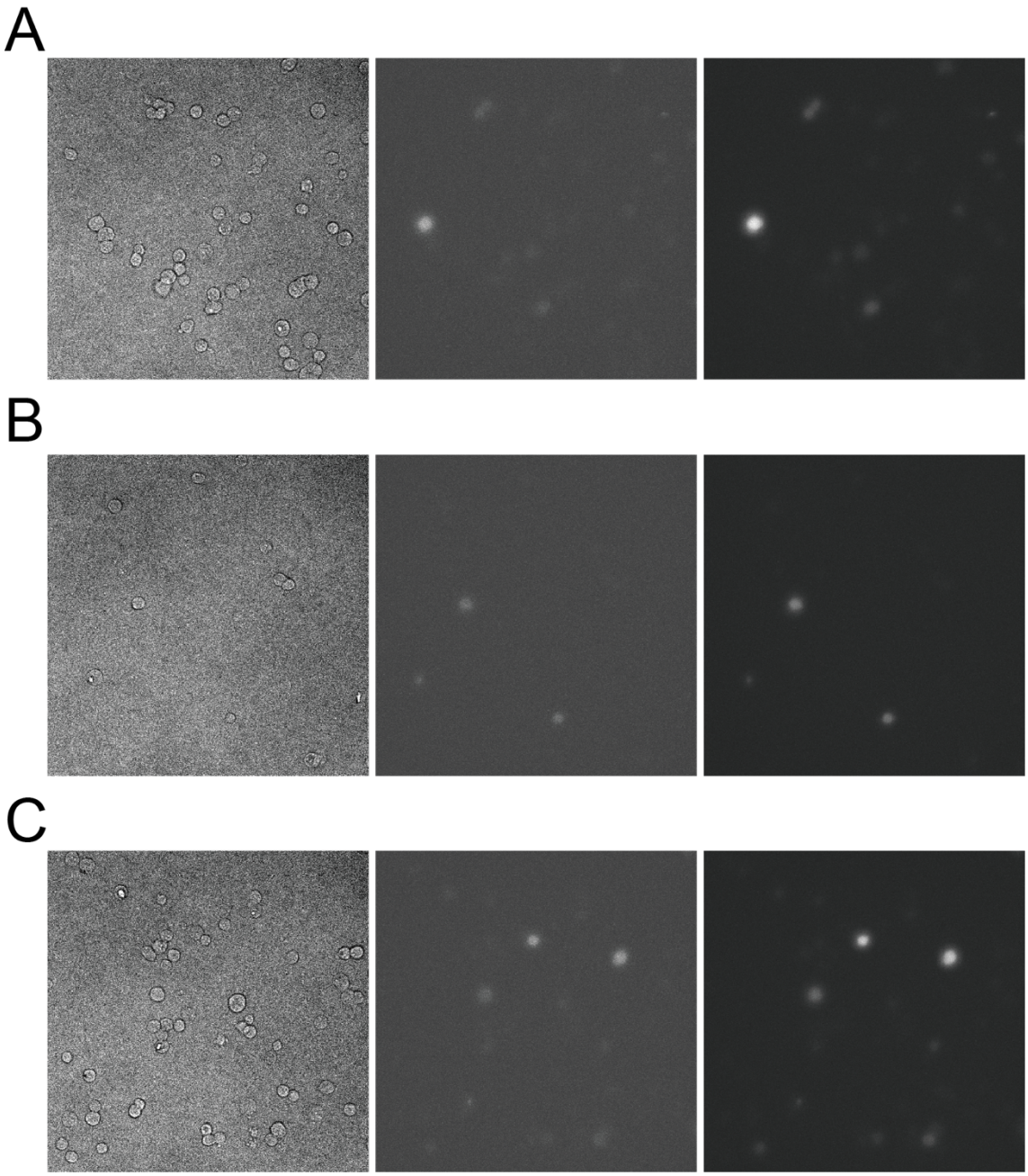

Figure 5.6. Fluorescence microscope images of the HEK293 into which vector encoding 553-575 was transfected. (A) Area 1. (B) Area 2. (C) Area 3. Left: blight field images Center: fluorescence images at 535 nm excited at 403nm (linear contrast from 1000 to 5000), Right: fluorescence images at 535 nm excited at 480 nm (linear contrast from 0 to 15000).

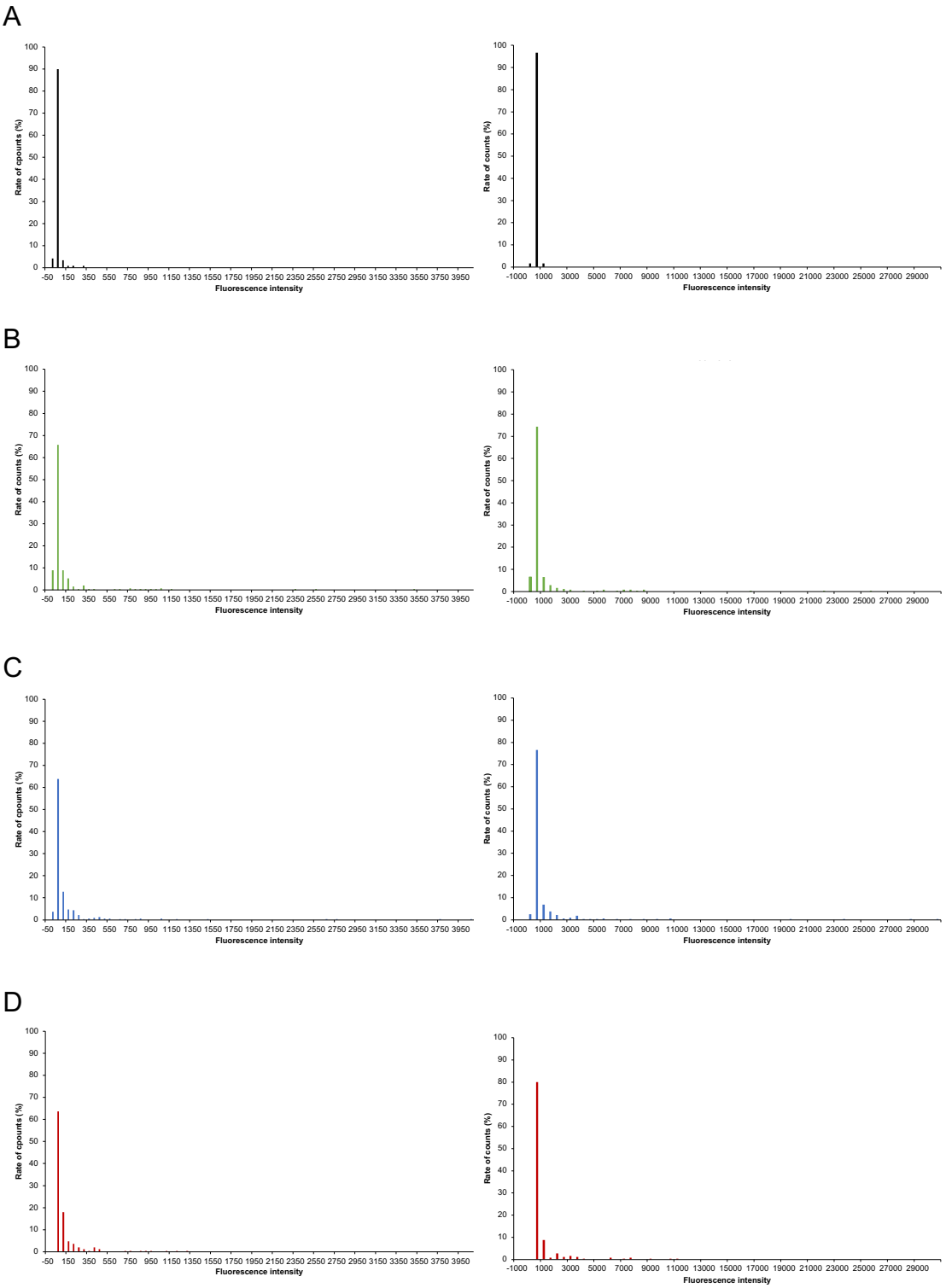

Figure 5.7. The percentage distributions of the fluorescence intensity at 535 nm when excited at 403 nm (Left) or 483 nm (Right) of HEK293 cells. Intensity of the background where cells did not exist was subtracted from the fluorescence intensity of each cell. (A) Autofluorescence deriving from the HEK293 cells (B) Fluorescence intensities of the

HEK293 cells into which the vector encoding 551-575 was transfected (245 cells were counted). (C) Fluorescence intensities of the HEK293 cells into which the vector encoding 552-575 was transfected (321 cells were counted). (D) Fluorescence intensities of the HEK293 cells into which the vector encoding 553-575 was transfected (495 cells were counted).

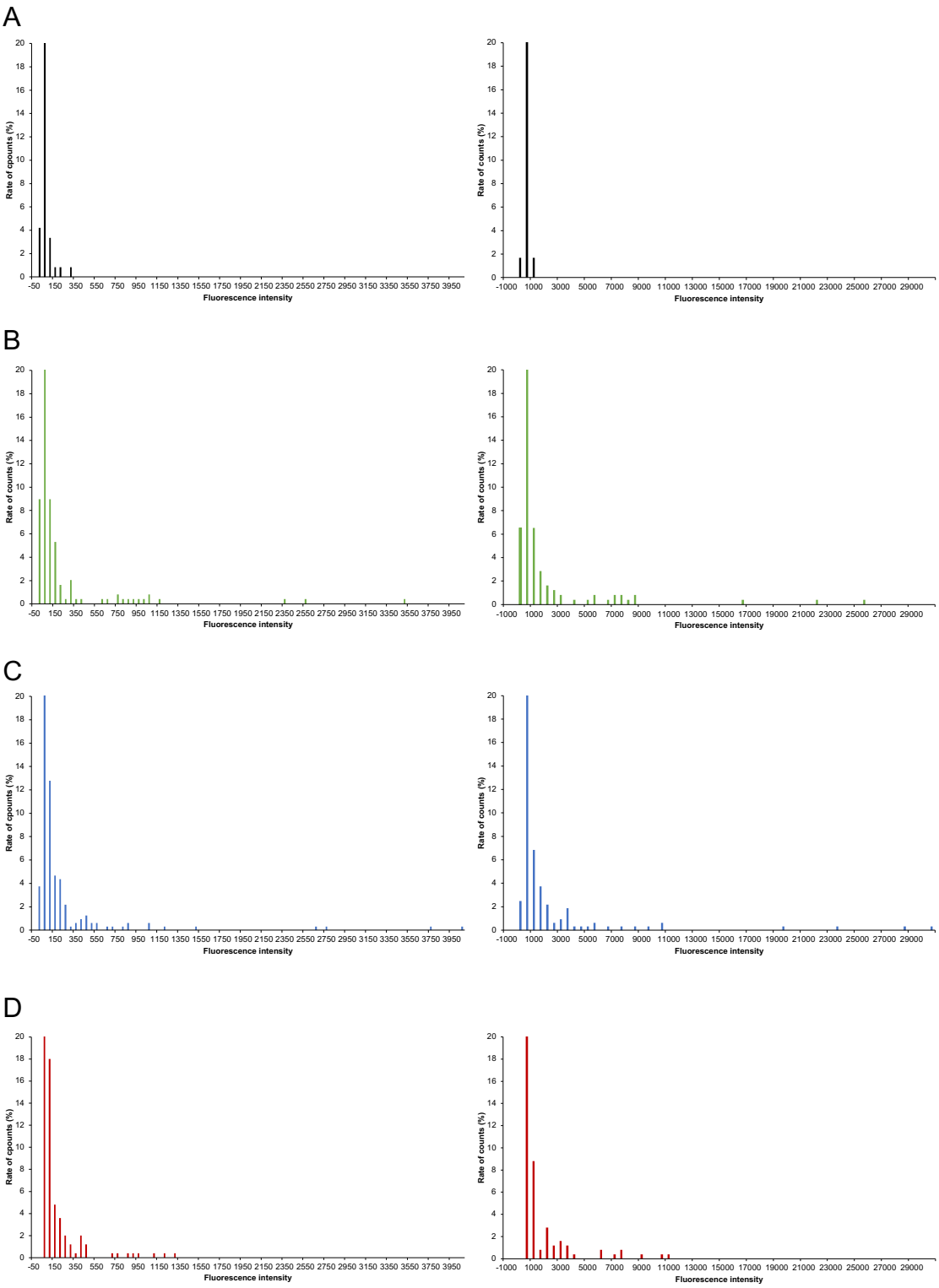

Figure 5.8. The percentage distributions of the fluorescence intensity at 535 nm when excited at 403 nm (Left) or 483 nm (Right) of HEK293 cells. y-axis of the percentage distributions described in Figure 5.7 was zoomed up. Intensity of the background where

cells did not exist was subtracted from the fluorescence intensity of each cell. (A) Autofluorescence deriving from the HEK293 cells (B) Fluorescence intensities of the HEK293 cells into which the vector encoding 551-575 was transfected (245 cells were counted). (C) Fluorescence intensities of the HEK293 cells into which the vector encoding 552-575 was transfected (321 cells were counted). (D) Fluorescence intensities of the HEK293 cells into which the vector encoding 553-575 was transfected (495 cells were counted).

5. 2. 3. Measurement of the fluorescence response of the redox sensors to the addition of H_2O_2

Next, fluorescence response to H_2O_2 was measured to investigate whether redox sensor 551-575 could function in the living cells. Extracellular H_2O_2 (500 μM) was added to the bulk solution where the cells were soaked, causing H_2O_2 to diffuse freely and invade the cells. Upon addition of H_2O_2, the cells were not damaged severely because their plasma membranes remained with slight change in the cell size (Figure 5.9A). Although the fluorescence intensity varied depending on the cells, the R values of the cells increased to the similar extent, ranging from 0.12 to 0.15 (Figure 5.9A, 5.9B, and 5.9C). Analysis of R values indicates they increased from 18% in cells showing a minimum increase, to 49% in cells showing a maximum increase upon addition of H_2O_2, with 34% as the average (Figure 5.9C and 5.9D). Considering 31% of the change in R values upon reaction with H_2O_2 in the redox sensor 551-575 *in vitro* measurement, the signal responses of redox sensor 551-575 upon reaction with H_2O_2 in cells were comparable with those of the *in vitro* measurements, whereas the signal responses varied in different cells. In contrast, the original EGFP did not show changes in R values (Figure 5.10). These results indicate that redox sensor 551-575 detected H_2O_2 with an increase in R value in mammalian cells, and therefore can be used as a redox biosensor in a cellular system.

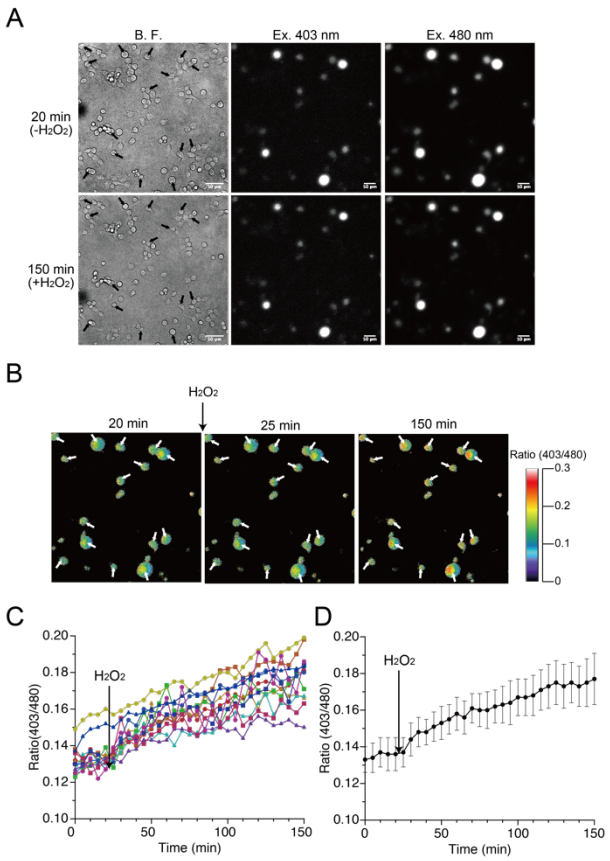

Figure 5.9. (A) Blight field images (left) and fluorescent images of fluorescence emission at 535 nm when excited at 403 nm (middle) and 480 nm (right) of redox sensor 551-575 expressed in HEK293 cells in response to H_2O_2. Cells indicated by arrows show sufficient fluorescence. Half of the pool volume of 1.5 mM H_2O_2 was added to a final concentration of 500 µM H_2O_2, with H_2O_2 freely and uniformly spread, between 20 and 25 min. (B) Time-lapse of pseudo color images of fluorescence emission ratios of redox sensor 551-575 expressed in HEK 293 cells in response to H_2O_2. R value was calculated by dividing the fluorescence intensity when excited at 403 nm with 480 nm from which the background intensity was subtracted. (C, D) Analysis of the fluorescence response of redox sensor 551-575 expressed in HEK293 cells upon addition of extracellular H_2O_2 of (C) individual cells and (D) average. Time-lapses of fluorescence images when excited at 403 nm and 480 nm were analyzed with ImageJ software (NIH) (n = 14 for two cultures).

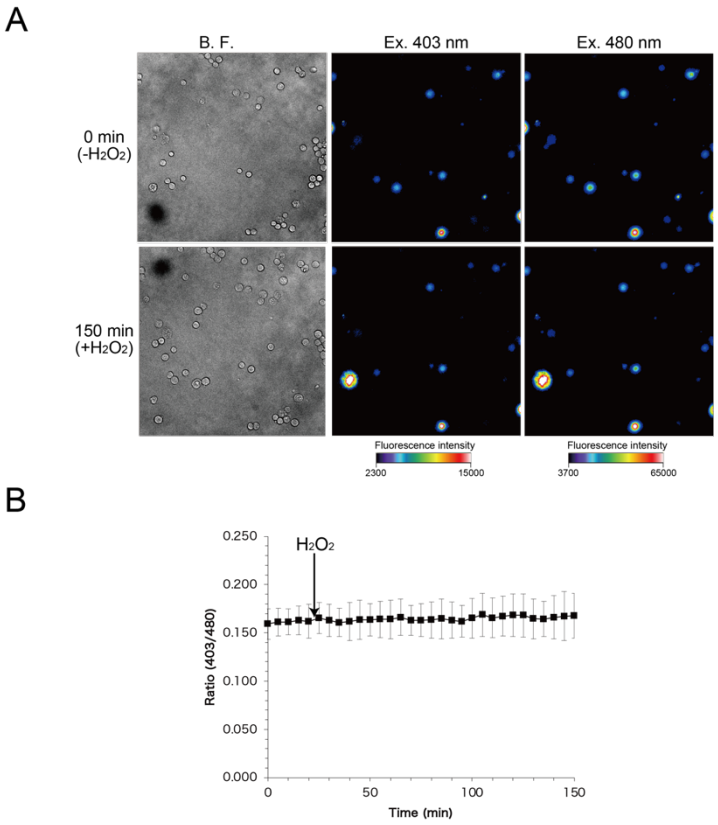

Figure 5.10. (A) Blight field images (left), pseudocolor images of fluorescence images at 535 nm when excited at 403 nm (middle) and 480 nm (right) of EGFP expressed in HEK293 cells in the absence and presence of H_2O_2. Cells indicated in arrow showed sufficient fluorescence. Half volume of the pool volume of 1.5 mM H_2O_2 was added to final 500 μM H_2O_2, desiring H_2O_2 spread freely to uniform concentration, between 20 and 25 min. (B) Analysis of the fluorescence response of EGFP expressed in the HEK293 cells upon the addition of extracellular H_2O_2. The time-lapse of the fluorescence images when excited at 403 nm and 480 nm were analyzed with using ImageJ software (NIH) (n=5 for 1 cultures).

5. 3. Conclusions

It was confirmed whether redox sensors 551-575, 552-575, or 553-575, constructed in the chapter 3 and 4, could work as biosensors in living cells. Upon the expression in the HEK293 cells, redox sensors 551-575, 552-575, 553-575 showed

sufficient fluorescence in the HEK293 cells. Furthermore, the redox sensor 551-575 showed the change of the fluorescence emission ratio in response to H_2O_2 in the mammalian HEK293 cells. Therefore, it was confirmed that the redox sensor 551-575, which was obtained from a facile two-step screening, could be applicable in the redox biosensor for *in vivo* measurements. These results indicated that our screening strategy for enhancing the ratiometric signal response successfully provided the mutants showing larger ΔR value by effectively transducing the structural change associated with the disulfide bond formation for application *in vivo* measurements.

5. 4. Materials and methods

5. 4. 1. Materials

The restriction enzymes (*EcoR*I, *Sal*I and *Dpn*I) were purchased from New England Biolabs. Purified oligonucleotide primers for gene construction were purchased from Thermo Fisher Scientific Inc. (Waltham, MA, USA). Mini Elute Gel Extraction Kit was purchased from QIAGEN (Tokyo, Japan). PrimeSTAR HS DNA polymerase, T4 DNA ligase, and *E. coli* DH5α competent cells were purchased from TaKaRa Bio Inc. (Shiga, Japan). All the other chemicals were purchased from Wako Chemicals (Osaka, Japan), Tokyo Chemical Industry Co., Ltd (Tokyo, Japan), Sigma-Aldrich Japan (Tokyo, Japan) and Nacalai Tesque (Kyoto, Japan).

5. 4. 2. Construction of plasmids

The gene encoding EGFP-TRPC5 was obtained by digesting peT29a encoding EGFP-TRPC5 with *Nde*I and *Xho*I and sequentially amplified by PCR using the primers listed in Table 5.1. The PCR products were run on 1% agarose gels (TAE) and purified using a Mini Elute Gel Extraction Kit. The PCR products and pCI-neo were digested with *EcoR*I and *Sal*I, purified in the same manner, and incubated with T4 DNA ligase. The mixture was transformed into *E. coli* DH5α competent cells for amplification. The vector encoding the parent EGFP with TRPC5 (L538-L575) was purified and sequenced.

The NO-sensing segments of TRPC5 (L538-L575) were shortened to N551-L575 with same procedure to that of *in vitro* measurement as described in chapter 3.

Table 5. 1. Nucleotide sequences of primers for construction of an expression vector for the parent EGFP with TRPC5 (L538-575).

primer	from 5' to 3'
Primer 1 (F-EcoRI-EGFP)	AAAAAAAAAAGAATTCGCCACCATGGTGAGCAAGGGCGAG
Primer 2 (R-EGFP-SalI)	AAAAAAAAAAGTCGAGTCAGTGGTGGTGGTGGTGGTG

5. 4. 3. Cell culture and transfection of vectors

HEK293 cells were cultured in DMEM (Gibco) containing 10% FBS, 30 units/ml penicillin, and 30 mg/ml streptomycin at 37 ºC under 5% CO_2. pCI-neo encoding 551-575, 552-575, or 553-575 was transfected using Lipofectamine 2000 (Invitrogen). The medium was replaced 3h after transfection.

5. 4. 4. Measurement of fluorescence responses of redox sensors

HEK293 cells were seeded onto a poly-L-lysin coated 35 mm glass-bottom dish (IWAKI) and incubated for 1h. The cells were washed with HBS containing 107 mM NaCl, 6 mM KCl, 11.5 mM Glucose, 20 mM HEPES, 1.2 mM $MgSO_4$, 2 mM $CaCl_2$, pH 7.4 twice and 200 μL HBS was added to the dish. Fluorescence was observed using an IX-81 fluorescence microscope (Olympus) equipped with a 20× objective lens (UPlanSApo). For time-lapse imaging to observe the fluorescence response to H_2O_2, 100 μl 1.5 mM H_2O_2 dissolved in HBS was gently added to the dish. Time-lapse images were acquired every 5 min.

5. 4. 5. Analysis of the fluorescence intensity and responses of redox sensors

Fluorescence images were modified with MetaFluor (Molecular devices). Pseudo color images of fluorescence emission ratios was calculated by dividing the fluorescence intensity when excited at 403 nm with 480 nm from which the background intensity was subtracted. Fluorescence images and intensities of cells were analyzed using ImageJ

software (NIH). First, cells were circulated based on bright images to determine the area for calculating the fluorescence intensity. The average fluorescence intensity within each circle was then calculated. The background signal was also estimated by circulating regions of any size without cells in each captured area. Fluorescence intensity of cells was determined by subtracting the background intensity from the raw fluorescence intensity of cells.

5. 5. References

1. Jaffrey SR, Erdjument-Bromage H, Ferris CD, Tempst P, Snyder SH. Protein S-nitrosylation: a physiological signal for neuronal nitric oxide. Nature Cell Biol. 2001;3:193-197.
2. Leonard SE, Reddle KG, Carroll KS. Mining the thiol proteome for sulfenic acid modifications reveals new targets for oxidation in cells. ACS Chem. Biol. 2009;4:783-799.
3. Hunter T. Signaling-2000 and Beyond. Cell. 2000;100:113-127.
4. Wilson GS, Gifford R. Biosensors for real-time *in vivo* measurement. Biosens. Bioelectron. 2005;20:23882403.
5. Liu W, Deng M, Yang C, Liu F, Guan X, Du Y, Wang L, Chu J. Genetically encoded single circularly permuted fluorescent protein-based intensity indicators. J. Phys. D: Appl. Phys. 2020;53:113001.
6. Stephens DJ, Allan VJ. Light Microscopy Techniques for Live Cell Imaging. Science. 2003;300:82-86.
7. Giepmans BN, Adams SR, Ellisman MH, Tsien RY. The Fluorescent Toolbox for Assessing Protein Location and Function. Science 2006;312:217-224.
8. Johnsson N, Johnsson K. Chemical Tools for Biomolecular Imaging. ACS Chem. Biol. 2007;2:31-38.
9. Rao J, Dragulescu-Andrasi A, Yao H. Fluorescence Imaging *in vivo*: Recent Advances. Curr. Opin. Biotechnol. 2007;18:17-25.
10. Johnsson K. Visualizing Biochemical Activities in Living Cells. Nat. Chem. Biol. 2009;5:63-65.

11. Wang H, Nakata E, Hamachi I. Recent Progress in Strategies for the Creation of Protein-Based Fluorescent Biosensors. ChemBioChem 2009;10:2560-2577.
12. Nakata E, Liew FF, Nakano S, Morii T. Recent progress in the constructin methodology of fluorescent biosensors based on biomolecules. Biosensors-Emerging materials and Applications. Serra, P. A. Ed. pp. 123-140 (2011).
13. Rodriguez EA, Campbell RE, Lin JY, Michael Z, Lin MZ, Miyawaki A, Amy E, Palmer AE, Shu X, Zhang J, Tsien RY. The Growing and Glowing Toolbox of Fluorescent and Photoactive Proteins. Trends Biochem. Sci. 2017;42:111-129.
14. Heim R, Tsien RY. Engineering green fluorescent protein for improved brightness, longer wavelengths and fluorescence resonance energy transfer. Curr. Biol. 1996;6:178-182.
15. Campbell RE, Tour O, Palmer AE, Steinbach PA, Baird GS, Zacharias DA, Tsien RY. A monomeric red fluorescent protein. Proc. Natl. Acad. Sci. U.S.A. 2002;99: 7877-7882.
16. Shaner NC, Campbell RE, Steinbach PA, Giepmans BNG, Palmer AE, Tsien RY. Improved monomeric red, orange and yellow fluorescent proteins derived from Discosoma sp. red fluorescent protein. Nat. Biotechnol. 2004;22:1567-1572.
17. Yoshida T, Inoue R, Morii T, Takahashi N, Yamamoto S, Hara Y, Tominaga M, Shimizu S, Sato Y, Mori Y. Nitric oxide activates TRP channels by cysteine S-nitrosylation. Nat. Chem. Biol. 2006;2:596-607.
18. Tajima S, Nakata E, Sakaguchi R, Saimura M, Mori Y, Morii T. Fluorescence detection of the nitric oxide-induced structural change at the putative nitric oxide sensing segment of TRPC5. Bioorg. *Med. Chem.* 2020;28:115430.
19. Schaefer PM, Kalinina S, Rueck A, von Arnim CAF, von Einem B. NADH Autofluorescence—A Marker on its Way to Boost Bioenergetic Research. Cytometry A. 2019;95:34-46.
20. Wagnieres GA, Star WM, Wilson BC. ln Vivo Fluorescence Spectroscopy and Imaging for Oncological Applications *Photochem Photobiol.* 1998;68:603-632.

Chapter 6
General conclusions

In this thesis, two new strategies related to the application of auto-fluorescent protein (AFP) based biosensors were developed. One strategy is the detection method for structural change of proteins upon the activation, as described in the chapter 2. The other strategy is a facile screening method on the optimization process of AFP-based biosensor, as described in the chapter 3, 4, and 5.

In the chapter 2, the putative structural change of TRPC5 upon reaction to NO was detected with utilizing the detection mechanism of AFP-based biosensors. It was suggested that TRPC5 stabilize the open state with forming the intramolecular disulfide bond with nucleophilically attacks of Cys558 to S-nitrosylated Cys553. On the other hand, AFP-based biosensors detected the structural change of the recognition modules induced by the recognition/reaction event as the fluorescence signal changes of AFP. A partial segment of TRPC5 containing two cysteine residues was embedded into a near chromophore of AFP, termed as EGFP-TRPC5, to evaluate its structural changes in response to NO. The quantitation of the change of the free thiol group and the measurement of the change of the fluorescence intensity indicated that the fluorescence emission ratio increased upon formation of disulfide bond with rection to NO. This result indicated that the structural change of the partial segment of TRPC5 induced by the disulfide bond formation between Cy553 and Cys558 transduced to the chromophore of EGFP. Therefore, proposed activation mechanism for the NO response of TRPC5 could be detected.

In the chapter 3, a facile two-step screening strategy for enhancing the signal response of AFP-based biosensor was developed. NO biosensor could be constructed with the optimization of a slight signal response of EGFP-TRPC5 as the first generation. One of the strategies to efficiently transduce the structural change upon disulfide bond formation to the EGFP chromophore is deletion of amino acid residues between the

disulfide bond formation site and EGFP. However, even the simplest one by one deletion of amino acid residues from the N- and/or the C-terminal provided 47 mutants as the candidates of deletion mutants. Instead of the *in vitro* evaluation of 47 mutants, a degree of structural change of each mutant was estimated as a RMSD value based on *in silico* simulation. 10 mutants could be selected for *in vitro* screening effectively because these were expected to show larger signal response. In fact, three mutants, termed as 551-575, 552-575, and 553-575, showed 2-4 times larger changes of the fluorescence emission ratios than EGFP-TRPC5, first generation, with evaluation of signal responses upon the cleavage of disulfide bond *in vitro* screening.

In chapter 4, further investigation of three NO sensor candidates 551-575, 552-575, and 553-575 obtained in the chapter 3 were measured to confirm whether these NO sensor candidates could detect NO. With the evaluation of the free thiol group and fluorescence intensity change, all three NO sensor candidates could detect NO with the increment of fluorescence emission ratios upon formation of disulfide bond. Additionally, reduction of these NO sensor candidates showed the decrease of the fluorescence emission ratios upon cleavage of disulfide bond, indicating these NO sensor candidates could work as the reversible sensors. However, these NO sensor candidates did not show specificity to NO but reacted to H_2O_2 as well as EGFP-TRPC5. The kinetics of the reaction to both NO and H_2O_2 all three NO sensor candidates became slower than EGFP-TRPC5.

In the chapter 5, it was confirmed whether the three redox sensors, 551-575, 552-575, and 553-575, investigated in the chapter 4, could function a in the living cells. These redox sensors showed sufficient fluorescence intensity upon the expression in the HKE293 cell. Upon the addition of extracellular H_2O_2, 551-575 showed the increment of the fluorescence intensity ratio as well as *in vitro* evaluation as described in the chapter 4. These results indicated that these redox sensors could work in the living cells.

In summary, firstly, the putative structural change of TRPC5 was detected with applying the detection mechanism of AFP-based biosensors. This result suggested that AFP-based biosensors could be applied for detecting the structural changes of the proteins at the activation. Secondly, to enhance the signal response at the construction of AFP-based biosensors, a new facile two-step screening strategy was developed. Structural changes of recognition modules were estimated as the RMSD values with *in silico* simulation. Obtained redox sensors could show measurable signal response in the living

cells, indicating that this two-step screening method was applicable for enhancement of signal response of AFP-based biosensors working in the living cells. This optimization strategy will promote the effective constructions of the AFP-based biosensors because this two-step screening method could be also applied to the essential optimization process of the introduction sites of the recognition modules upon the constructions of AFP-based biosensors. Especially, this two-step screening method show the advantage in the case that proteins of which structural information was lack were used as the recognition modules.

Finally, These methods described in this thesis showed the new application of AFP and a facile construction method of AFP-based biosensor to unveil the functions of the proteins in the signal transduction to utilize the bioenergy in the cells.

List of publications

1. Detection of Inositol Phosphates by Split PH Domains

Reiko Sakaguchi, Shunsuke Tajima, Yasuo Mori, Takashi Morii

Methods Mol. Biol. **2020***, 2091, 47-57.* doi: 10.1007/978-1-0716-0167-9_4.

(Chapter 1)

2. Fluorescence detection of the nitric oxide-induced structural change at the putative nitric oxide sensing segment of TRPC5

Shunsuke Tajima, Eiji Nakata, Reiko Sakaguchi, Masayuki Saimura, Yasuo Mori, Takashi Morii

Bioorg. Med. Chem. **2020**, *28*, 115430. doi: 10.1016/j.bmc.2020.115430.

(Chapter 2)

3. A two-step screening to optimize the signal response of autofluorescence protein-based biosensor

In preparation

(Chapter 3, 4, 5)

List of presentations

International conference

1. Construction of nitric oxide sensor based on fluorescent protein

Shunsuke Tajima, Eiji Nakata, Reiko Sakaguchi, Masayuki Saimura, Yasuo Mori, Takashi Morii

1st Japan-India Bilateral Symposium on Energy and Environmental Science, Dec. 2-5, 2018, Bangalore, India

2. Direct observation of CUG repeat RNAs assembled on DNA nanostructure.

Musashi Shimizu, Shun Nakano, Shunsuke Tajima, Takashi Morii

The 46th International Symposium on Nucleic Acids Chemistry (ISNAC2019), Oct. 29-31, 2019, Koganei Civic Center (Miyaji Gakki Hall), Koganei, Tokyo, Japan

Domestic conference

1. 蛍光タンパク質を基本骨格とする一酸化窒素センサー

田嶋　竣介、中田　栄司、才村　正幸、森井　孝

日本化学会第 96 春季年会、2016 年 3 月 24 日~ 27 日、同志社大学京田辺キャンパス

2. 蛍光タンパク質を基本骨格とした一酸化窒素センサー

田嶋　竣介、中田　栄司、才村　正幸、森井　孝

第 10 回バイオ関連化学シンポジウム、2016 年 9 月 7 日~9 日、石川県立音楽堂・もてなしドー地下イベント広場

3. 蛍光タンパク質を基本骨格とした一酸化窒素センサーの構築

田嶋　竣介、中田　栄司、才村　正幸、森井　孝

日本化学会第 97 春季年会、2017 年 3 月 16 日~ 19 日、慶應義塾大学日吉キャンパス

4. 蛍光タンパク質を基本骨格とした一酸化窒素センサーの構築

田嶋　竣介、中田　栄司、才村　正幸、森井　孝

第 29 回生体機能関連化学若手の会サマースクール、2017 年 7 月 10 日~ 11 日、松江ニューアーバンホテル

5. 蛍光タンパク質を基本骨格とした一酸化窒素センサーの機能評価

田嶋　竣介、中田　栄司、才村　正幸、森井　孝

第 11 回バイオ関連化学シンポジウム、2017 年 9 月 7 日~ 9 日、東京大学弥生キャンパス

6. 蛍光タンパク質を用いた一酸化窒素センサーの作製

田嶋　竣介、中田　栄司、才村　正幸、森井　孝

第 30 回生体機能関連化学若手の会サマースクール、2018 年 7 月 19 日~ 20 日、ANA ホリデイ・イン　リゾート宮崎

7. 蛍光タンパク質を用いた一酸化窒素センサーの機能評価

田嶋　竣介、坂口　怜子、才村　正幸、中田　栄司、森　泰生、森井　孝

第 12 回バイオ関連化学シンポジウム 2018、2018 年 9 月 9 日~ 11 日、大阪大学吹田キャンパス、大阪府吹田市

8. Design of fluorescent sensor detecting nitric oxide using auto-fluorescent protein

Shunsuke Tajima, Yoshitaka Toyoshima, Eiji Nakata, Reiko Sakaguchi, Masayuki Saimura, Yasuo Mori, Takashi Morii

日本化学会第 99 春季年会、2019 年 3 月 16 日~19 日、甲南大学岡本キャンパス、兵庫県神戸市

9. Detecting structural changes if the putative nitric oxide domain in TRPC5 channel

Shunsuke Tajima, Eiji Nakata, Reiko Sakaguchi, Masayuki Saimura, Yasuo Mori, Takashi Morii

日本化学会第 100 春季年会、2020 年 3 月 22 日~25 日、東京理科大学野田キャンパス、千葉県野田市

10.　蛍光タンパク質を用いた一酸化窒素センサーの構築

豊島　慶峻、田嶋　竣介、中田　栄司、才村　正幸、森井　孝

日本化学会第 100 春季年会、2020 年 3 月 22 日~25 日、東京理科大学野田キャンパス、千葉県野田市

11.　CUG リピート RNA が形成する高次構造体の直接観察

清水　武蔵、仲野　瞬、田嶋　竣介、森井　孝

日本化学会第 100 春季年会、2020 年 3 月 22 日~25 日、東京理科大学野田キャンパス、千葉県野田市

12.　構造変化が不明なタンパク質に対する蛍光タンパク質を用いたバイオセンサーの設計戦略

田嶋　竣介、中田　栄司、坂口　怜子、才村　正幸、森　泰生、森井　孝

第 15 回バイオ関連化学シンポジウム、2021 年 9 月 8 日~10 日、オンライン開催